

Surface Dynamics of Pd₂Ga and its Reactivity in the Liquid Phase Hydrogenation of Phenylacetylene

vorgelegt von
Diplom-Chemiker
Gregor Wowsnick
aus Dresden

Von der Fakultät II - Mathematik und Naturwissenschaften
der Technischen Universität Berlin
zur Erlangung des akademischen Grades
Doktor der Naturwissenschaften
Dr. rer. nat.
genehmigte Dissertation

Promotionsausschuss:

Vorsitzender: Prof. Dr. Thorsten Ressler

Berichter/Gutachter: Prof. Dr. Robert Schlögl

Berichter/Gutachter: Prof. Dr. Reinhard Schomäcker

Berichter/Gutachter: Prof. Dr. Michael Ruck

Tag der wissenschaftlichen Aussprache: 2. 9. 2013

Berlin, 2013

D 83

Zusammenfassung

Intermetallische Verbindungen des Pd-Ga Systems zeigen eine hochselektive und stabile katalytische Aktivität in der Gasphasenhydrierung von Acetylen. Dies wurde mit einer, von Pd verschiedenen, wohlgeordneten Kristallstruktur und einer starken Modifikation der elektronischen Struktur begründet sowie einer hohen Stabilität unter *in situ* Bedingungen. In dieser Arbeit wurde die Stabilität der intermetallischen Verbindung Pd₂Ga und ihre Eignung als Katalysator für die partielle Hydrierung von Phenylacetylen in flüssiger Phase untersucht.

Pd₂Ga ist inert gegenüber Hydridbildung und das Volumen wird auch in einer Atmosphäre aus 20% O₂ in He nicht unter 300 °C angegriffen, wie durch *in situ* XRD und *in situ* DTA/TG/MS Messungen gezeigt werden kann. Allerdings wurde, abweichend von bisherigen Annahmen, eine deutliche Diskrepanz zwischen der Struktur des Volumens und der Oberfläche von Pd₂Ga festgestellt. Mit Hilfe von HR-TEM sowie XPS konnte nachgewiesen werden, dass selbst Spuren von H₂O oder O₂ intermetallisches Ga unter partieller Zersetzung von Pd₂Ga zu oxidieren vermögen. Mechanische Belastung induziert Segregation von Ga des Volumens an die Oberfläche, welches anschließend oxidiert. Die Anwesenheit von Pd bewirkt eine hohe Reversibilität dieser Prozesse, wodurch die jeweilige elektronische Struktur der Oberfläche von Pd₂Ga stark von der Vorbehandlung und der umgebenden Atmosphäre abhängt. Eine Rekonstruktion der intermetallischen Verbindung auf der Oberfläche findet unter den Bedingungen der Flüssigphasenhydrierung nicht statt, wird jedoch durch eine Hochtemperaturvorbehandlung in einer 5% H₂/Ar-Atmosphäre erreicht unter Ausprägung einer nur sehr dünnen Passivierungsschicht. Gegenüber Pd zeigt Pd₂Ga eine erwartete, deutlich verminderte Hydrieraktivität, die Oberfläche oxidiert allerdings auch unter diesen Bedingungen. Unter weitestgehendem Ausschluss von Spuren von H₂O und O₂ wird die Oxidation verhindert, es findet in diesem Fall jedoch ein Angriff auf das Volumen von Pd₂Ga durch Phenylacetylen statt.

Die Ergebnisse zeigen beispielhaft, dass eine gezielte starke elektronische Modifizierung eines Übergangsmetall mit einem unedlen Metall eine verringerte Stabilität der Oberfläche bewirkt. Eine Terminierung der Volumenstruktur an der Oberfläche kann, wenn überhaupt, nur unter stark reduzierenden Bedingungen erhalten werden.

Abstract

Intermetallic compounds of the Pd-Ga system provide a highly selective and stable catalytic activity in the gas phase hydrogenation of acetylene, which was explained by the modified, well-ordered crystal structures and electronic structures as well as their high *in situ* stability, as compared to Pd. In this work the stability of the bulk and the surface of Pd₂Ga and its reactivity towards the partial hydrogenation of phenylacetylene in the liquid phase were investigated.

Pd₂Ga is resistant against hydride formation and the bulk of the material is not affected in a 20% O₂/He atmosphere at temperatures below 300 °C. However, in contrast to former suggestions, a considerable discrepancy between the bulk and the surface structure of Pd₂Ga was found. By means of HR-TEM and XPS evidence was found that traces of O₂ or H₂O are sufficient for the oxidation of intermetallic Ga at the surface leading to partial decomposition of Pd₂Ga. Mechanical load induces Ga segregation from the bulk to the surface with subsequent oxidation. The presence of Pd explains the relatively high reversibility of these processes, which ultimately leads to strong dependence of the surface structure on the pre-treatment and surrounding atmosphere. A re-formation of the intermetallic surface does not take place under the conditions of the liquid phase hydrogenation but is only achieved by a high temperature reduction in a 5% H₂/Ar atmosphere, resulting in the formation of only a very thin passivation layer. Compared to Pd, Pd₂Ga shows an expected, significantly lowered hydrogenation activity. Though, the surface oxidizes even under these conditions. Under the exclusion of traces of O₂ and H₂O to the greatest possible extent, the oxidation is prevented, however, in this case even the bulk material is attacked by phenylacetylene.

The results exemplify, that a well-defined strong modification of a transition metal with a less noble metal causes a considerably lowered stability. A direct termination of the bulk structure at the surface can be - if at all - achieved only under strongly reducing conditions.

Danksagung

Mein erster Dank gilt Herrn Prof. Dr. Robert Schlögl, unter dessen Anleitung ich die Forschungsarbeiten in der Abteilung Anorganische Chemie des Fritz-Haber-Institutes durchführen konnte. Seine konstruktiven Anmerkungen und Kritiken, sein Motivationsvermögen sowie sein großer Erfahrungsschatz haben diese Arbeit maßgeblich geprägt.

Dr. Malte Behrens gebührt ein ganz besonderer Dank. Abgesehen von den vielen, zu jeder Zeit möglichen wissenschaftlichen Diskussionen und Anreizen ist seine moralische Unterstützung unschätzbar. Ohne sein stets offenes Ohr und sein großes Engagement in Zeiten, in denen nicht die Wissenschaft im Vordergrund stand, hätte ich diese Arbeit nicht beendet.

Dr. Detre Teschner möchte ich besonders hervorheben. Er unterstützte mich in allen Fragen zur Photoelektronenspektroskopie am Synchrotron und bei deren Auswertung sowie zur Hydrierung allgemein und er hat mit stetem Interesse den Fortgang der Arbeit verfolgt. Dankeschön!

Die Forschungsarbeiten wurden in Zusammenarbeit mit dem Max-Planck-Institut für Chemische Physik fester Stoffe in Dresden durchgeführt. Bei Herrn Prof. Dr. Juri Grin bedanke ich mich für die von ihm gegebene Möglichkeit der Nutzung der Infrastruktur des Institutes zur Synthese und Charakterisierung der intermetallischen Verbindungen. Ich danke weiterhin Dr. Marc Armbrüster für nützliche Hinweise und Anregungen.

Ich möchte mich bei Dr. Igor Kasatkin, Dr. Ullrich Burkhardt, Monika Eckert, Petra Scheppan und Gisela Weinberg für die metallographischen und elektronenmikroskopischen Analysen bedanken. Dr. Horst Bormann, Dr. Yuri Prots, Dr. Frank Girgsdies und Steffen Hückmann danke ich für die Durchführung und die Hilfe bei der Auswertung der Röntgenbeugungsmessungen.

Mein großer Dank gilt allen, die mich bei den täglichen Laborarbeiten unterstützt haben: Dr. Edward Kunkes, Timur Kandemir, Dr. Matthias Friedrich und Yuan Luo. Die äußerst angenehme, lockere Atmosphäre im Büro mit Dr. Olaf Timpe und Klaus Friedel war von unschätzbarem Wert.

Mein letzter, großer Dank gilt meiner Familie für ihre Liebe und ihr großes Vertrauen in mich sowie für ihre immerwährende Unterstützung in jeglicher Hinsicht.

Table of Contents

Zusammenfassung.....	I
Abstract.....	III
Danksagung	V
Table of Contents	VII
Table of Figures.....	XI
List of Tables	XIX
List of abbreviations	XXI
1 Introduction.....	1
1. 1 Syntheses of alkenes by the reduction of alkynes	1
1. 2 Thermodynamics of alkyne hydrogenation with H ₂	2
1. 3 Gas phase hydrogenation of acetylene	3
1. 4 Hydrogenation of higher alkynes	3
1. 5 The relationship between the electronic structure of a transition metal surface and the strength of surface-adsorbate interactions	5
1. 6 Mechanism and selectivity control of alkyne hydrogenation over Pd	7
1. 7 Modifiers	10
1. 7. 1 Pd-Ag catalysts	11
1. 7. 2 Lindlar's catalyst.....	12
1. 8 Pd-Ga intermetallic compounds as catalysts for the semi-hydrogenation of acetylene.	13
1. 8. 1 The phase diagram of the Pd-Ga system.....	13
1. 8. 2 Crystal structure of PdGa.....	14
1. 8. 3 Crystal structure of Pd ₂ Ga	15
1. 8. 4 Previous studies of Pd-Ga intermetallic compounds as hydrogenation catalysts ...	16
1. 9 References	20
2 Aim and outline of the current work.....	26
3 Surface Dynamics of the Intermetallic Catalyst Pd₂Ga, Part I - Structural Stability in UHV and Different Gas Atmospheres	28
Abstract.....	28
3. 1 Introduction	29
3. 2 Materials and Methods	34
3. 2. 1 Synthesis of Pd ₂ Ga.....	34

3. 2. 2	X-ray powder diffraction	34
3. 2. 3	Metallography and scanning electron microscopy	35
3. 2. 4	Surface area characterization	35
3. 2. 5	Transmission electron microscopy	36
3. 2. 6	<i>In situ</i> thermal analysis	36
3. 2. 7	X-ray photoelectron spectroscopy	36
3. 3	Results and Discussion.....	37
3. 3. 1	Characterization and stability of the bulk of Pd ₂ Ga.....	37
3. 3. 2	Characterization and stability of the surface.....	41
3. 3. 3	XPS investigation of the metallographic specimen	41
3. 3. 4	XPS and HR-TEM investigations of milled Pd ₂ Ga in the as prepared state	45
3. 3. 5	XPS investigations of ground Pd ₂ Ga	48
3. 3. 6	XPS and HR-TEM investigations of <i>ex situ</i> pre-reduced milled Pd ₂ Ga.....	48
3. 3. 7	<i>In situ</i> H ₂ treatment of pre-reduced milled Pd ₂ Ga and re-oxidation.....	52
3. 4	Summary	53
3. 5	Conclusion.....	56
3. 6	Supporting information	57
3. 6. 1	Microscopy	57
3. 6. 2	<i>In situ</i> XRD.....	59
3. 6. 3	Further XPS analyses.....	61
3. 7	References	65
4	Surface Dynamics of the Intermetallic Catalyst Pd₂Ga, Part II – Reactivity and Stability in Liquid Phase Hydrogenation of Phenylacetylene.....	69
4. 1	Introduction	70
4. 2	Materials and Methods	73
4. 2. 1	Synthesis of Pd ₂ Ga.....	73
4. 2. 2	X-ray diffraction	74
4. 2. 3	X-ray photoelectron spectroscopy	74
4. 2. 4	HR-TEM	74
4. 2. 5	Catalytic hydrogenation	75
4. 3	Results and Discussions	77
4. 3. 1	Hydrogenation of phenylacetylene with as prepared milled Pd ₂ Ga, Pd powder, Pd/Al ₂ O ₃ and Lindlar's catalyst	77
4. 3. 2	Hydrogenation of phenylacetylene with Pd ₂ Ga after different pre-treatments.....	80

4. 3. 3 Activity of styrene hydrogenation with pre-reduced Pd ₂ Ga, Pd powder and Lindlar's catalyst.....	86
4. 4 Summary	89
4. 5 Conclusion.....	91
4. 6 Supporting information	92
4. 7 References	97
5 Summary.....	101
Appendix.....	104
Bulk and surface analyses of PdGa.....	104
Personal information.....	108

Table of Figures

Figure 1-1: Density of states projected on H 1s state as presented in [37] for H atoms chemisorbed on (111) metal surfaces. The antibonding states of the complex get filled in the case of Cu and Au, where the d-band of the metal surface is shifted away from the Fermi level (dashed lines), resulting in repulsive interactions. The antibonding states are not filled in the case of Ni and Pt.....	6
Figure 1-2: Potential energy diagram for acetylene hydrogenation (top) and ethylene hydrogenation on Pd(111) taken from [55].	8
Figure 1-3: Phase diagram of the Pd-Ga system [108]	13
Figure 1-4: Unit cell (left) and coordination of Pd (right) in the intermetallic compound PdGa crystallizing in space group $P2_13$ (FeSi-type). The Pd atoms are isolated from each other and are surrounded exclusively from seven Ga atoms in the first coordination sphere (right).	14
Figure 1-5 Left: Unit cell of Pd ₂ Ga. Top right: Coordination of Pd1. Down right: Coordination of Pd2. The compound crystallizes in the Co ₂ Si-type. The short Pd-Ga distances (2.54-2.56 Å) are shown as straight line, dashes lines represent atomic distances between 2.81-2.99 Å.	15
Figure 1-6: Pd 3d _{5/2} core-level spectra of Pd, Pd ₂ Ga, PdGa and Pd ₃ Ga ₇ ^[128] recorded in UHV at ambient temperature.	18
Figure 3-1: Left: Unit cell of Pd ₂ Ga. Top right: First coordination shell of Pd1. Down right: First coordination shell of Pd2. The compound crystallizes in the Co ₂ Si type of structure. The short Pd-Ga distances (2.54-2.62 Å) are shown as full lines, dashes lines represent atomic distances between 2.81-2.99 Å. The structural motif of elemental palladium, i.e. Pd-triangles, are preserved within the crystal structure.	33
Figure 3-2: X-ray diffraction patterns of Pd ₂ Ga after different treatments. a) calculated pattern ^[56] b) ground c) milled d) milled and subsequently treated 4 h in 5% H ₂ /Ar at 400 °C.	38

- Figure 3-3: *In situ* DTA/TG/MS measurement of as prepared milled Pd₂Ga. Top: The powder was initially heated in He to 200 °C (10 K/min) to desorb water from the surface. After cooling the atmosphere was changed to 10% H₂/He and the powder was heated to 500 °C (10 K/min) revealing an exothermic peak at 180 °C accompanied by H₂O formation due to surface oxide reduction. Bottom: No further phase transformations were detected also during the long time treatment of the powder in 10% H₂/He with a stepwise increase of the temperature from 50 to 150 °C.....40
- Figure 3-4: Pd 3d XP spectra of a Pd foil (black) and a metallographic specimen (polished under Ar) in an as prepared state (blue) and after thermal treatment at 400 °C in dynamic vacuum (red).42
- Figure 3-5: Ga 3d and valence spectra of different Pd₂Ga samples. The change of the valence band structure with the amount of oxidized Ga is obvious.43
- Figure 3-6: Pd 3d depth profiling of milled Pd₂Ga in an as prepared state (blue) and heated to 400 °C (red). The black line represents Pd₂Ga powdered by grinding in air.46
- Figure 3-7: HR-TEM of milled Pd₂Ga in an as-prepared state. Large crystalline Pd₂Ga particles are surrounded by an inhomogeneous amorphous Ga oxide layer. At certain parts of the layer nanoparticles are embedded.....47
- Figure 3-8: Ga 3d spectra of different pre-reduced Pd₂Ga powder samples. a) *ex situ* pre-reduced powder, cooled under Ar b) *ex situ* pre-reduced cooled under H₂ c) *in situ* H₂ treatment after *ex situ* pre-reduction and cooling under Ar d) sample of c) after slow oxidation in the cell and subsequent air exposure e) sample of c) after abrupt exposure to air. Red lines represent fits of the intermetallic Ga 3d doublet while blue lines correspond to oxidized Ga species. In the case of a high oxidation grade also a broad signal of O 2s (green) is observed ~ 23 eV.49
- Figure 3-9: Pd 3d spectra of *ex situ* pre-reduced powders at a kinetic energy of 145 eV. The red curve represents the *ex situ* pre-reduced milled powder cooled under 5% H₂/Ar and is almost similar to the metallographic specimen heated to 400 °C (black curve) and the samples treated *in situ* with H₂ at 1 mbar (not shown). *Ex situ* pre-reduction and cooling under 100% Ar leads to significant disruption of

the surface (blue curve) as well as the abrupt exposure to air of an freshly reduced sample (green).	49
Figure 3-10: XP spectra of the valence band at a photon energy of 710 eV. a) Pd foil b) <i>ex situ</i> pre-reduced milled powder and cooled under Ar c) <i>ex situ</i> pre-reduced milled powder cooled under H ₂ d) metallographic specimen heated to 400 °C and e) sample of b) during treatment in 1 mbar H ₂ at 400 °C.	51
Figure 3-11: HR-TEM of Pd ₂ Ga powder after pre-reduction at 400 °C. These particles consist of large domains and are surrounded only by a thin amorphous over-layer. According to the XP spectra Ga oxide contribute to the thin over-layer but also contaminations in the microscope likely response therefore.	51
Figure 3-12: Scheme of the observed dynamic changes of Pd ₂ Ga after different treatments. The rectangle shown in (A) and (B) indicate the metallographic specimen. The spherical sketches (C-J) represent a microcrystalline particle after milling. The non-uniform morphologies and distribution of the nanostructures in particular that of the smaller Pd agglomerates (Pd _x , light blue spheres), larger metallic Pd accumulations (dark blue spheres), Pd oxide (green) and C accumulations (black rectangles) at the surface are simplified. The bulk of Pd ₂ Ga (red areas) is always stable. Ga oxide is shown in yellow color. A layer of varying thickness at the interface of the bulk and the Ga oxide, shown in purple, marks slightly Pd enriched Pd ₂ Ga due to Ga surface segregation. The grey cover visible in (H and J) should indicate the irreversible enrichment of metallic Ga on top of the surface during <i>in situ</i> H ₂ treatment in the XPS chamber.....	54
Figure 3-13: Microscopic analysis of an embedded metallographic specimen of Pd ₂ Ga polished under Ar. The material is homogeneous as visible by optical microscopy (a) and SEM (c). The color shading observed in polarized light (b) indicates the polycrystallinity of the specimen.	57
Figure 3-14: SEM images of milled Pd ₂ Ga. a) overview on the powder in the as prepared state. b) a closer look to a large particle and the elemental mapping of Pd, Ga and W c) overview on the powder after treatment at 400 °C for 4 h in 5% H ₂ /Ar.	58
Figure 3-15: Calculated Rietveld scale factor of <i>in situ</i> XRD pattern of Pd ₂ Ga in different atmospheres, representing the overall intensity of the Pd ₂ Ga reflections. A	

significant drop starting at about 300 °C in 20% O ₂ /He indicates starting bulk oxidation.	59
Figure 3-16: Selected <i>in situ</i> XRD pattern of Pd ₂ Ga recorded at 25 °C. a) after stepwise heating and cooling in 100% He and 25% H ₂ /He respectively. The sample remains single phase b) Decomposition products were detected after high temperature treatment in 20% O ₂ /He accompanied by a decrease in the overall intensity of the Pd ₂ Ga diffraction lines. Black lines represent the obtained pattern, red lines correspond to the Rietveld fit and bottom lines reveal the difference between both.	59
Figure 3-17: Observed Pd 3d reference spectra of the Pd ₂ Ga metallographic specimen, heated to 400 °C (left) and a Pd foil (right). Both line profiles can be fit with a Donjach-Sunjic function. The asymmetry is very small for the IMC compared to elemental Pd. Blue lines in the Pd spectra represent shake-up satellites due to final state effects.	61
Figure 3-18: Left: The Pd 3d _{5/2} peak of the metallographic specimen in the as prepared state. The almost symmetric but relatively broad peak (black dots) cannot be described with a combination (black lines) of the line shapes of elemental Pd (green) and Pd ₂ Ga (red). Right: One broad fitting curve perfectly match the obtained line profil (a). The use of three fitting components (b and c), including Pd ₂ Ga and Pd is somehow arbitrary and do not match a perfect peak fitting. (d) represents a spectra, obtained after <i>in situ</i> reduction of milled Pd ₂ Ga powder, which was abruptly exposed to air and subsequently measured in UHV at room temperature.	62
Figure 3-19: C 1s depth profiling of the metallographic specimen in the as prepared state and after heating to 400 °C.	63
Figure 3-20: Comparison of absolute peak intensities of Ga 3d and Pd 3d recorded at E _{Kin} = 145 eV obtained after <i>ex situ</i> pre-reduction and subsequent cooling under H ₂ atmosphere.	64
Figure 4-1: Concentration profiles during the hydrogenation of phenylacetylene at 4 bar, 40 °C in octane using Pd ₂ Ga (10 mg), Pd powder (10 mg), Lindlar's catalyst (3.5 mg, 5 wt-% Pd) and Pd/Al ₂ O ₃ (0.8 mg, 5 wt-% Pd).	80

- Figure 4-2: Concentration profiles of phenylacetylene hydrogenation for Pd₂Ga after different pre-treatments as well as Pd powder and Lindlar's catalyst as reference catalysts. For better visualization of the strongly different activity of the Pd₂Ga catalyst after the pre-treatments, the reaction time was multiplied by the catalysts mass on the x axis. Note their very different scales. All reactions were carried out at 40 °C in octane at ~ 1 bar, except Pd₂Ga pre-treated in static vacuum (4 bar, compare Table 4-3).....82
- Figure 4-3: X-ray diffraction pattern of pre-reduced Pd₂Ga (a) after liquid phase hydrogenation of phenylacetylene under inert conditions; (b) after styrene hydrogenation. c) represents the calculated pattern according to [46].84
- Figure 4-4: HR-TEM of a sample spent for phenylacetylene hydrogenation. In contrast to a pre-reduced fresh sample, the particles are cracked in smaller domains. According to Fourier analysis the surface consists of Pd₂Ga nanoparticles. An amorphous phase is also detected, which can be related either to carbon or Ga oxide. The sample was exposed to air after reaction and before TEM imaging. .85
- Figure 4-5: Hydrogenation of styrene (circles) with pre-reduced Pd₂Ga to ethylbenzene (stars). Adding small amounts of H₂O under H₂ atmosphere result in spontaneous increase in reaction rate.87
- Figure 4-6: Schematic sketch of the structure of a microcrystalline Pd₂Ga particle before and after liquid phase hydrogenation and subsequent air contact. Red: Pd₂Ga, purple: Pd₂Ga_{1-x} (within the homogeneity range), yellow: surface Ga oxide, black: carbon, blue: elemental Pd, green: Pd oxides, light blue particles represent the presence of undefined Pd species. However, the exact nature and morphology of the Pd species is not known.90
- Figure 4-7: Arrhenius-plot for the hydrogenation of phenylacetylene carried out in octane at 4 bar H₂ pressure. The temperature was set to 25 °C, 35 °C, 40 °C, 50 °C and 60 °C.92
- Figure 4-8: Image of a part of the hydrogenation reactor for reactions under very inert conditions: 1 Catalyst containing ampoule, 2 burner, 3 hydrogenation vessel with baffles, 4 thermo-couple, 5 cannula terminated with a 4-way valve (not shown)

for sample taking, 6 spindle valve to introduce liquids, 7 H₂ source, 8 connections to the Schlenk line for vacuum and inert gas.....93

Figure 4-9: XPS depth profiling of the Pd 3d core level for different Pd₂Ga samples. Blue lines represent the as-prepared milled Pd₂Ga consisting mainly of Pd. At the outermost surface oxidized Pd also seems to be present as indicated by the long tail of the peak. Green lines represent a sample used for liquid phase hydrogenation. The Pd oxides vanish during reduction but the surface consists still mainly of elemental Pd, possibly alloyed with some Ga. Red lines represent the metallographic specimen of Pd₂Ga heated to 400 °C and is shown as reference here.....94

Figure 4-10: Conversion, selectivity and carbon balance vs. time observed for the liquid phase hydrogenation of phenylacetylene at 4 bar, 40 °C with Lindlar's catalyst (stars), Pd/Al₂O₃ (spheres), as prepared milled Pd₂Ga (squares) and Pd powder (triangles).....95

Figure 4-11: Conversion, selectivity and carbon balance versus (time*catalyst mass) for Pd₂Ga after different pre-treatments at ~1.3 bar, 40 °C. On the right site a zoom is shown, to highlight the different initial activities. The highest initial activity is found for as prepared milled Pd₂Ga (squares), followed by milled Pd₂Ga treated at 400 °C in static vacuum (stars, this reaction was performed at 4 bar in the commercial autoclave). A reductive pre-treatment leads to a considerably lower initial activity. It increases rapidly with time, using the commercial autoclave (spheres), but can be stabilized at least in the beginning under very inert conditions (Schlenk reactor). Under these conditions the carbon balance decreases significantly more.....96

Figure A1: Optical microscopy of an embedded metallographic specimen (a, b) reveals no additional phases. Leaks and rifts, visible in the SEM image (c), are present to a small extent, which certainly originate from sample preparation. The distribution of Pd (d) and Ga (e) is homogeneous with an elemental composition of Pd_{49.8}Ga_{50.2} according to WDX. Small holes, close to the edge are slightly enriched on Ga.....105

Figure A2 left: X-ray diffraction pattern of ground PdGa (a) and a calculated pattern (b).

Right: *In situ* TG/MS of a ground PdGa. The heating rate was 5°C/min in 5% H₂/Ar. The X-ray diffraction pattern of ground PdGa verifies the absence of additional crystalline phases within its detection limit. The *in situ* TG/MS analysis of ground PdGa show a slight mass loss starts at ~270 °C accompanied with the formation of CO₂ which is likely attributed to carbonate decomposition. At 400 °C, a further mass loss accompanied by signals for CO₂ and H₂O is visible, which indicates simultaneous carbonate decomposition and surface oxide reduction. 106

Figure A3 left: XPS depth-profiling of the Pd 3d core-level of the as prepared metallographic specimen of PdGa in UHV at ambient temperature (blue), the metallographic specimen heated *in situ* to 450 °C in 1 mbar H₂ (red) and of ground PdGa, pre-reduced *ex situ* in 5% H₂/Ar at 200 °C for 1 h, recorded under UHV at ambient temperature. A binding energy of 336.3 eV is observed for the *in situ* reduced specimen. This binding energy is similar to that of a PdGa($\bar{1}\bar{1}\bar{1}$) [D. Rosenthal et al., Langmuir 28 (2012) 7848] after several sputtering and annealing cycles. The other signals must be attributed to partially decomposed Pd species. On the right side the corresponding valence bands are shown. 106

Figure A4: XPS depth-profiling of the Ga 3d core-level. a) an as prepared metallographic specimen of PdGa b) metallographic specimen during *in situ* treatment at 450 °C in 1 mbar H₂, c) ground PdGa, pre-reduced *ex situ* in 5% H₂/Ar at 200 °C for 1 h and recorded under UHV at ambient temperature. In a) and c) large amounts of Ga oxides (blue fitting lines) the relative amount increases with increasing surface sensitivity. The signal at 19.2 eV in c) is attributed to Ga sub-oxides. Only the *in situ* reduced specimen (c) shows Ga almost completely in intermetallic state (red doublet). Green lines correspond to O 2s. 107

List of Tables

Table 1-1: Selected thermodynamic data for the hydrogenation of acetylene and phenylacetylene. ^[8,9,10]	2
Table 1-2: Comparison of the minimum chemisorption energies of Ni(111), Cu(111), Pt(111) and Au(111) obtained from DFT calculations by Hammer et al. ^[38]	6
Table 1-3: Structure type, lattice parameters and corresponding references for the known Pd-Ga compounds	14
Table 3-1: Lattice parameters of Pd ₂ Ga after grinding (a), milling (b) and milling with subsequent thermal treatment at 400 °C in 5% H ₂ /Ar (c) as determined by XRD. While no distinctive differences in lattice parameters are observed, after milling, a significant diffraction line broadening (values are given for the 203 reflection) is visible.	38
Table 3-2: Comparison of peak maxima and FWHM of Pd 3d _{5/2} at different kinetic energies: metallographic specimen as prepared (a), metallographic specimen heated to 400 °C in dynamic vacuum (b) and a Pd foil (c). The ratios of Pd and Ga in dependence on the information depth and the amount of oxidized Ga are also given.	43
Table 3-3: Comparison of peak maxima and FWHM of Pd 3d _{5/2} at different kinetic energies: milled powder as prepared (a), powder heated to 400 °C in dynamic vacuum (b) and ground powder as prepared (c). The quantification of Pd and Ga always shows a large excess of Ga. Due to the high content of oxidized Ga the surface is enriched on Pd with respect to the present metallic Ga.	48
Table 3-4: Peak position and FWHM of Pd 3d _{5/2} and elemental quantification of Pd and Ga and Ga oxide content of <i>ex situ</i> pre-reduced milled Pd ₂ Ga recorded at a kinetic energy of 145 eV. a) sample cooled down under 100% Ar, b) <i>in situ</i> H ₂ treatment (1 mbar) of the sample of a) at 400 °C, c) sample of b) after slow <i>in situ</i> oxidation and subsequent exposure to air, d) <i>ex situ</i> pre-reduced and cooled down under 5% H ₂ /Ar, e) <i>in situ</i> H ₂ treatment (1 mbar) of samples of d) at 400 °C, f) sample of e) after abrupt exposure to air (2 signals).	53

Table 3-5: Carbon content of different Pd ₂ Ga samples dependent on the information depth.	64
Table 4-1: Comparison of initial activity and selectivity towards styrene S _{Sty} at low and full conversion and the carbon balance CB of as prepared, milled Pd ₂ Ga with Pd, Pd/Al ₂ O ₃ and Lindlar's catalyst in the hydrogenation of phenylacetylene at 4 bar, 40 °C in octane in a commercial autoclave.	79
Table 4-2: Lattice parameters and FWHM of the 203 reflex of pre-reduced Pd ₂ Ga used for hydrogenation of a) phenylacetylene and b) styrene. The values for a fresh sample pre-reduced at 400 °C are given for comparison (c).	84
Table 4-3: Initial activity towards styrene formation (A _{Sty}) and selectivities to styrene (S _{Sty}) as a function of the pre-treatment and the used reactor for hydrogenation of phenylacetylene. Pre-reduction was 5% H ₂ /Ar for 4 h at 400 °C. ~ 3 ml phenylacetylene were solved in octane (80-100 ml). The reaction temperature was always 40 °C.	86
Table 4-4: Initial reaction rate of ethylbenzene formation (A _{EB}) for Pd, pre-reduced Pd ₂ Ga and Lindlar's catalyst. All reactions were carried out in the Schlenk reactor and the reaction conditions for styrene hydrogenation are similar to that described for phenylacetylene hydrogenation. A _{Sty} is given for comparison. The ratio between both activities is calculated for the catalysts.	88
Table 4-5: Comparison of peak maxima and FWHM of Pd 3d _{5/2} at different kinetic energies and quantification of Pd and Ga: a) milled powder as prepared b) spent sample without pre-reduction. The similarity of Ga oxide content and metal ratios is obvious.	93
Table A1: Pd 3d _{5/2} peak maxima and FWHM of a) an as prepared metallographic specimen b) metallographic specimen during <i>in situ</i> treatment at 450 °C in 1 mbar H ₂ , c) ground PdGa, pre-reduced <i>ex situ</i> in 5% H ₂ /Ar at 200 °C for 1 h and recorded under UHV at ambient temperature. The calculated surface stoichiometry (<i>ab initio</i>) and the relative content of oxidized Ga are also given. In particular note the massive Ga enrichment for the ground sample c).	107

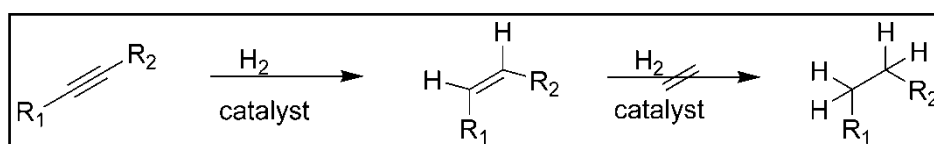
List of abbreviations

A	specific activity
BE	binding energy
BET	adsorption isotherm model (Brunauer, Emmet, Teller)
CB	carbon balance
CCD	charge coupled device
DFT	density functional theory
DOS	density of states
DSC	differential scanning calorimetry
DTA	differential thermal analysis
EDX	energy dispersive X-ray spectroscopy
EXAFS	extended X-ray absorption fine structure
fcc	face centered cubic
FID	flame ionization detector
FTIR	fourier transformed infrared spectroscopy
FWHM	full width at half maximum
GC	gas chromatograph
HR-TEM	high resolution transmission electron microscopy
IMC	intermetallic compound
LEED	low energy electron diffraction
MS	mass spectrometry
S	selectivity
SEM	scanning electron microscopy
TG	thermo gravimetry
UHV	ultra high vacuum
WDX	wavelength dispersive X-ray spectroscopy
X	conversion
XPS	X-ray photoelectron spectroscopy
XRD	X-ray diffraction

1 Introduction

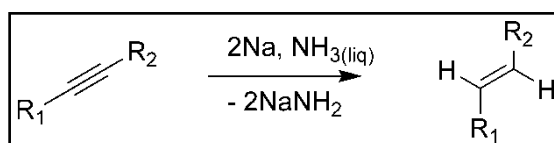
1.1 Syntheses of alkenes by the reduction of alkynes

In 1897 Paul Sabatier reported about the high reducing power of H_2 in presence of finely divided Ni and received the Nobel prize in 1912 for his work on catalytic hydrogenation and its application in organic synthesis^[1,2]. Today, a widely applied method for alkyne reduction to an alkene is the heterogeneous catalytic hydrogenation in presence of a catalytically active transition metal^[3]. Di-substituted alkynes are generally hydrogenated with high stereoselectivity to the (Z)-alkene (Scheme 1-1). The further reaction of the alkene to the alkane is an undesired consecutive reaction and must be prevented.



Scheme 1-1: Catalytic hydrogenation of an alkyne to a (Z)-alkene with H_2 . The further hydrogenation to the saturated hydrocarbon is undesired.

The catalytic hydrogenation might be also carried out in homogeneous manner, e.g. with Pd(0) complexes^[4,5]. Another method is the chemical reduction of alkynes with dissolved Na in liquid NH_3 ^[6], an important approach for the syntheses of (E)-alkenes (Scheme 1-2).



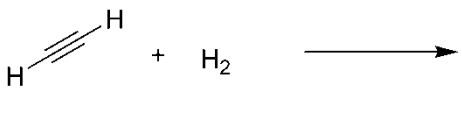
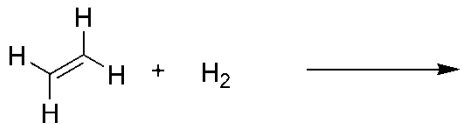
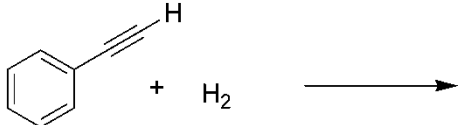
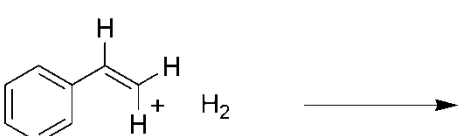
Scheme 1-2: Reduction of an alkyne to an alkene with Na dissolved in liquid NH_3 . This reaction occurs with high (E)-stereoselectivity.

The alkyne is reduced stepwise by two solvated electrons, formed by dissolving Na in liquid NH_3 and the resulting carbanions deprotonate NH_3 to NH_2^- . Alkynes can also be transformed by ionic hydrogenation^[7] using a protic acid and a hydride ion donor, e.g. a mixture of CF_3SO_3H and $Cp(CO)_3WH$. This work addresses exclusively the heterogeneously catalyzed hydrogenation.

1.2 Thermodynamics of alkyne hydrogenation with H₂

The direct hydrogenation of an alkyne to an alkene with molecular hydrogen is generally a strongly exothermic reaction^[8,9,10]. At ambient temperature the equilibrium lies on the products side. This is also true for the hydrogenation of an alkene to an alkane and from thermodynamic point of view, the reaction of H₂ with an alkyne takes place spontaneously resulting in the corresponding alkane as preferred product. Table 1-1 summarizes some thermodynamic data for the hydrogenation of acetylene, ethylene, phenylacetylene and styrene.

Table 1-1: Selected thermodynamic data for the hydrogenation of acetylene and phenylacetylene.^[8,9,10]

reaction			$\Delta_R H^\circ_{298} /$ kJ·mol ⁻¹	$\Delta_R S^\circ_{298} /$ J·mol ⁻¹ K ⁻¹	$\Delta_R G^\circ_{298} /$ kJ·mol ⁻¹
			-174.5	-111.9	-141.1
			-136.9	-120.6	-101.0
			-158.8	-123.7	-129.9
			-118.0	-145.9	-74.5

However, the equilibrium constant K_P for the required dissociation of H₂ in two H atoms ($\Delta H_{\text{diss}} = 436 \text{ kJ·mol}^{-1}$), at 25 °C is 10^{-71} ^[11]. Hence, the equilibrium lies completely on the molecular side and e.g. at 300 °C only $10^{-34}\%$ of H₂ molecules are dissociated in its atoms. Therefore, at moderate temperatures the hydrogenation does practically not proceed in absence of a catalyst

1.3 Gas phase hydrogenation of acetylene

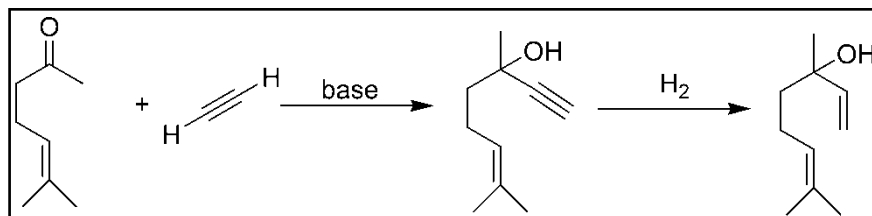
The simplest alkyne - acetylene - is an impurity (0.5-2%) in the pyrolysis products obtained by steam cracking of light alkanes, which contain mainly H_2 , methane, ethane and ethylene and other C_{2+} hydrocarbons^[12]. De-ethanizer units separate C_2 hydrocarbons from all other products. The ethylene is mainly used for further polymerization to polyethylene (worldwide production ~ 50 Mt/a) by the Ziegler-Natta process^[13]. The concentration of acetylene has to be lowered to ppm range because acetylene poisons the polymerization catalyst and lowers the quality of the polyethylene. Industrially this is realized by catalytic hydrogenation of acetylene to ethylene. Industrially an eggshell Pd-Ag/ Al_2O_3 alloy catalyst is applied today^[14,15]. The hydrogenation is carried out continuously either before (front-end method^[16]) or after (tail-end method^[17]) the de-ethanizer units. It is observed, that the high H_2 content (H_2/C_2H_2 ratio ~ 110) in the front-end method is beneficial for fast removal of acetylene, causes a low rate of carbonaceous deposits (oligomers, “green-oil”) and decelerates catalyst deactivation^[12]. However, under these conditions highly undesired ethylene hydrogenation to ethane can easily occur, which lowers the ethylene yield and might lead to thermal runaway of the reactor. In tail-end reactors stoichiometric amounts of H_2 , optionally co-feed with CO are added to the C_2 feed. This approach is more selective towards the semi-hydrogenation but due to enhanced formation of carbonaceous deposits the catalyst deactivates quickly which necessitates its frequent regeneration.

1.4 Hydrogenation of higher alkynes

The alkyne removal from alkenes to low ppm level is furthermore relevant for the substituted alkynes propyne^[18] and phenylacetylene, where the corresponding alkenes can be further polymerized to polypropylene and polystyrene, respectively. Styrene is produced by dehydrogenation of ethylbenzene and contains phenylacetylene and its substituted derivatives, which can be removed by hydrogenation in liquid phase^[19,20].

Alkyne semi-hydrogenation is further important for fine-chemical syntheses. Ketones or organohalogen can be subjected to an alkynylation with a terminal alkyne, aiming at the formation of a C-C bond. The resulting alkyne or propargylic alcohol is usually of low

interest and can be further converted by means of hydrogenation to the corresponding alkene or alkane or is further coupled to higher alkynes. Examples are the syntheses of Linalool (see Scheme 1-3)^[21], Vitamin A, E and K or insect pheromons^[22,23].



Scheme 1-3: The last two steps of Linalool synthesis as example for the application of alkyne semi-hydrogenation in fine chemical syntheses. The 6-methylhept-5-en-2-one is subjected to an alkynylation to Dehydrolinalool, followed by the hydrogenation of the propargylic alcohol to the vinyl alcohol Linalool.

When higher alkynes are hydrogenated chemo- and stereo-selectivity must be considered in addition to complete hydrogenation to the alkane and formation of carbonaceous deposits. Isomerization of the (Z)-alkene to the (E)-alkene is a frequently occurring side reaction^[24]. Double bond migration and reduction of other easily reducible functional groups, for instance the reduction of NO₂-group or hydrogenolysis of carbon-halogen bond, can additionally diminish the yield of the desired cis-alkene^[25].

Ni^[26,27] or Fe^[28] based catalysts were successfully applied for alkyne hydrogenation but the vast majority of catalysts is based on Pd, which is often further modified by heavy metals or organic nitrogen-bases^[3]. The most important and most widely utilized catalyst for liquid phase hydrogenations is Lindlar's catalyst^[29]. This catalyst consists of Pd supported on CaCO₃ and poisoned with Pb(OAc)₂ and in many cases displays very high alkene yields accompanied by low isomerization rates.

The alkyne hydrogenation in laboratory syntheses or in industrial fine chemical production is usually carried out in discontinuous operation mode. This mode is favored because it offers lower operating costs combined with a relatively easy maintenance^[30]. Batch systems are relatively flexible with respect to educts, reaction time and conditions, offering a high degree of selectivity control. For alkyne hydrogenation temperatures below 100 °C and H₂ pressures of 1 bar or slightly above are usually applied. A solvent is often present, which additionally influences the reaction behavior^[31]. The most important difference from the continuous operation mode is that the composition is steadily changing during the reaction and therefore

also the reaction rates^[32]. A direct measurement of reaction rates is not possible but can be interfered by the calculation of the initial slope, when measuring the concentration of educts and products as a function of the time.

1.5 The relationship between the electronic structure of a transition metal surface and the strength of surface-adsorbate interactions

Following the Langmuir-Hinshelwood mechanism^[33] for a heterogeneously catalyzed reaction the alkyne and H₂ must adsorb on the surface of an active catalyst prior to reaction. Subsequently, the products must desorb from the surface. Nørskov^[34,35] revealed a nearly linear relationship between the d-band center of the valence band of a transition metal surface and the strength of surface-adsorbate interactions: The valence band of a transition metal consists in general on a broad s-p band, whose electrons behave in first approximation as free electrons, and a more narrow and localized d-band. Firstly, adsorbate orbitals become broadened and downshifted by the metals s-p band. This contribution is roughly the same for every transition metal. These states become further hybridized by the presence of the d-orbitals of the metal. The interaction with the adsorbate involves the entire d-band and gets weaker the more the d-band is shifted away from the Fermi level, which occurs with increasing group number of the transition metal in the periodic table.

Molecular H₂ adsorbs on the surface very weakly (~3.5-15 kJ/mol)^[36] and needs to dissociate prior to stronger adsorption of atomic H. Its heat of adsorption is between 65 and 110 kJ/mol for different transition metal surfaces of group 8-10 Fe, Ru, Co, Rh, Ir, Ni, Pd and Pt. Metals of group 3-7 adsorb H₂ generally stronger with a maximum in group 5^[36]. The d-band of the coinage metals (group 11) is essentially filled and strongly shifted away from the Fermi level. The formation of the surface-adsorbate complex also causes repulsive interactions, due to occupation of antibonding states. Additionally a decrease in adsorption strength of adsorbates is observed when going from the 3d to the 5d metals. This is explained by the more extended 5d states compared to the 3d states, which demand higher orthogonalization energies as a consequence of Pauli repulsion that accompanies the formation of a chemical bond. This leads, in the case of Au, even to endothermic adsorption energies. In Figure 1-1 the change in the electronic structure of the surface during adsorption of hydrogen is compared for the

(111) surfaces of Ni, Cu, Pt and Au^[37]. Table 1-2 summarizes the corresponding calculated minimum chemisorption energies.

Table 1-2: Comparison of the minimum chemisorption energies of Ni(111), Cu(111), Pt(111) and Au(111) obtained from DFT calculations by Hammer et al.^[37]

Element surface	Ni(111)	Cu(111)	Pt(111)	Au(111)
$E_{\text{ads}} / \text{kJ}\cdot\text{mol}^{-1}$	-110	-14	-86	+45

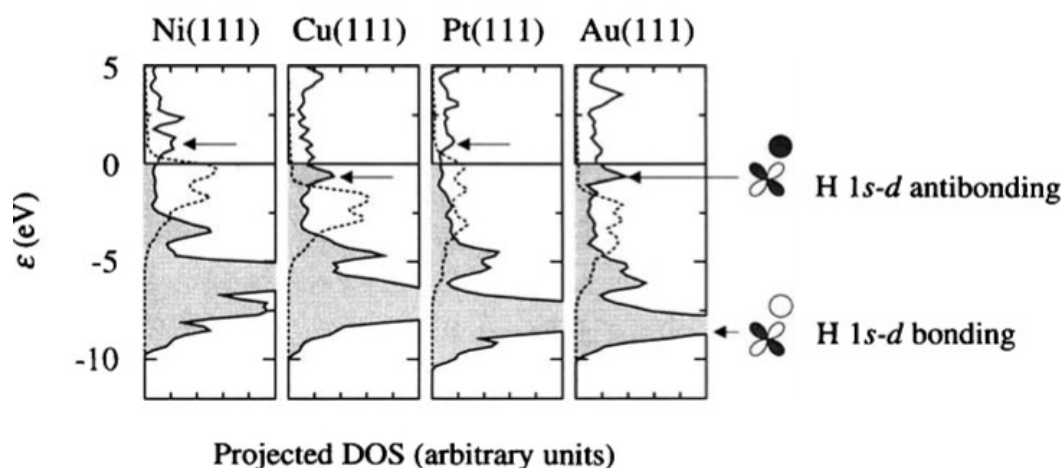


Figure 1-1: Density of states projected on H 1s state as presented in [37] for H atoms chemisorbed on (111) metal surfaces. The antibonding states of the complex get filled in the case of Cu and Au, where the d-band of the metal surface is shifted away from the Fermi level (dashed lines), resulting in repulsive interactions. The antibonding states are not filled in the case of Ni and Pt.

Apart from the nature of the transition metal, the d-band structure also depends on the local coordination of a surface atom. Atoms of different crystal facets, edges, defects or strained surfaces^[38,39] will have a modified d-band structure resulting in different adsorption strength. A modification can be achieved by alloying with a second metal^[40,41,42]. Furthermore with increasing coverage the adsorbate itself induce a shift of the d-band centre away from the Fermi level^[43].

The observed tendencies among the transition metals are in principle also valid for the adsorption of alkynes and alkenes^[42]. Alkynes adsorb considerably stronger than alkenes. According to Sabatier's^[44] principle for an efficient alkyne hydrogenation catalyst the alkyne adsorption must not neither be too weak nor be too strong. Transition metal surfaces of group 3 to 7 are highly reactive and are prone to irreversible dehydrogenation and C-C dissociation of hydrocarbons. This ultimately leads to strong deactivation of the surface and hence the pure transition metals are no effective hydrogenation catalysts. The elements of group 8, 9

and 10 are active hydrogenation catalysts even if the formation of carbonaceous deposits is often a reason for deactivation of the catalyst. The coinage metals, in turn, show no or only low activity, unless they are highly defective or present as very small particles. Such Cu^[45,46] or Au^[47,48,49] catalysts are active for alkyne hydrogenation.

1.6 Mechanism and selectivity control of alkyne hydrogenation over Pd

Among the transition metals Pd based catalysts provide an outstanding selectivity for the hydrogenation of alkynes^[50]. Bond and Wells^[51,52] found a selectivity decrease in the order Pd >> Rh \geq Pt > Ru >> Ir > Os in the gas phase hydrogenation of acetylene, propyne and 2-butyne. The fundamental mechanism of acetylene and ethylene hydrogenation was studied by DFT calculations on a clean Pd(111) surface^[53,54,55]: acetylene and ethylene are, following the Horiuti-Polanyi mechanism^[56], converted by subsequent half-hydrogenation with vinyl and ethyl, respectively, as intermediates on the surface, which requires an ensemble of Pd atoms, see Figure 1-2. H₂ generally prefers adsorption on the three-fold hollow sites. These sites are also preferred for acetylene, which competes with H₂. Ethylene adsorption is less exothermic and proceeds either by formation of a di- σ complex on two Pd atoms or a π complex on one Pd atom, which was calculated to be more stable at higher coverage.

Alkynes always adsorb stronger than the corresponding alkenes on Pd, which give rise to the early explanation that the selectivity of Pd towards the semi-hydrogenation of alkynes originates solely from a strong thermodynamic factor, meaning that as long as an alkyne is present the alkene is displaced from the surface. However, it is well-known that Pd-based catalyst can operate in a selective as well as in an unselective manner favoring formation of the alkene and alkane respectively.

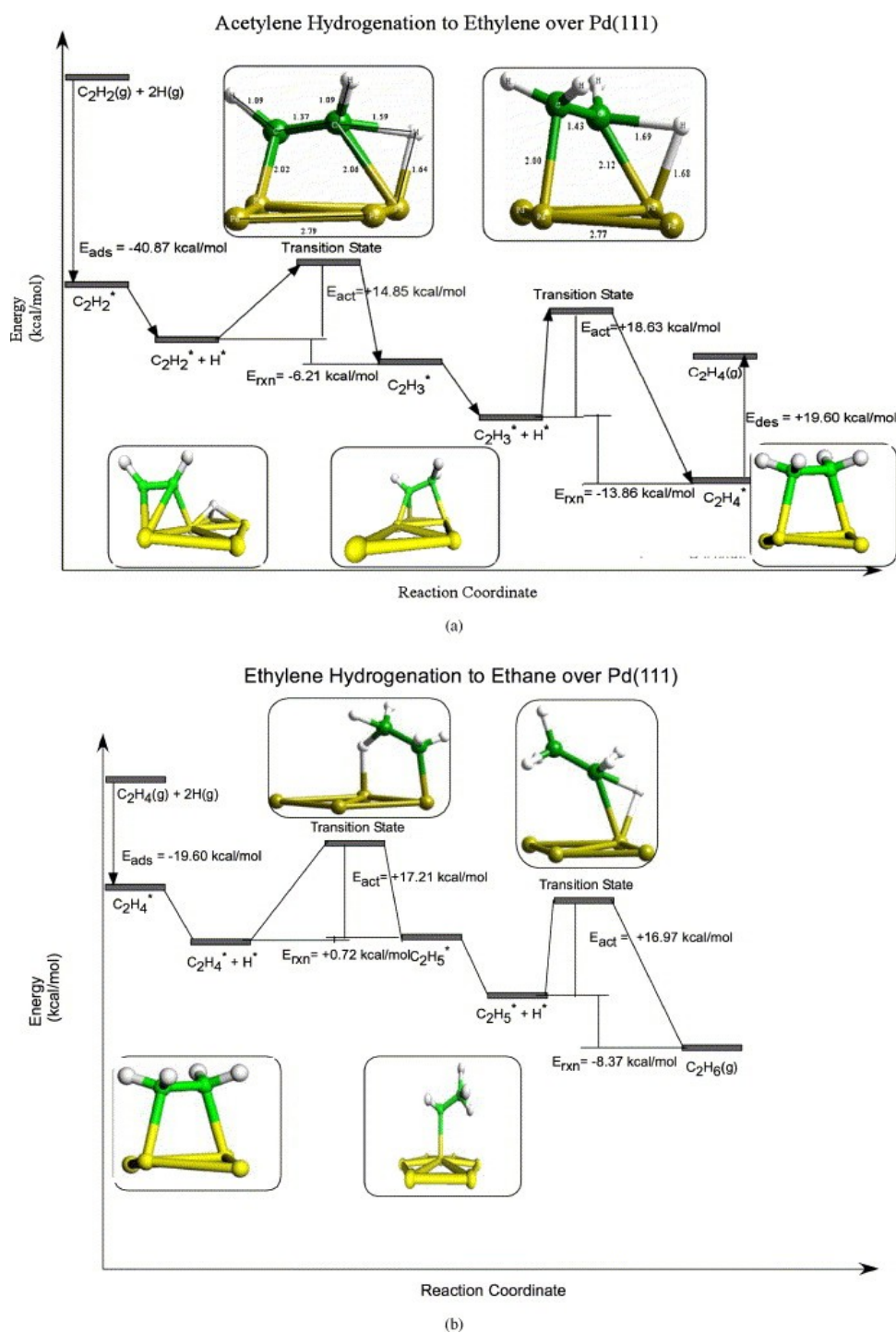


Figure 1-2: Potential energy diagram for acetylene hydrogenation (top) and ethylene hydrogenation on Pd(111) taken from [55].

Bond and Wells^[57] showed that the selectivity of Pd for acetylene hydrogenation decreases as the initial H_2 : acetylene ratio increases and at sufficiently high ratios the reaction becomes completely non-selective. Furthermore, it was shown that acetylene and ethylene can be indeed adsorbed and hydrogenated simultaneously and ethylene hydrogenation proceeds faster than the acetylene hydrogenation^[58]. The formation of oligomers and carbonaceous

deposits on the catalyst surface due to dissociative adsorption are additional observed side reactions. In particular ethylidyne but also other intermediates resulting from dissociative adsorption like vinylidene or acetylide are observed intermediates in various studies^[59,60] and could act as precursors for carbonaceous deposits and oligomers. The observed surface species could lead to active sites with varying activity towards acetylene and ethylene hydrogenation^[60]. Azad et al.^[61] determined the acetylene hydrogenation to vinyl as rate limiting step as detected by combine TPD and IR absorption measurements on Pd(111) under UHV conditions and ethylidyne was detected after heating the surface above 160 K. Comparable results were obtained on Pt(111). Cremer et al.^[62,63] investigated the hydrogenation of ethylene by optical sum frequency generation. Di- σ bonded ethylene is stable only until 240 K and dehydrogenates subsequently to ethylidyne with an ethylidene species as intermediate. Ethylidyne is thought to be only a spectator intermediate, competing with di- σ bonded ethylene for sites, while the rate of hydrogenation of π -bonded ethylene was not effected by the ethylidyne coverage^[64]. Coexistence of π -bonded and di- σ bonded ethylene was also observed for Pd(110) and Pd/SiO₂ at low temperatures^[65] but the di- σ bonded species decomposes to ethylidyne at even 195 K^[59]. Ethylidyne binds strongly to the surface with 636 kJ/mol^[54] on Pd(111). The situation become even more complex, because Pd is able to dissolve H^[66] as well as C^[67] forming subsurface and bulk species, whose formation depends strongly on the chemical potential. Doyle et al.^[68,69] showed, that the hydrogenation of ethylene over Pd under low pressure conditions requires in sharp contrast to acetylene hydrogenation not only adsorbed H at the surface but the presence of weaker bound subsurface H. The accessibility of these H atoms is higher for nanoparticles than for a Pd(111) surface, which lead to the fact, that under reduced pressure only the nanoparticles show a reasonable activity.

The catalytic hydrogenation of alkynes with supported Pd catalysts shows an antipathetic structure sensitivity^[70,71]. The activation energy given in the literature on different Pd catalysts for acetylene hydrogenation vary between 40 and 60 kJ/mol^[12,57,72]. For supported Pd catalysts the π bound intermediate is preferred for smaller particles^[73] and the hydrogenation of ethylene is found to be structure insensitive over a broad range of dispersions^[74]. The determined activation energies for ethylene hydrogenation for supported metal systems over various transition metals including Pd are typically between to 35-40 kJ/mol and thus generally equal or smaller than for acetylene hydrogenation.

In general, there are three main influences discussed, which determine the desired selectivity of Pd towards the alkene. Firstly, there is a geometric effect^[12]: The isolation of active sites and the presence of exclusively small ensembles of active atoms leads to the suppression of reaction requiring larger ensembles of atoms, in general known as ensemble effect^[75,76]. This leads to reduced oligomerization by C-C coupling a reaction that requires large ensembles and less strongly bound hydrogen deficient species^[77]. In particular the presence of only small ensembles also reduces the availability of hydrogen^[78] and hinders over-hydrogenation. Secondly, Pd easily forms Pd hydrides^[66]: Compared to dissociatively bonded H atoms on the surface, the hydrogen incorporated in the subsurface or in the bulk of Pd provides a higher reactivity and lowers the selectivity towards the alkene due to enhanced alkene hydrogenation^[68,69,79,80]. Thirdly, the selectivity could be enhanced if an electronic effect enhances the barrier for alkene hydrogenation and thus favoring alkene desorption^[42].

Recently, it has been shown that the selective phase in a Pd catalyst during hydrogenation of C-C triple-bonds is not the pure Pd itself but an *in situ* formed subsurface palladium-carbon phase formed by a rapid decomposition of the substrate as a first step of the reaction^[81,82]. The subsurface C modifies the electronic structure of Pd at the surface and slows down diffusion of H through the Pd-C surface phase into the Pd lattice. It weakens the adsorption strength of surface bonded H and thus further lowers the availability of H at the surface. As a result, over-hydrogenation and formation of the alkane is suppressed on this modified surface. Unfortunately, the existence of the Pd-C phase depends strongly on the chemical potential of C and H^[80]. High potentials of H or low potentials of the acetylene lead to hydrogenation of the subsurface C and, hence, Pd loses its selectivity. This dependence is crucial, because it can play a role in a large industrial ethylene purification reactor as well as in batch-wise operated reaction systems.

1.7 Modifiers

Modifiers and additives are frequently added to Pd to enhance the selectivity as already briefly stated in chapter 1. 4. Modifiers could be based on alkaline metals, e.g. K^[83], transition metals like Zn^[84], Cu^[85], Au^[47], Zr^[86], Nb^[87], Ti^[87,88] or main group metals for instance Pb^[29] or Bi^[89]. Organic bases containing N^[3], for example quinoline, and CO^[78] are

typically additives. Generally, their exact principle of operation varies and is still under debate. The state of the modifiers might change under reaction conditions, which further complicates their investigation^[90,91], as evidenced by the following discussion of two economically important catalysts.

1. 7. 1 Pd-Ag catalysts

Pd-Ag alloy catalysts are applied in industrial acetylene hydrogenation. It has been shown by DFT calculations^[42] and by X-ray absorption measurements^[92] that the electronic structure of Pd can be slightly changed by alloying with Ag resulting in a lowered heats of adsorption for acetylene and ethylene, which favors the desorption of ethylene and thus suppresses over-hydrogenation. Shet et al.^[93] found a decrease in exothermicity of the undesired dissociative adsorptions but an increase of the exothermicity in bond-forming reactions. They confirmed a slight shift of the d-band center from 2.35 eV (Pd) to 2.40 eV (Pd₅₀Ag₅₀), which weakens the adsorbate binding strength. However, the geometric effect was more influential because the reduction of the ensemble size lead to a change in the preferred adsorption site and disfavored the dissociative adsorption of H₂. In contrast to the well-ordered surface model of Shet et al.^[93] atoms in alloys are statistically ordered and ensembles of Pd might still be present. Generally, atoms in alloys tend to segregate under reactive atmosphere^[94]. Zea et al.^[95] found that an oxidative pre-treatment of Pd-Ag/SiO₂ lead to low selectivities for acetylene hydrogenation and explained this by an enhanced surface roughness and Pd segregation, while subsequent high-temperature reductive pre-treatments increase the ethylene selectivity significantly. CO-IR absorption measurements revealed a higher content of linear compared to bridged adsorbed CO for samples pre-treated in H₂ at high temperature, which suggests a decreased number of Pd ensembles due to Ag segregation and restructuring of the surface. On the other hand it was suggested for Pd-Ag alloys^[96], that H₂ treatment lead to segregation of Pd to the surface leaving behind an Ag enrichment in the subsurface, which prevents the formation of the undesired subsurface H species.

1. 7. 2 Lindlar's catalyst

Lindlar's catalyst^[29] consists of Pd supported on CaCO_3 and poisoned with $\text{Pb}(\text{OAc})_2$ showing in many cases very high (Z)-alkene yields and low isomerization rates. It is produced by impregnation of $\text{Pd}(\text{OH})_2$ on CaCO_3 followed by reduction in H_2 and subsequent wet-impregnation with $\text{Pb}(\text{OAc})_2$ ^[29]. The catalyst can be optionally further poisoned by a nitrogen base, e.g. quinoline, before reaction. The H_2 uptake normally significantly decreases or even stops after 1 equivalent H_2 is consumed in the case of internal alkynes. Although Lindlar's catalyst^[97] is one of the most common catalysts, it is not always sufficiently stable and selective^[98], in particular if H_2O was used as solvent. When phenylacetylene was hydrogenated, Lindlar^[99] and also Sobczak^[100] noticed a considerable excess H_2 uptake. Further poisoning by N-doped polymers, however, gave excellent yields (~98% selectivity at 100% phenylacetylene conversion)^[101]. The role of the support, the Pb additive and the base are still controversially discussed in literature. Lindlar's catalyst consists on at least seven different species and the selective sites of Lindlar's catalyst are formed *in situ*^[102]. It is likely that the function of Pb is not an electronic modification of Pd but rather to block sites for alkene adsorption^[103]. Palczewska et al.^[104] did not find evidence for significant diffusion of Pb in the Pd lattice as observed by means of H_2 chemisorption methods. However, the intermetallic compound Pd_3Pb was even more selective than Lindlar's catalyst for hydrogenation of acetylene, 2-butyne and phenylacetylene to the corresponding alkenes^[100]. The well-ordered structure of the intermetallic compound was claimed to be the reason for enhanced selectivity. García-Mota et al.^[105] used quantum chemical calculations and concluded that the role of quinoline is to reduce the ensemble size and hence to suppress C-C coupling reactions. The role of Pb was found to reduce the overall amount of H available at the surface and to induce a strong modification in the adsorption strength of the hydrocarbons. In other studies^[106,107] the role of the modifiers of Lindlar's catalyst was attributed to a change in polarization of the Pd-H bond, which leads to different reactivity of H.

1.8 Pd-Ga intermetallic compounds as catalysts for the semi-hydrogenation of acetylene

1.8.1 The phase diagram of the Pd-Ga system

The Pd-Ga phase diagram^[108] (Figure 1-3) was firstly established by studies of Schubert et al.^[109,110] and was extended by the work of Wannek et al.^[111,112] by the intermetallic compounds (IMCs) Pd_7Ga_3 and $\text{Pd}_{13}\text{Ga}_5$.

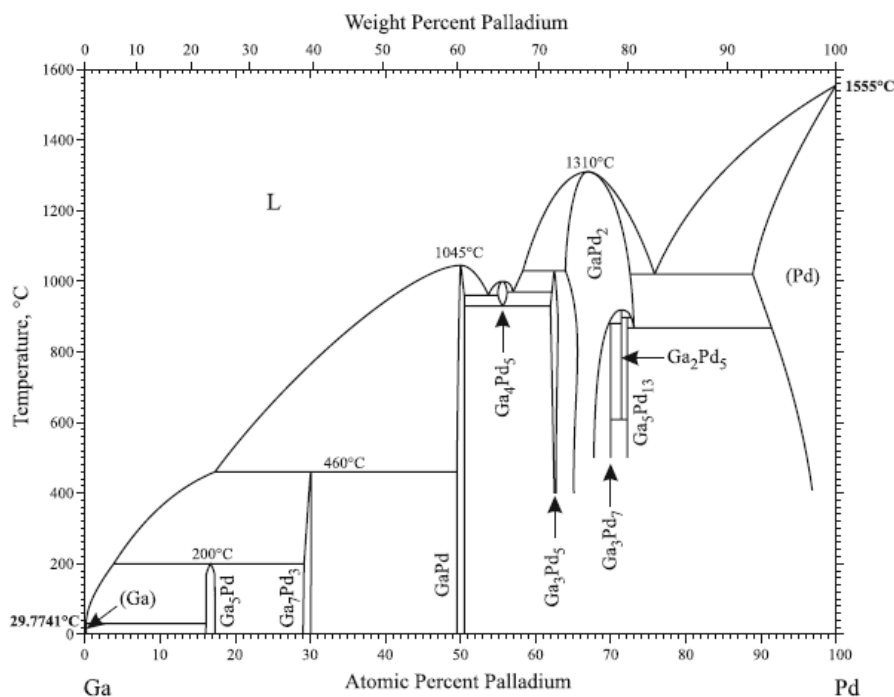


Figure 1-3: Phase diagram of the Pd-Ga system [108]

Ga displays a temperature dependent solubility in elemental Pd forming a solid solution. The highest solubility is reached at about 1283 K forming a solid solution $\text{Pd}_{90}\text{Ga}_{10}$, where the atoms are randomly distributed and the *fcc* crystal structure of elemental Pd is exhibited. In the regions richer in Ga several intermetallic compounds are formed. By definition, an intermetallic compound consists of two or more metals that form an at least partly ordered crystal structure which differs from the crystal structure of the pure elements and provide a stoichiometric or close to stoichiometric composition^[113]. The compounds Pd_2Ga , PdGa , Pd_3Ga_7 and PdGa_5 are accessible by melting the elements in stoichiometric ratio in an induction furnace with a subsequent thermal treatment. The compounds Pd_5Ga_2 , $\text{Pd}_{13}\text{Ga}_5$,

Pd_7Ga_3 , Pd_5Ga_3 and Pd_5Ga_4 are obtained only by chemical transport reactions. Selected crystallographic data of the compounds are summarized in Table 1-3. The nomenclature is not uniform in literature. According to the IUPAC recommendation 2005^[114] these compounds are named Pd_xGa_y in this work.

Table 1-3: Structure type, lattice parameters and corresponding references for the known Pd-Ga compounds

Compound	Structure type	Space group	Lattice parameters / Å			References
			<i>a</i>	<i>b</i>	<i>c</i>	
Pd_5Ga_2	Pd_5Ga_2	<i>Pnma</i>	5,48(5)	4,08(3)	18,39(6)	110
$\text{Pd}_{13}\text{Ga}_5$	$\text{Pd}_{13}\text{Ga}_5$	<i>C2/m</i>	24,2599(5)	4,05060(7) $\beta = 102,690(1)^\circ$	5,4437(1)	112
Pd_7Ga_3	Pd_7Ga_3	<i>C2/m</i>	13,5946(2)	4,05510(5) $\beta = 105,2219(7)^\circ$	5,44339(6)	111
$\text{Pd}_{2+x}\text{Ga}_{1-x}$	Co_2Si	<i>Pnma</i>	5,4762(1)	4,0570(1) für $x = 0$	7,7973(2)	111,115
Pd_5Ga_3	Rh_5Ge_3	<i>Pbam</i>	5,42	10,51	4,03	110
Pd_5Ga_4	CsCl	<i>Pm\bar{3}m</i>	3,040	3,040	3,040	110
PdGa	FeSi	<i>P2_13</i>	4,8959(1)	4,8959(1)	4,8959(1)	116
Pd_3Ga_7	Ir_3Ge_7	<i>Im\bar{3}m</i>	8,7716(1)	8,7716(1)	8,7716(1)	110
PdGa_5	PdGa_5	<i>I4/mcm</i>	6,436(6)	6,436(6)	9,990(8)	117

1. 8. 2 Crystal structure of PdGa

PdGa crystallizes in the cubic space group $P2_13$ (No. 198, FeSi structure type) with $a = 4.8959 \text{ Å}$ ^[116]. Pd is coordinated by four Ga atoms with distances between 2.54 and 2.56 Å and furthermore by three Ga atoms with a distance of 2.71 Å resulting in the coordination number seven. The shortest Pd-Pd distance is 3.01 Å. The structure can be seen as a distorted modification of the NaCl structure type. The space group $P2_13$ is chiral and two enantiomers exists along (111)^[118].

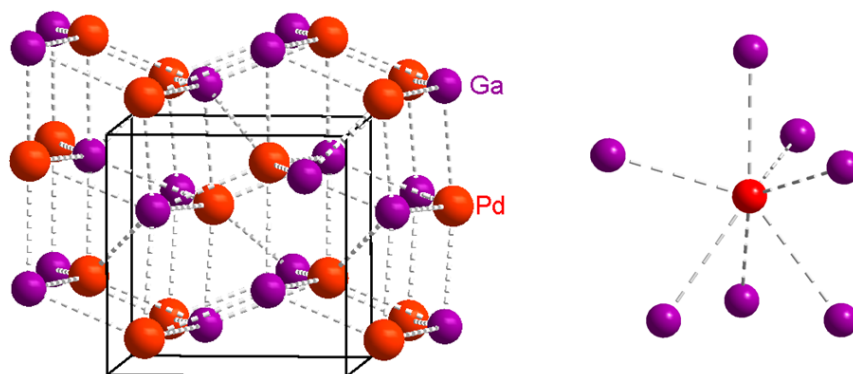


Figure 1-4: Unit cell (left) and coordination of Pd (right) in the intermetallic compound PdGa crystallizing in space group $P2_13$ (FeSi -type). The Pd atoms are isolated from each other and are surrounded exclusively from seven Ga atoms in the first coordination sphere (right).

1. 8. 3 Crystal structure of Pd₂Ga

Pd₂Ga crystallizes in the orthorhombic space group *Pnma* in the Co₂Si structure type^[115]. Pd occupies two symmetrically nonequivalent positions, Pd1 and Pd2. Pd1 is coordinated by four Ga atoms with short distances between 2.54 and 2.56 Å and one Ga atom with a significant longer distance of 2.96 Å. Pd2 is coordinated by three Ga atoms with distances between 2.56 and 2.62 Å and two Ga atoms with a distance of 2.84 Å. In contrast to PdGa there is no full isolation of the Pd atoms. Pd1 and Pd2 in Pd₂Ga are furthermore coordinated by eight Pd atoms with distances between 2.81 - 2.99 Å. Thus all distances are extended compared to elemental Pd (2.75 Å) and the coordination by neighboring Pd atoms is lowered from twelve to eight. However, ensembles of Pd atoms - forming triangles with side length smaller than 3 Å - are present.

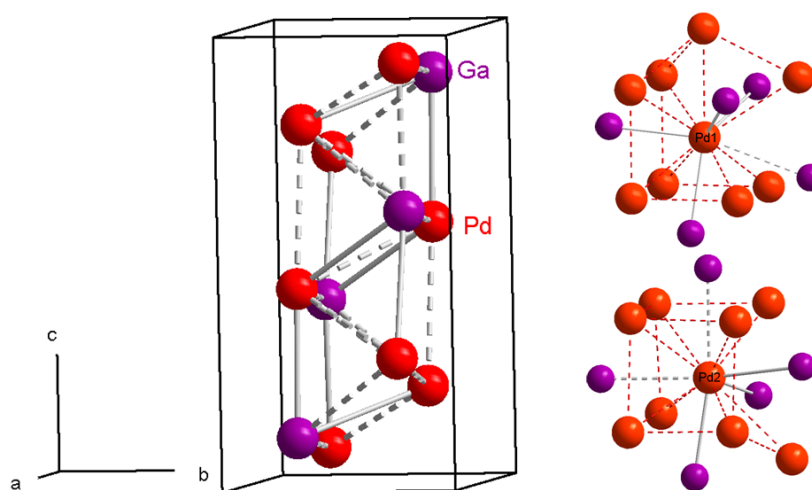


Figure 1-5 Left: Unit cell of Pd₂Ga. Top right: Coordination of Pd1. Down right: Coordination of Pd2. The compound crystallizes in the Co₂Si-type. The short Pd-Ga distances (2.54-2.56 Å) are shown as straight line, dashes lines represent atomic distances between 2.81-2.99 Å.

In contrast to the other intermetallic compounds of the Pd-Ga system Pd₂Ga shows a significant homogeneity range in particular at high temperatures. At 673 K the composition of Pd_{2+x}Ga_{1-x} is in the range of $-0.04 < x < 0.02$. At higher temperatures the slightly Pd richer intermetallic compounds decompose peritectoid (Pd₁₃Ga₅ and Pd₇Ga₃) and congruently (Pd₅Ga₂) to Pd_{2+x}Ga_{1-x} offering a broad homogeneity range with $-0.05 < x < 0.18$ at 1253 K^[111]. Pd partially substitutes Ga positions in the Pd rich regime of Pd, leading to

decreased Pd-Pd distances. There is a close structural relationship between the Co₂Si-type like Pd_{2+x}Ga_{1-x} and a fcc solid solution Pd_xGa_{1-x}.

1. 8. 4 Previous studies of Pd-Ga intermetallic compounds as hydrogenation catalysts

Intermetallic compounds (IMCs) like Pd₃Pb^[23], PdGa or NiZn^[42] were discussed as alternative catalyst for the acetylene hydrogenation, owing to their well-ordered crystal structure and their modified electronic structure. The modification of the electronic structure of Pd and Ni IMCs is generally stronger compared to substitutional alloys^[75,119] or for non-stoichiometric surface phases. This effect becomes more pronounced with decreasing electronegativity of the second metal^[40,41]. Recently, the intermetallic compounds Pd₂Ga, PdGa and Pd₃Ga₇ were extensively studied and characterized as catalysts for the semi-hydrogenation of acetylene^[120,121,122,123].

In contrast to traditional transition metal hydrogenation catalysts, these materials were primarily prepared by metallurgical syntheses and subsequently ground or milled to obtain a microcrystalline powder. The use of such unsupported single-phase powders allows a very reliable characterization, e.g. by XRD or XPS, and allows simultaneously to study the intrinsic catalytic properties because additional influences, for instance by the support, can be avoided. However, the major disadvantage is a considerably low surface area, which necessitates a high amount of catalyst to achieve reasonable conversions. The dispersion is below the detection limit of CO or H₂ chemisorption, typically used for the determination of the active surface area, and due to a low abundance of surface sites CO-IR adsorption methods fail^[124].

In Pd-Ga intermetallic compounds covalent bonds are present, which distinguish these compounds sharply from pure Pd or disordered alloys. For PdGa the presence of covalent interactions was proven by means of the calculation of the electron localizability indicator (ELI)^[121]. This characteristic suggests PdGa as promising catalyst for alkyne hydrogenation, superior to elemental Pd. PdGa satisfies the three main criteria for selectivity: Firstly, the expanded Pd-Pd distances due to complete surrounding by Ga atoms induces a geometric effect. Secondly, the presence of Ga provides a strong electronic modification. DFT

calculations confirmed a significant shift of the d-band center away from the Fermi level, comparable to the coinage metals. XPS indicated a symmetric Pd 3d_{5/2} core-level signal for ground PdGa with a shift to 336.0 eV. The presence of Ga oxide was recognized, which was explained by Ga segregation from the bulk and subsequent oxidation during preparation. Thirdly, PdGa is stable under *in situ* conditions and does not form hydrides or decompose, as evidenced by *in situ* DTA/TG, *in situ* XRD, *in situ* EXAFS, PGAA and *in situ* XPS. Indeed, under the applied reaction conditions of acetylene hydrogenation (plug-flow reactor, feed-gas: 0.5% C₂H₂, 5% H₂, 50% C₂H₄ in He, T = 200 °C) without a pre-treatment of the catalysts the IMCs show no or only slight deactivation within 20 h in contrast to a commercial Pd/Al₂O₃ catalyst. Ethane and oligomers are produced only as a minor product even in a large excess of ethylene.

Studies on a PdGa($\bar{1}\bar{1}\bar{1}$) single crystal surface under UHV conditions clearly demonstrated the intermetallic character of PdGa at the surface^[125]. Low energy electron diffraction as well as X-ray photoelectron diffraction pattern confirmed an unreconstructed bulk terminated surface of PdGa after several sputtering and annealing cycles, whereupon four different surface terminations can occur, dependent on the annealing temperature. In contrast to disordered substitutional alloys segregation of Pd or Ga in the intermetallic compound was not observed. XPS results indicated a binding energy of 336.3 eV, thus slightly higher as observed for the powdered samples.

In contrast to the aforementioned observation, Osswald et al.^[123] applied ball-milling to increase the surface area and noticed a Pd 3d_{5/2} peak of only 335.7 eV and only a partial reduction of Ga oxide even after pre-reduction at 400 °C in 200 mbar H₂. Furthermore, an unusual temperature dependence of hydrogenation activity was observed with a volcano shape providing a maximum in activity at 200 °C. Interestingly, the activity decreases continuously to almost zero when going to 600 °C.

Pd₂Ga turned out to be more appropriate than PdGa towards catalytic application. The powdered bulk material exhibits a similar high selectivity and long-term stability^[120] in the acetylene hydrogenation and is relatively easy to obtain as supported high-performance catalyst by bottom-up approaches^[126,127]. Although Pd₂Ga provides only a partial isolation of

Pd by Ga atoms, it still exhibits a strong electronic modification as evidenced by its Pd 3d_{5/2} peak observed at 335.7 eV.

Experiments have led to the conclusion, that besides the Ga oxide the “metallic part” of the surfaces of Pd-Ga compounds are terminations of the bulk. The degree of electronic modification of Pd is tunable by the Ga content as shown by the increasing Pd 3d_{5/2} core-level shift in Figure 1-6^[128]. The developed concept provides, thus, the possibility to design an intrinsically stable catalyst, which can emulate the Pd-C phase without being subjected to a dynamic subsurface chemistry.

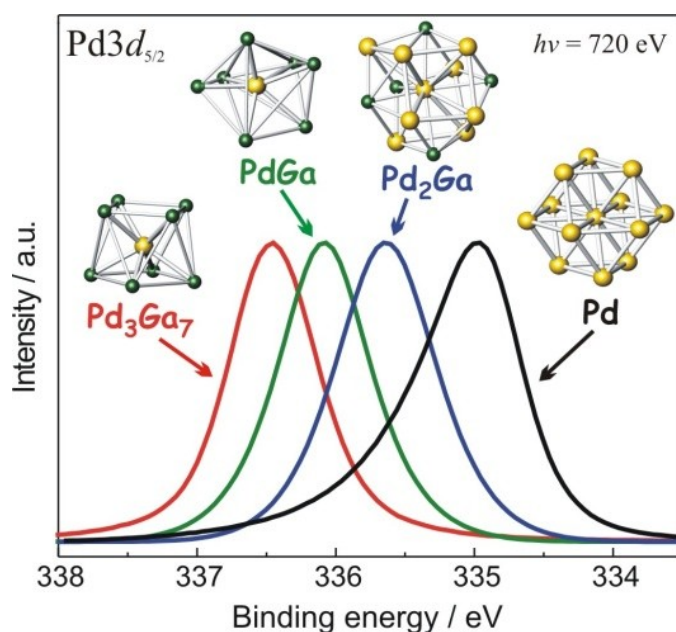


Figure 1-6: Pd 3d_{5/2} core-level spectra of Pd, Pd₂Ga, PdGa and Pd₃Ga₇^[128] recorded in UHV at ambient temperature.

However, several very recent investigations reveal doubts about the stability of supported Pd₂Ga nanoparticles. Recently, Haghofer et al.^[129] studied the *in situ* stability of Pd₂Ga nanoparticles under H₂ and O₂ atmosphere by means of *in situ* XRD, *in situ* EXAFS and CO-FTIR. While the formation of hydrides could be excluded, decomposition was detected at the surface already at room temperature in O₂ atmosphere as indicated by EXAFS and CO adsorption. They also investigated the *in situ* stability of Pd₂Ga during methanol steam reforming and found that CO promotes the at least partially decomposition of Pd₂Ga leading to catalytic properties comparable to elemental Pd^[130]. In a very recent publication^[131] it was pointed out, that the role of Pd₂Ga in methanol steam reforming is to produce a highly active Ga oxide while remaining Ga depleted Pd₂Ga particles might act as a sink for atomic H. Ota

et al.^[132] studied the catalytic performance of Pd₂Ga supported on MgGa₂O₄/MgO for the semi-hydrogenation of acetylene. The selectivity of this catalyst was only slightly decreasing with time and comparable high as in the case of the metallurgical prepared powder. The major difference is, that this catalyst shows a long activation period until a stable conversion is achieved, after a high temperature reductive pre-treatment. Microscopic analyses of a spent sample suggest segregation of small Pd particles. The activation period could be significantly shortened by an O₂ treatment after reduction - surprisingly without loss of the high selectivity.

1.9 References

- [1] P. Sabatier, J. B. Senderens, *Compt. Rend.* 124 (1897) 1358.
- [2] A. F. Hollemann, N. Wiberg, *Lehrbuch der Anorganischen Chemie*, 101st edition, Berlin, de Gruyter, 1995, 1847.
- [3] S. Nishimura, *Handbook of Heterogeneous Catalytic Hydrogenation for Organic Synthesis*, New York, Wiley-Interscience, 2001, 148.
- [4] M. W. van Laren, C. J. Elsevier, *Angew. Chem. Int. Ed.* 38 (1999) 3715.
- [5] E. W. Stern, P. K. Maples, *J. Catal.* 27 (1972) 120.
- [6] R. Brückner, *Reaktionsmechanismen*, 3rd Edition, Munich, Spektrum Akademischer Verlag, 2004, 810.
- [7] L. Luan, J-S. Song, R. M. Bullock, *J. Org. Chem.* 60 (1995) 7170.
- [8] R. C. Weast, M. J. Astle, *Handbook of Chemistry and Physics*, 60th edition, Boca Raton, CRC Press, 1979
- [9] H. E. Davis, N. L. Allinger, *J. Org. Chem.* 50 (1985) 3601.
- [10] B. V. Lebedev, T. A. Bykova, N. N. Smirnova, T. G. Kulagina, *Zhur. Obshch. Khim.* 52 (1982) 2630.
- [11] A. F. Hollemann, N. Wiberg, *Lehrbuch der Anorganischen Chemie*, 101st edition, Berlin, de Gruyter, 1995, 258.
- [12] A. Borodzinski, G. C. Bond, *Catal. Rev.* 48 (2006) 91.
- [13] H. Arnold, F. Döbert, J. Gaube, in: G. Ertl, H. Knözinger, F. Schüth, J. Weitkamp (Eds.), *Handbook of Heterogeneous Catalysis*, Weinheim, Wiley-VCH, 2008, 3271.
- [14] C. N. Thanh, B. Didillon, P. Sarrazin, C. Cameron, US patent 6054409 (2000).
- [15] A. Pachulski, R. Schödel, P. Claus, *Appl. Catal. A* 445-446 (2012) 107.
- [16] C. Godinez, A. L. Cabanes, G. Villora, *Chem. Eng. Proc.* 34 (1995) 459.
- [17] C. Godinez, A. L. Cabanes, G. Villora, *Chem. Eng. Comm.* 164 (1998) 225.
- [18] D. R. Kennedy, G. Webb, S. D. Jackson, D. Lennon, *Appl. Catal. A* 259 (2004) 109.
- [19] M. Galobardes, B. R. Maurer, US patent 4822936 A (1989).
- [20] R. A. Basimova, M. L. Pavlov, S. I. Myachin, A. V. Prokopenko, A. V. Askarova, B. I. Kutepov, S. A. Sychkova, *Petrol. Chem.* 49 (2009) 360.
- [21] V. V. Rusak, M. I. Zaretskii, A. S. Mozzhukhin, I. V. Usyshkina, L. A. Pushkina, *Russ. J. Appl. Chem.* 67 (1995) 1066.

- [22] P. Mercier, P. Chabardes, *Pure & Appl. Chem.* 66 (1994) 1509.
- [23] J. Sobczak, T. Bolesławska, M. Pawłowska, W. Palczewska, *Stud. Surf. Sci. Catal.* 41 (1988) 197.
- [24] N. A. Dobson, G. Eglinton, M. Krishnamurti, R. A. Raphael, R. G. Willis, *Tetrahedron* 16 (1961) 16.
- [25] H. U. Blaser, H. Steiner, M. Studer, *ChemCatChem* 1 (2009) 210.
- [26] K. N. Campbell, B. K. Campbell, *Chem. Rev.* 31 (1942) 145.
- [27] C. A. Brown, V. K. Ahuja, *J. Org. Chem.* 38 (1973) 2226.
- [28] A. F. Thompson, S. B. Wyatt, *J. Am. Chem. Soc.* 62 (1940) 2555.
- [29] H. Lindlar, *Helv. Chim. Acta* 35 (1952) 446.
- [30] E. Ignatowicz, *Chemietechnik*, Haan-Gruiten, Verlag Europa Lehrmittel, 2003, 409.
- [31] V. Vajt, L. Kurc, L. Cervený, *Int. J. Chem. Kinet.* 40 (2008) 240.
- [32] M. E. Davis, R. J. Davis, *Fundamentals of Chemical Reaction Engineering*, New York, McGraw-Hill, 2003, 64.
- [33] A. D. McNaught, A. Wilkinson, *IUPAC Compendium of Chemical Terminology*, 2nd edition, Oxford, Blackwell Scientific Publications, 1997.
- [34] B. Hammer, J. K. Nørskov, *Surf. Sci.* 343 (1995) 211.
- [35] J. K. Nørskov, T. Bligaard, A. Logadottir, S. Bahn, L. B. Hansen, M. Bollinger, C. J. H. Jacobsen, *J. Catal.* 209 (2002) 275.
- [36] K. Christmann, *Surf. Sci. Rep.* 9 (1988) 1.
- [37] B. Hammer, J. K. Nørskov, *Nature* 376 (1995) 238.
- [38] M. Mavrikakis, B. Hammer, J. K. Nørskov, *Phys. Rev. Lett.* 81 (1998) 2819.
- [39] B. Hammer, *Top Catal.* 37 (2006) 3.
- [40] J. C. Fuggle, F. U. Hillebrecht, R. Zeller, Z. Zolnierrek, P. A. Bennett, *Phys. Rev. B* 27 (1983) 2145.
- [41] F. U. Hillebrecht, J. C. Fuggle, P. A. Bennett, Z. Zolnierrek, *Phys. Rev. B* 27 (1983) 2179.
- [42] F. Studt, F. Abild-Pedersen, T. Bligaard, R. Z. Sørensen, C. H. Christensen, J. K. Nørskov, *Science* 320 (2008) 1320.
- [43] N. İnoğlu, J. R. Kitchin, *Phys. Rev. B* 82 (2010) 045414.
- [44] A. A. Balandin, *Adv. Catal.* 19 (1969) 1.
- [45] B. Bridier, N. López, J. Pérez-Ramírez, *DaltonTrans* 39 (2010) 8412.

- [46] B. Bridier, N. López, J. Pérez-Ramírez, *J. Catal.* 269 (2010) 80.
- [47] T. V. Choudhary, C. Sivadinarayana, A. K. Datye, D. Kumar, D. W. Goodman, *Catal. Lett.* 86 (2003) 1.
- [48] Y. Segura, N. López, J. Pérez-Ramírez, *J. Catal.* 247 (2007) 383.
- [49] S. A. Nikolaev, V. V. Smirnov, *Gold Bull.* 42 (2009) 182.
- [50] G. C. Bond, D. A. Dowden, N. Mackenzie, *Trans. Faraday Soc.* 54 (1958) 1537.
- [51] G. C. Bond, P. B. Wells, *Adv. Catal.* 15 (1964), 205.
- [52] P. B. Wells, *Chem. Ind. (Lond.)* 1964, 1742.
- [53] P. A. Shet, M. Neurock, C. M. Smith, *J. Phys. Chem. B* 107 (2003) 2009.
- [54] M. Neurock, R. A. van Santen, *J. Phys. Chem. B* 104 (2000) 11127.
- [55] D. Mei, D. A. Shet, M. Neurock, C. M. Smith, *J. Catal.* 224 (2006) 1.
- [56] J. Horiuti, M. Polanyi, *Trans. Faraday Soc.* 30 (1934) 1164.
- [57] G. C. Bond, P. B. Wells, *J. Catal.* 5 (1965) 65.
- [58] A. S. Al-Ammar, G. Webb, *J. Chem. Soc. Faraday Trans. 74* (1978) 195.
- [59] N. Sheppard, C. de la Cruz, *Adv. Catal.* 42 (1998) 181.
- [60] A. N. R. Bos, K. R. Westerterp, *Chem. Eng. Proc.* 32 (1993) 1.
- [61] S. Azad, M. Kaltchev, D. Stacciola, G. Wu, W. T. Tysoe, *J. Phys. Chem. B* 104 (2000) 3107.
- [62] P. S. Cremer, G. A. Somorjai, *J. Chem. Soc. Faraday Trans.* 91 (1995) 3671.
- [63] P. Cremer, C. Stanners, J. W. Niemantsverdriet, Y. R. Shen, G. Somorjai, *Surf. Sci.* 328 (1995) 111.
- [64] P. S. Cremer, X. Su, Y. R. Shen, G. A. Somorjai, *J. Am. Chem. Soc.* 118 (1996) 2942.
- [65] M. A. Chesters, G. S. McDougall, M. E. Pemble, N. Sheppard, *Appl. Surf. Sci.* 22/23 (1985) 369.
- [66] F. D. Manchester, A. San-Martin, J. M. Pitre, *J. Phase Equilib.* 15 (1994) 62.
- [67] S. B. Ziemecki, G. A. Jones, D. G. Swartzfager, R. L. Harlow, J. Faber, *J. Am. Chem. Soc.* (1985) 4547.
- [68] A. M. Doyle, S. K. Shaikhutdinov, H.-J. Freund, *J. Catal.* 223 (2004) 444.
- [69] A. M. Doyle, S. K. Shaikhutdinov, S. D. Jackson, H.-J. Freund, *Angew. Chem. Int. Ed.* 42 (2003) 5240.
- [70] M. Che, C. O. Bennett, *Adv. Catal.* 36 (1989) 55.
- [71] A. Sárkány, A. H. Weiss, L. Guczi, *J. Catal.* 98 (1986) 550.

- [72] H. Molero, B. F. Bartlett, W. T. Tysoe, *J. Catal.* 181 (1999) 49.
- [73] M. Frank, M. Bäumer, *Phys. Chem. Chem. Phys.* 2 (2000) 3723.
- [74] G. Rupprechter, *Annu. Rep. Prog. Chem. Sect. C* 100 (2004) 237.
- [75] W. M. H. Sachtler, in: G. Ertl, H. Knözinger, F. Schüth, J. Weitkamp (Eds.), *Handbook of Heterogeneous Catalysis*, Weinheim, Wiley-VCH, 2008, 1585.
- [76] V. Ponec, W. M. H. Sachtler in: J. W. Hightower (Ed.), *Proceedings of 5th International Congress on Catalysis*, Amsterdam, (1972), 6541.
- [77] Á. Molnár, A. Sárkány, M. Varga, *J. Mol. Catal. A* 173 (2001) 185.
- [78] M. García-Mota, B. Bridier, J. Pérez-Ramírez, N. López, *J. Catal.* 273 (2010), 92.
- [79] N. A. Khan, S. Shaikhutdinov, H.-J. Freund, *Catal. Lett.* 108 (2006) 159.
- [80] D. Teschner, Z. Révay, János Borsodi, M. Hävecker, A. Knop-Gericke, R. Schlögl, D. Milroy, S. D. Jackson, D. Torres, P. Sautet, *Angew. Chem. Int. Ed.* 47 (2008) 9274.
- [81] D. Teschner, E. M. Vass, M. Hävecker, S. Zafeiratos, P. Schnörch, H. Sauer, A. Knop-Gericke, R. Schlögl, M. Chamam, A. Wootsch, A. S. Canning, J. J. Gamman, S. D. Jackson, J. McGregor, L. F. Gladden, *J. Catal.* 242 (2006) 26.
- [82] D. Teschner, J. Borsodi, A. Wootsch, Zs. Révay, M. Hävecker, A. Knop-Gericke, S. D. Jackson, R. Schlögl, *Science* 320 (2008) 86.
- [83] Y. H. Park, G. L. Price, *Ind. Eng. Chem. Res.* 31 (1992) 469.
- [84] V. Engels, A. E. H. Wheatley, A. Berenguer-Murcia, D. A. Jefferson, B. F. G. Johnson, *Mater. Sci. Forum* 604-605 (2009) 13.
- [85] L. Guczi, Z. Schay, Gy. Stefler, L. F. Liotta, G. Deganello, A. M. Venezia, *J. Catal.* 182 (1999) 456.
- [86] P. N. Rylander, *Catalytic Hydrogenation over Platinum Metals*, New York, Academic press, 1967, 62.
- [87] J.H. Kang, E. W. Shin, W. J. Kim, J. D. Park, S. H. Moon, *Catal. Today* 63 (2000) 183.
- [88] J. H. Kang, E. W. Shin, W. J. Kim, J. D. Park, S. H. Moon, *J. Catal.* 208 (2002) 310.
- [89] J. A. Anderson, J. Mellor, R. P. K. Wells, *J. Catal.* 261 (2009) 208.
- [90] T. Mallat, A. Baiker, *Appl. Catal. A* 200 (2000) 3.
- [91] A. Borodzinski, G. C. Bond, *Catal. Rev.* 50 (2008) 379.
- [92] D. C. Huang, K. H. Chang, W. F. Pong, P. K. Tseng, K. J. Hung, W. F. Huang, *Catal. Lett.* 53 (1998) 155.
- [93] P. A. Shet, M. Neurock, C. M. Smith, *J. Phys. Chem. B* 109 (2005) 12449.

- [94] S. Zafeiratos, S. Piccinin, D. Teschner, *Catal. Sci. Technol.* 2 (2012) 1787.
- [95] Y. Jin, A. K. Datye, E. Rightor, R. Gulotty, W. Waterman, M. Smith, M. Holbrook, J. Maj, J. Blackson, *J. Catal.* 203 (2001) 292.
- [96] S. González, K. M. Neyman, S. Shaikhutdinov, H.-J. Freund, F. Illas, *J. Phys. Chem. C* 111 (2007) 6852.
- [97] H. Lindlar, *Helv. Chim. Acta* 35 (1952) 446.
- [98] N. Semagina, M. Grasemann, N. Xanthopoulos, A. Renken, L. Kiwi-Minsker, *J. Catal.* 251 (2007) 213.
- [99] H. Lindlar, R. Dubius, *Org. Synth, Coll. Vol.* 5 (1973) 880.
- [100] J. Sobczak, W. Palczewska, T. Boleslawska, M. Pawlowska, *Stud. Surf. Sci. Catal.* 41 (1988) 197.
- [101] D. Dhamodharan, *Chem. Lett.* 235 (1996) 235.
- [102] R. Schlögl, K. Noack, H. Zbinden, *Helv. Chim. Acta* 70 (1987) 627.
- [103] J. Rajaram, A. P. S. Narula, H. P. S. Chawla, S. Dev, *Tetrahedron* 39 (1983) 2315.
- [104] W. Palczewska, A. Jablonski, Kaszkur, *J. Mol. Catal.* 25 (1984) 307.
- [105] M. García-Mota, J. Gómez-Díaz, G. Novell-Leruth, C. Vargas-Fuentes, L. Bellarosa, B. Bridier, J. Pérez-Ramírez, N. López, *Theor. Chem. Acc.* 128 (2011) 663.
- [106] J. Yu, J. B. Spencer, *Chem. Commun* (1998) 1103.
- [107] J. Yu, J. B. Spencer, *J. Org. Chem.* 62 (1997) 8618.
- [108] H. Okamoto, *J. Phase Equil.* 29 (2008) 466.
- [109] K. Schubert, H. L. Lukas, H.-G. Meissner, S. Bhan, *Z. Metallkunde* 50 (1959) 534.
- [110] K. Khalaff, K. Schubert, *J. Less-Comm. Met.* 37 (1974) 129.
- [111] C. Wannek, B. Harbrecht, *J. Alloys Comp.* 316 (2001) 99.
- [112] C. Wannek, B. Harbrecht, *Z. Anorg. Allg. Chem.* 626 (2000) 1540.
- [113] H. Kohlmann, in: R. A. Meyers (Ed.), *Encyclopedia of Physical Science and Technology*, San Diego, Academic Press, 2002, 441.
- [114] N. G. Connelly, T. Damhus, R. M. Hartshorn, A. T. Hutton, *Nomenclature of Inorganic Chemistry - IUPAC Recommendations 2005*, Cambridge, The Royal Society of Chemistry, 2005.
- [115] K. Kovnir, M. Schmidt, C. Waurisch, M. Armbrüster, Y. Prots, Y. Grin, *Z. Kristallogr. New Cryst. Struct.* 223 (2008) 7.

- [116] M. Armbrüster, H. Borrmann, M. Wedel, Yu. Prots, R. Giedigkeit, P. Gille, Z. Kristallogr. New Cryst. Struct. 225 (2010) 617.
- [117] Yu. Grin, K. Peters, H.-G. van Schnering, Z. Kristallogr. New Cryst. Struct. 212 (1997) 6.
- [118] D. Rosenthal, R. Widmer, R. Wagner, P. Gille, M. Armbrüster, Yu. Grin, R. Schlögl, O. Gröning, Langmuir 28 (2012) 6848.
- [119] H. C. de Jongste, V. Poncet, Bull. Soc. Chim. Belg. 88 (1979) 453.
- [120] M. Armbrüster, K. Kovnir, M. Behrens, D. Teschner, Yu. Grin, R. Schlögl, J. Am. Chem. Soc. 132 (2010) 14745.
- [121] K. Kovnir, M. Armbrüster, D. Teschner, T. V. Venkov, F. C. Jentoft, A. Knop-Gericke, Yu. Grin, R. Schlögl, Sci. Technol. Adv. Mater. 8 (2007) 420.
- [122] J. Osswald, R. Giedigkeit, R. E. Jentoft, M. Armbrüster, F. Girgsdies, K. Kovnir, T. Ressler, Yu. Grin, R. Schlögl, J. Catal. 258 (2008) 210.
- [123] J. Osswald, R. Giedigkeit, R. E. Jentoft, M. Armbrüster, F. Girgsdies, K. Kovnir, T. Ressler, Yu. Grin, R. Schlögl, J. Catal. 258 (2008) 219.
- [124] Private communication with Günther Rupprechter, Technical University of Vienna
- [125] D. Rosenthal, R. Widmer, R. Wagner, P. Gille, M. Armbrüster, Yu. Grin, R. Schlögl, O. Gröning, Langmuir 28 (2012), 6848.
- [126] A. Ota, M. Armbrüster, M. Behrens, D. Rosenthal, M. Friedrich, I. Kasatkin, F. Girgsdies, W. Zhang, R. Wagner, R. Schlögl, J. Phys. Chem. C 115 (2011) 1368.
- [127] L. Li, B. Zhang, E. Kunkes, K. Föttinger, M. Armbrüster, D. S. Su, W. Wei, R. Schlögl, M. Behrens, ChemCatChem 4 (2012) 1764.
- [128] K. Kovnir, D. Teschner, M. Armbrüster, P. Schnörch, M. Hävecker, A. Knop-Gericke, Yu. Grin, R. Schlögl, BESSY Highlights 2007 (2008) 22.
- [129] A. Haghofer, K. Föttinger, M. Nachtegaalm, M. Armbrüster, G. Rupprechter, J. Phys. Chem. C 116 (2012) 21816.
- [130] A. Haghofer, K. Föttinger, F. Girgsdies, D. Teschner, A. Knop-Gericke, R. Schlögl, G. Rupprechter, J. Catal. 286 (2012) 31.
- [131] A. Haghofer, D. Ferri, K. Föttinger, G. Rupprechter, ACS Catal. 2 (2012) 2305.
- [132] A. Ota, PhD thesis (2012), TU Berlin.

2 Aim and outline of the current work

The aim of this work is to provide an understanding of the observed discrepancy between the described dynamics of supported Pd₂Ga catalysts on the one hand and the pronounced high stability of unsupported Pd-Ga intermetallic compounds in the gas phase hydrogenation of acetylene on the other hand. Therefore, the bulk and the surface stability as well as the catalytic properties of Pd₂Ga with respect to the liquid phase hydrogenation of phenylacetylene were studied. In spite of a considerably low specific surface area, metallurgical prepared unsupported Pd₂Ga was utilized to study the intrinsic properties of this material.

The findings are described in two main chapters.

Chapter III - Surface Dynamics of Pd₂Ga Part I – Structural Stability in UHV and Different Gas Atmospheres describes the omnipresent discrepancy between the bulk and the surface structure of Pd₂Ga. It includes:

- the synthesis of single-phase Pd₂Ga
- the characterization of the material by bulk sensitive methods
- surface analyses of Pd₂Ga after several pre-treatments
- possibilities to obtain and preserve an almost intact intermetallic surface are demonstrated with regard to its utilization in liquid phase hydrogenation

Chapter IV - Surface Dynamics of Pd₂Ga Part II – Reactivity and Stability in the Liquid Phase Hydrogenation of Phenylacetylene describes the consequences of the dynamic behavior of Pd₂Ga with respect to its catalytic properties. The following key aspects are emphasized:

- description of the used reactor set-ups and reaction procedures of phenylacetylene hydrogenation

- the comparison of the reactivity of Pd₂Ga after different pre-treatments towards phenylacetylene hydrogenation, whereby the stability of the catalyst is emphasized.
- the comparison with different reference catalysts including the activity towards styrene hydrogenation

Chapter V – Summary summarizes the obtained results. General conclusions, which can be drawn from the observed results, concerning intermetallic compounds for catalytic applications are stated. The validity of the described stability issue for the formerly discussed PdGa is briefly proven in the appendix.

3 Surface Dynamics of the Intermetallic Catalyst Pd₂Ga, Part I - Structural Stability in UHV and Different Gas Atmospheres

Authors: Gregor Wowsnick, Detre Teschner, Igor Kasatkin, Frank Girgsdies, Marc Armbrüster, Aiping Zhang, Yuri Grin, Robert Schlögl, Malte Behrens

Abstract

The structural and electronic properties of unsupported Pd₂Ga were investigated after different pre-treatments. Pd₂Ga provides with respect to elemental Pd a significantly modified electronic structure with its d-band centre being shifted away from the Fermi level. It was found that the electronic structure of the surface depends strongly on its pre-treatment and on the chemical environment. We report a detailed bulk and surface characterization of the intermetallic compound by means of XRD, DTA/TG/MS, SEM, XPS and HR-TEM. At moderate temperatures the bulk of Pd₂Ga is chemically resistant against H₂ or O₂ atmosphere and against mechanical load. Contrariwise its surface is highly sensitive against even traces of oxidizing agents leading quickly to a disparity between bulk and surface structure and composition. The reversibility of this dynamic effect depends on the degree of decomposition and on the sample history. An almost pure intermetallic surface can only be achieved in highly reducing atmospheres.

3.1 Introduction

The selective hydrogenation of alkynes to alkenes is applied in hydro-refining processes to remove impurities of acetylene or methylacetylene in corresponding alkene streams^[1], which are further used for polymerization. Furthermore (Z)-alkenes can be synthesized by liquid phase hydrogenation of internal (often propargylic) alkynes resulting from C-C-coupling by alkynylation, which is frequently applied during the syntheses of fine chemicals, flavours and pharmaceuticals, e.g. Linalool, Vitamin A, E and K or insect pheromons^[2,3,4].

Pd based catalysts provide an outstanding activity and selectivity for the hydrogenation of alkynes^[5,6,7,8]. The fundamental mechanism of acetylene and ethylene hydrogenation following the Horvut-Polanyi mechanism^[9] was studied by DFT calculations on a clean Pd(111) surface^[10,11]: acetylene and ethylene are converted by subsequent half-hydrogenation with vinyl and ethyl, respectively, as intermediates on the surface, which requires ensembles of Pd atoms. Azad et al.^[12] determined the acetylene hydrogenation to vinyl as rate limiting step as detected by joint TPD and IR absorption measurements on Pd(111) under UHV conditions. Ethylidyne was detected after heating the surface above 160 K.

Generally, alkynes are adsorbed stronger than alkenes. An early explanation for the high selectivity of Pd was a strong thermodynamic factor, meaning that as long as an alkyne is present the alkene is displaced from the surface. However, it is well-known that Pd-based catalyst can operate in a selective as well as in an unselective manner favoring formation of the alkene and alkane respectively. Bond and Wells^[13] showed that the selectivity of Pd for acetylene hydrogenation decreases as the initial H₂ : acetylene ratio increases and at sufficiently high ratios the reaction becomes completely non-selective. It was shown furthermore, that acetylene and ethylene can be indeed adsorbed and hydrogenated simultaneously and ethylene hydrogenation proceeds faster than the acetylene hydrogenation^[14]. The formation of oligomers and carbonaceous deposits due to dissociative adsorption are additionally observed side reactions. In particular ethylidyne, but also other intermediates resulting from dissociative adsorption like vinylidene or acetylidyne, are intermediates that have been observed in various studies^[15,16]. They were suggested to be precursors for carbonaceous deposits as well as oligomers.

In general, there are three main influences discussed, which determine the desired selectivity of Pd towards the alkene. Firstly, there is a geometric effect^[17]: The isolation of active sites and the presence of exclusively small ensembles of active atoms leads to the suppression of reactions requiring larger ensembles, e.g. oligomerization or formation of strongly bound hydrogen deficient species^[18], in general known as ensemble effect^[19,20]. In particular the presence of only small ensembles reduces the availability of hydrogen^[21] and hinders over-hydrogenation. Secondly, Pd easily forms Pd hydrides^[22]: Compared to dissociatively bonded H atoms on the surface, the hydrogen incorporated in the subsurface or in the bulk of Pd provides a higher reactivity and lowers the selectivity towards the alkene due to enhanced alkene hydrogenation^[23,24,25,26]. Thirdly, the selectivity could be increased if an electronic effect enhances the barrier for alkene hydrogenation and thus favoring alkene desorption^[27].

Recently, it has been shown that the selective phase in an initially pure Pd catalyst during hydrogenation of C-C triple-bonds is not the pure Pd itself but an *in situ* formed subsurface palladium-carbon phase formed by a rapid decomposition of the substrate as a first step of the reaction^[28,29]. The subsurface C modifies the electronic structure of Pd at the surface and slows down diffusion of H through the Pd-C surface phase into the Pd lattice. It weakens the adsorption strength of surface bonded H and thus further lowers the availability of H at the surface. As a result, over-hydrogenation and formation of the alkane is suppressed on this modified surface. Unfortunately, the existence of the Pd-C phase is highly dynamic and depends strongly on the chemical potential of C and H^[26]. High potentials of H or low potentials of the acetylene lead to hydrogenation of the subsurface C and, hence, Pd loses its selectivity.

Thus, less volatile additional modifiers are frequently added. In the semi-hydrogenation of acetylene eggshell Pd-Ag/Al₂O₃ alloy catalysts are applied^[30,31]. It is evidenced theoretically^[32,33] and experimentally^[34] that the electronic structure of Pd can be slightly changed by alloying with Ag resulting in lower heats of adsorption for acetylene and ethylene, which favors the desorption of ethylene and thus suppresses over-hydrogenation. However, the geometric effect was more influential because the reduction of the ensemble size lead to a change in the preferred adsorption site and disfavor the dissociative adsorption of H₂^[33]. Deviating from an ordered surface model, the constituting atoms in alloys are

statistically disordered and large ensembles of Pd might be still present. Generally atoms in alloys tend to segregate under reactive atmosphere^[35] and their surface structure can strongly depend on the pre-treatment^[36]. It was also suggested, that a H₂ treatment leads to segregation of Pd to the surface leaving behind a Ag enrichment in the subsurface. This prevents from the formation of the undesired subsurface H species and alkene hydrogenation^[37]. Optionally, co-feeding of CO during operation can strongly suppress over-hydrogenation^[38]. It simultaneously lowers the barrier for C-C coupling reactions^[39] and with increasing CO/H₂ ratio oligomer formation takes place in which CO itself is involved (“green oil”).

Beside the insights in the reaction mechanisms of acetylene hydrogenation over Pd under typical low pressure conditions, the role of different modifiers and additives is still controversially discussed and they are, as described briefly by means of Pd-Ag alloys and CO, not necessarily stable under reaction conditions. This is likewise the case for Pd catalysts in liquid phase hydrogenations of alkynes. Although Lindlar’s catalyst^[40], optionally poisoned with organic nitrogen bases, is one of the most common catalysts, it is not always sufficiently stable and selective^[41], for instance, if H₂O is used as solvent. Furthermore, impregnated heavy metals can be subjected to a dynamic redox chemistry and can leach and C-N bonds of organic bases could be cleaved by hydrogenolysis in presence of Pd^[42]. Works of Mallat et al.^[43] and López et al.^[44] highlight the role of important modifiers. It is still necessary and a challenge to find catalyst materials, which are not reliant on a complex subsurface chemistry or additional modifiers.

Intermetallic compounds (IMCs) like Pd₃Pb^[45] or NiZn^[32] were discussed as alternative catalyst for acetylene hydrogenation with their well-ordered crystal structure and their modified electronic structure. The modification of the electronic structure of Pd and Ni IMCs is generally stronger compared to substitutional alloys^[19,46] or for non-stoichiometric surface phases. This effect is more pronounced with decreasing electronegativity of the second metal^[47,48]. In the last years Pd-Ga intermetallic compounds were found to be stable and selective catalysts for the semi-hydrogenation of acetylene^[49,50,51]. It was shown, that the ordered structure and the partially covalent bonds of these intermetallic compounds gives rise to the intrinsically modified electronic structure compared to elemental Pd. Detailed studies have been carried out for PdGa where covalent interactions between Pd and Ga lead to a shift

of the Pd 4d band centre away from the Fermi level, which has been confirmed by XPS and NMR studies^[52,53]. An increasing d-band shift away from the Fermi level with increasing gallium content was proven for Pd₂Ga, PdGa and Pd₃Ga₇ by XP spectroscopy in the valence band region^[55]. The partially covalent chemical bonding in these materials leads to an enhanced structural stability suppressing a dynamic subsurface chemistry. PdGa exhibits an ordered crystal structure where Pd atoms are fully surrounded by Ga atoms resulting in expanded Pd-Pd distances compared to elemental Pd^[54]. Various bulk and surface sensitive methods, applied *ex situ* and under reaction conditions, like XRD, EXAFS, DTA and XPS supported the stability of PdGa and Pd₃Ga₇ and emphasized the similarity between bulk and surface^[49,50,51]. Theoretical calculations supported the superior catalytic properties of PdGa systems^[32].

A significant d-band shift is also observed for Pd₂Ga^[55] but, different from PdGa, Pd₂Ga does not show a perfect site-isolation. Pd₂Ga crystallizes in the Co₂Si-type structure (space group *Pnma* No. 62, orthorhombic, see Figure 3-1)^[56]. The two symmetrically nonequivalent positions of Pd are both surrounded by eight Pd atoms with distances of 2.82-2.99 Å, which is slightly enlarged compared to elemental Pd (2.75 Å)^[57]. Five Ga atoms with Pd-Ga distances between 2.54 and 2.84 Å complete the first coordination sphere. Thus, there is only a partial isolation of Pd by Ga in the first coordination sphere and triangular arrangements of Pd - similar to elemental palladium - are still present. In contrast to PdGa and Pd₃Ga₇, Pd₂Ga exhibits a significant homogeneity range (Pd_{2+x}Ga_{1-x}, -0.04 ≤ *x* ≤ 0.02 at 500 °C). In the Pd richer regime Pd atoms partially substitute Ga positions. Wannek et al.^[58] draw up the structural relationship between the Co₂Si-type like Pd_{2+x}Ga_{1-x} and a fcc solid solution Pd_xGa_{1-x}. However, a metallurgically prepared powdered Pd₂Ga sample without pre-treatment also shows a high selectivity in the hydrogenation of acetylene and provides the same long-term stability^[59] as in the case of PdGa and Pd₃Ga₇. In contrast to the more Ga-rich materials, one advantage of Pd₂Ga is that it can be obtained comparably easy way in a highly active nanostructured form by co-reduction of Ga-oxide supported Pd. For instance, a Pd₂Ga/MgO/MgGa₂O₄ catalyst was shown to maintain the higher selectivity compared to monometallic Pd nanoparticles^[60]. However, in the latter case, an unusual activation period of this catalyst over 40 hours has been observed before stable performance was reached. Such dynamic behavior might be related to an *in situ* change of the material surface. Haghofer et al.^[61] found a poor long-term stability of supported nanoparticulate Pd₂Ga in methanol steam-

reforming due to decomposition of the intermetallic surface under these conditions. In a combined *in situ* XRD, *in situ* EXAFS and CO-FTIR study^[62] under H₂ and O₂ atmosphere, the *in situ* formation of hydrides could be excluded but it was shown that the surface undergoes oxidative decomposition in O₂ forming Ga oxides and elemental Pd or a Ga depleted Pd₂Ga phase. Evidence for the structural disturbance of the surface due to oxidative decomposition was also reported in a HR-TEM study of unsupported Pd₂Ga nanoparticles^[63]. The close structural relationship between the compounds makes a straightforward distinction by HR-TEM challenging. However, larger accumulations of elemental Pd were not observed on the surface but an ordered and potentially fcc structured, only slightly Pd-enriched Pd₂Ga phase was suggested. These observations induce doubts with respect to the pronounced stability also of the unsupported, bulk Pd-Ga intermetallic compounds. The first experiments to determine the catalytic properties of powdered, unsupported Pd₂Ga and PdGa in the liquid phase hydrogenation of phenylacetylene, which were partly already reported in [64], did not show significant differences in selectivity towards styrene compared to elemental Pd powder (see part II of this work^[65]). This observation further suggests that the modified catalytic properties of the intermetallic compounds PdGa and Pd₂Ga, whose surfaces were reported to be unchanged before and during the gas phase hydrogenation of acetylene at high temperatures (T = 200 °C), are not present under the conditions of liquid phase hydrogenation at room temperature and provoked us to study in detail the stability of pure, metallurgically prepared Pd₂Ga in different chemical environments.

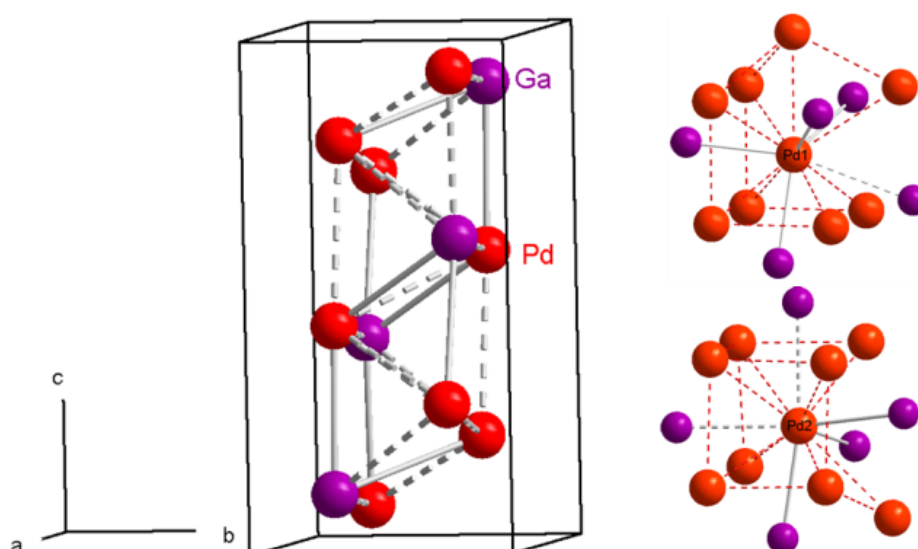


Figure 3-1: Left: Unit cell of Pd₂Ga. Top right: First coordination shell of Pd1. Down right: First coordination shell of Pd2. The compound crystallizes in the Co₂Si type of structure. The short Pd-Ga distances (2.54-2.62 Å) are shown as full lines, dashes lines represent atomic distances between 2.81-2.99 Å. The structural motif of elemental palladium, i.e. Pd-triangles, are preserved within the crystal structure.

Here we address the question, whether Pd₂Ga with its strong intrinsic modification of the d-band can transform its properties into chemical reactivity. In part I of this work, several bulk- and surface sensitive methods were applied with special focus on the resistance against oxidation, participation of sub-surface chemistry and its mechanical stability. Therefore, metallurgically prepared bulk-samples of Pd₂Ga in absence of supports or modifiers have been applied as model catalysts. This allowed studying the stability of the intermetallic compound and the potential of its intrinsically modified (electronic) structure for application. Part II^[65] focuses on the correlation of the surface structure with the catalytic properties in the selective hydrogenation of phenylacetylene in the liquid phase.

3. 2 Materials and Methods

3. 2. 1 Synthesis of Pd₂Ga

Pd₂Ga was synthesized by melting stoichiometric amounts of Pd granules (Chempur, 99.95%) and Ga pellets (Chempur, 99.99%) in a glassy carbon crucible in a high frequency induction furnace under Ar atmosphere in a glove box (O₂ < 1 ppm, H₂O < 1 ppm). The obtained regulus was annealed at 800 °C in an evacuated quartz glass ampoule for three days. A metallographic specimen was prepared by cutting 1 mm thick cylinders from the regulus. The slice was polished and stored under Ar. To obtain a fine powder of Pd₂Ga the material was either ground in air in an agate mortar or the material was powdered in air in a swing mill (Retsch, MM 200, 4 ml WC pot with two WC balls, 25 Hz) two times for 30 min with a break of 20 min. The absence of any additional phases was verified by X-ray powder diffraction and, in the case of the metallographic specimen, by optical microscopy and scanning electron microscopy.

3. 2. 2 X-ray powder diffraction

For *ex situ* X-ray powder diffraction the sample was placed on a 3 µm Kapton foil covered with vaseline. The measurement was performed on an image plate Guinier camera (G670, Huber, Cu Kα₁ radiation, λ = 1.54056 Å, curved Ge monochromator, 3° < 2Θ < 100°, CCD

detector). For determination of lattice parameters the powder was mixed with LaB₆ as internal standard ($a = 4.15695(6) \text{ \AA}$) prior to spreading on the Kapton foil. *In situ* X-ray powder diffraction was performed on a STOE theta/theta X-ray diffractometer (CuK α_{1+2} radiation, secondary graphite monochromator, scintillation counter) equipped with an Anton Paar XRK 900 *in situ* reactor chamber. The gas feed was mixed by means of Bronkhorst mass flow controllers, using helium as inert balance gas at a total flow rate of 100 ml/min. The effluent gas composition was monitored with a Pfeiffer OmniStar quadrupole mass spectrometer. XRD data were evaluated by total pattern analysis using the TOPAS software^[66]. The fitting procedure was based on the Rietveld method^[67] using the Pd₂Ga crystal structure model of Kovnir et al.^[56].

3. 2. 3 Metallography and scanning electron microscopy

For metallographic analysis samples were embedded in a conductive polymer (Polyfast[®], Struers), abraded with SiC paper and subsequently polished with diamond paste (minimum size 0.25 μm). The single phase nature of the material was confirmed by light microscopy (Axioplan 2, Zeiss) and scanning electron microscopy (Cameca microprobe SX100). WDX analysis was performed using a PdGa standard with known chemical composition (determined by ICP-OES) as reference. The particle morphology and homogeneity of the powdered samples was investigated by scanning electron microscopy using a Hitachi S4800 equipped with an EDAX Genesis 4000 detector.

3. 2. 4 Surface area characterization

The specific surface area was determined using Kr physisorption at 77 K in a Quantachrome AsiQ set-up by multi-point BET. Prior to the measurements samples were pre-treated either for 19 h in vacuum at ambient temperature or for 5 h at 400 °C in 5% H₂/Ar.

3. 2. 5 Transmission electron microscopy

A Philips CM200FEG microscope operated at 200 kV and equipped with a field emission gun, Gatan imaging filter, and energy-dispersive X-ray (EDX) analyzer was used. The coefficient of spherical aberration was $C_s = 1.35$ mm, and the information limit was better than 0.18 nm. High-resolution images with a pixel size of 0.016 nm were taken at the magnification of $1.083.000 \times$ with a CCD camera, and selected areas were processed to obtain the power spectra (square of the Fourier transform of the image), which were used for phase identification by measuring interplanar distances (± 0.5 %) and angles (± 0.5 deg).

3. 2. 6 *In situ* thermal analysis

In situ DTA/TG/MS measurements were performed with a Netzsch STA 449 Jupiter system connected to a Pfeiffer Omnistar 300 mass spectrometer. 248 mg of milled Pd₂Ga were weighted under air and placed inside a corundum crucible. The temperature program is described in the results and discussion section. The total gas flow during the measurement was either 40 ml/min He or a mixture of 5 ml/min H₂ in 45 ml/min He.

3. 2. 7 X-ray photoelectron spectroscopy

Near ambient pressure X-ray photoelectron spectroscopy^[68] was performed at the ISIS beamline at Bessy II, Helmholtz Zentrum Berlin. The metallographic specimen was prepared under Ar and transferred to the XPS chamber in a transport chamber without air contact. Approximately 250 mg of powdered samples were prepared by pressing the powder in air to a pellet with a diameter of 8 mm and a thickness of about 1 mm. Pellets of as prepared milled samples were introduced with air contact to the XPS chamber, while pellets of pre-reduced powder were annealed and reduced again for 1 h at 400 °C in 5% H₂/Ar and were subsequently transferred under Ar to the chamber. XPS measurements were performed under UHV (10^{-7} mbar) at temperatures between 25 °C and 400 °C or *in situ* in different atmospheres (H₂: Westfalengas, 99.999%; O₂: Westfalengas, 99.999%;) with a maximum total pressure of 1 mbar. Ga 3d, Pd 3d and C 1s core levels as well as the valence band region

were recorded. Spectra were taken with various excitation energies corresponding to kinetic electron energies of 145 eV, 385 eV or 785 eV. Using 3-times the inelastic mean free path given for elemental Pd^[69], these kinetic energies refer to an information depth of 1.3, 2.0 and 3.4 nm as a rough estimation. Analysis of the spectra was performed by the software CASA XPS^[70]. For details concerning the peak-fitting see supporting information. Quantification was performed using energy dependent cross sections from Yeh and Lindau^[71]. The peak intensities are normalized to the incoming photon flux.

3.3 Results and Discussion

In the present study three different kinds of Pd₂Ga samples were investigated: 1) A metallographic specimen, cut from compact regulus, 2) milled powder and 3) ground powder. The surface of the metallographic specimen was polished before analysis and handled exclusively under Ar atmosphere in a glove box. The ground and the milled Pd₂Ga samples were investigated in the as prepared state. Milled Pd₂Ga was subsequently subjected to different pre-treatments.

3.3.1 Characterization and stability of the bulk of Pd₂Ga

Single-phase Pd₂Ga was successfully prepared from the elements, as proven by XRD analysis of the ground sample (Figure 3-2). Metallographic analysis of the cross section of the regulus further verifies the absence of any additional minority phases (Figure 3-13). Inhomogeneities were not detected for the polycrystalline metallographic specimen in the SEM analysis. The composition of the specimen according to WDX is Pd_{66.2(±0.4)}Ga_{33.8(±0.1)}. The lattice parameters of the ground Pd₂Ga are $a = 5.4809(2)$, $b = 4.0556(1)$ and $c = 7.7895(1)$ Å, which is in good agreement with reported literature data^[56]. To decrease the particles size and increase the specific surface area, the material was milled in a swing mill. As shown in Table 3-1 and Figure 3-2 d, the milled powder provides, compared to the ground powder, significantly broader reflections. This is likely caused by the stress due to the harsh mechanical load during milling as already reported earlier in the case of PdGa^[50]. The milled powder still remains single-phase, which was also confirmed by a Rietveld refinement (not

shown) and the lattice parameters show only marginal changes (Table 3-1). According to SEM images (Figure 3-14) the particle size is in the range of 0.5-40 μm , and smaller particles cover larger ones due to agglomeration. As determined by Kr physisorption, the specific surface area of the powder is $0.27 \pm 0.01 \text{ m}^2\text{g}^{-1}$. Elemental mapping in the SEM microscope reveals a homogeneous distribution of Pd and Ga (Figure 3-14 b). The average composition of the powder according to EDX is $\text{Pd}_{68(\pm 3)}\text{Ga}_{32(\pm 3)}$ in reasonable agreement with the WDX results obtained on the regulus. Small particles of tungsten carbide were also detected in very low quantity originating from abrasion during milling. After 4 h of temperature treatment at 400 °C in reducing atmosphere (5% H₂/Ar, 100 ml/min) the XRD reflections become sharp again reaching similar full width at half maximum (FWHM) values as by crushing the sample (Figure 3-2 d). This is expected since the melting point of Pd₂Ga is about 1200 °C and 400 °C lies above the *Hüttig* temperature where structural healing becomes a fast process^[72].

Table 3-1: Lattice parameters of Pd₂Ga after grinding (a), milling (b) and milling with subsequent thermal treatment at 400 °C in 5% H₂/Ar (c) as determined by XRD. While no distinctive differences in lattice parameters are observed, after milling, a significant diffraction line broadening (values are given for the 203 reflection) is visible.

Sample preparation	<i>a</i>	<i>b</i>	<i>c</i>	FWHM / °
a)	5.4809(2)	4.0556 (1)	7.7895(1)	0.26
b)	5.4796(2)	4.0599(1)	7.7889 (2)	0.80
c)	5.4815(1)	4.0556(1)	7.7859(1)	0.23

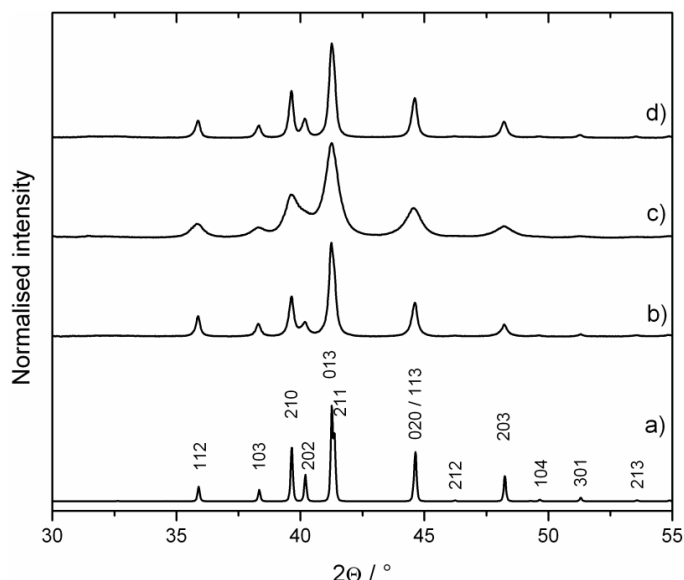


Figure 3-2: X-ray diffraction patterns of Pd₂Ga after different treatments. a) calculated pattern^[56] b) ground c) milled d) milled and subsequently treated 4 h in 5% H₂/Ar at 400 °C.

SEM images (Figure 3-14 c) reveal a somewhat lower amount of small particles, but no dramatic changes in particle size and morphology. Also the specific surface area remains unchanged ($0.28 \pm 0.01 \text{ m}^2 \text{ g}^{-1}$). Kohlmann^[73] studied the structural stability of Pd₂Ga against hydrogen by *ex situ* XRD and *in situ* DTA under harsh conditions ($p_{\text{H}_2} = 375 \text{ bar}$, $T = 250 \text{ }^\circ\text{C}$, $t = 60 \text{ h}$) and found no hints for the formation of hydrides. Also Haghofer et al.^[62] found no hint for the formation of hydrides by *in situ* EXAFS experiments for a Pd₂Ga/Ga₂O₃ catalyst at room temperature. Because the stability of hydrides is strongly dependent on the temperature, we studied the *in situ* stability of the milled Pd₂Ga in H₂ atmosphere by DTA/TG/MS (Figure 3-3) under elevated, but comparably mild conditions. After desorption of surface-adsorbed H₂O at 200 °C in pure He atmosphere, during the second heating cycle in 10% H₂/He (total pressure 1 bar) an exothermic peak with an onset temperature at 180 °C is observed, which is accompanied by a mass loss of 310 µg and H₂O formation. We assign the water formation to the reduction of surface Ga oxide which is reduced to metallic Ga corresponding to ~1% of the total Ga content. Further signals could not be detected under these conditions when heating to temperatures up to 500 °C and cooling under He atmosphere again.

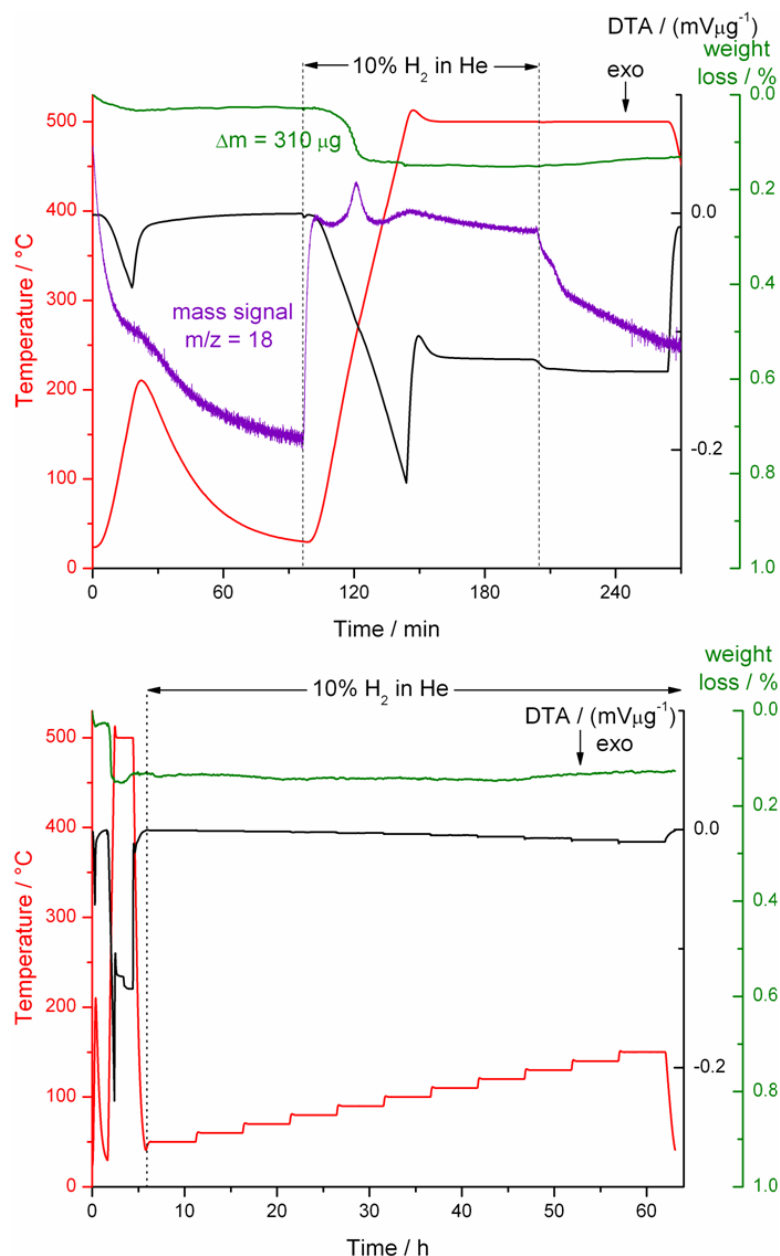


Figure 3-3: *In situ* DTA/TG/MS measurement of as prepared milled Pd₂Ga. Top: The powder was initially heated in He to 200 °C (10 K/min) to desorb water from the surface. After cooling the atmosphere was changed to 10% H₂/He and the powder was heated to 500 °C (10 K/min) revealing an exothermic peak at 180 °C accompanied by H₂O formation due to surface oxide reduction. Bottom: No further phase transformations were detected also during the long time treatment of the powder in 10% H₂/He with a stepwise increase of the temperature from 50 to 150 °C.

Also a subsequent long-time treatment in 10% H₂/He with stepwise increased temperature from 50 °C to 150 °C, i.e. in a temperature range where hydride formation and decomposition on elemental Pd takes place, revealed no significant thermal effects due to phase transformations. The bulk stability was furthermore investigated by *in situ* XRD in 100% He, 25% H₂/He and 20% O₂/He (details see Figure 3-15 and Figure 3-16). No hints for phase transformations of the bulk in He and H₂ were observed during stepwise heating to 400 °C

and subsequent cooling in agreement with the DTA/TG/MS measurement. Decomposition of the bulk starts at approximately 300 °C when treated in 20% O₂/He resulting in a mixture of Pd₂Ga, Pd₅Ga₃, Pd and PdO. Formed Ga oxide is probably amorphous and not detectable by XRD. In summary, the bulk of Pd₂Ga provides a high mechanical as well as chemical stability. Independent on the degree of mechanical load (polishing < grinding < milling) no decomposition or segregation could be observed. Milling induces a significant increase in disturbance of the crystal structure which can be easily reversed by annealing. Pd₂Ga is inert in H₂ atmosphere against formation of hydrides and starts to oxidize in 20% O₂ atmosphere not below 300 °C.

3. 3. 2 Characterization and stability of the surface

To investigate the surface of the Pd₂Ga powder, XPS and high-resolution TEM were applied. XPS is an integral method and provides information about the electronic structure, the chemical composition and the oxidation state of the material in the near-surface region. Using synchrotron radiation with variable photon energies allows measurements at different information depths. On the other hand, HR-TEM gives a complementary and direct local view on the micro- and nano-structure of the surface of the particles.

3. 3. 3 XPS investigation of the metallographic specimen

Figure 3-4 represents the Pd 3d core level XP spectra of the as prepared metallographic specimen of Pd₂Ga, which was recorded under UHV and ambient temperature as well as after heating to 400 °C. Additional reference spectra obtained from a Pd foil are also shown. The fits of the specimen heated to 400 °C and the Pd foil are shown in Figure 3-17.

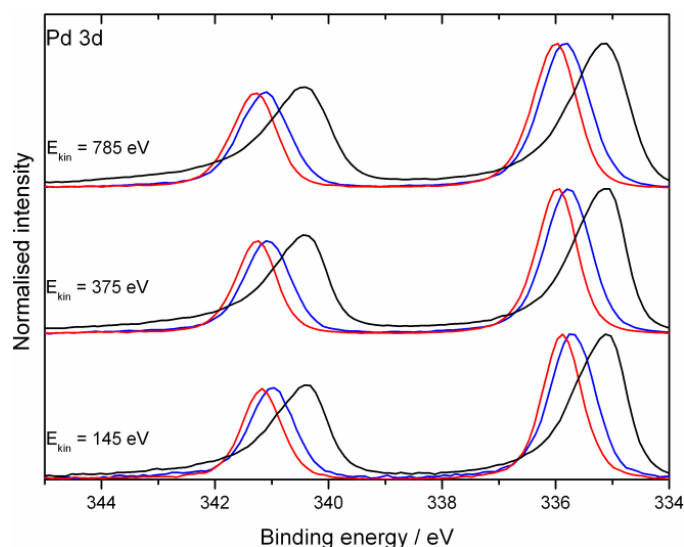


Figure 3-4: Pd 3d XP spectra of a Pd foil (black) and a metallographic specimen (polished under Ar) in an as prepared state (blue) and after thermal treatment at 400 °C in dynamic vacuum (red).

An asymmetric Pd 3d_{5/2} peak of elemental Pd located at a binding energy of 335.1 eV is observed for the palladium foil in agreement with the literature^[74]. On the other hand the Pd 3d_{5/2} peak of the Pd₂Ga specimen, heated to 400 °C, is significantly shifted towards a higher binding energy of 336.0 eV (335.9 eV at $E_{\text{kin}} = 145$ eV) accompanied by a loss of asymmetry. The core-level shift is in agreement with previous results for supported Pd₂Ga^[60,61] but - remarkably - as high as reported earlier for the more Ga rich unsupported PdGa sample^[49]. We attribute the slightly lower binding energy obtained at the lowest excitation energy (highest surface sensitivity) to a further surface core-level shift. The asymmetry of metallic core levels originates from the probability of excitation of electron-hole pairs at the Fermi level (final state effects)^[48,75] and is thus correlated with the number of electronic states at the Fermi level. Figure 3-5 compares the observed valence bands (with the main contribution of the Pd 4d states) and the Ga 3d core level spectra for the different samples at an excitation energy of 710 eV. Compared to elemental Pd the d-band centre of Pd₂Ga, heated to 400 °C, is significantly shifted away from the Fermi level towards higher binding energies resulting in a lower density of states at the Fermi edge, which is the consequence of intermetallic compound formation and the associated filling of the 4d states of Pd as it was reported for PdGa^[49]. The Ga 3d spectra of the Pd₂Ga specimen, heated to 400 °C reveal a doublet at approximately 18.4 and 18.8 eV, which can be assigned to (inter)-metallic Ga^[76]. A weak signal at 20.3-20.8 eV corresponds to oxidized Ga, whose atomic proportion increases from ~1 to 9% with decreasing information depth (see Table 3-2). The

ratios of Pd to metallic Ga are in the range of 2.3-1.6 depending on the kinetic energy of the photons, thus they are close to the stoichiometric composition of 2:1, confirming the presence of an almost clean intermetallic surface under these conditions.

Table 3-2: Comparison of peak maxima and FWHM of Pd 3d_{5/2} at different kinetic energies: metallographic specimen as prepared (a), metallographic specimen heated to 400 °C in dynamic vacuum (b) and a Pd foil (c). The ratios of Pd and Ga in dependence on the information depth and the amount of oxidized Ga are also given.

E _{kin}	Peak-maximum / eV			FWHM / eV			Pd ^{total} :Ga ^{total}			Pd ^{total} :Ga ⁰			Ga ³⁺ :(Ga ³⁺ +Ga ⁰)/%		
	785	375	145	785	375	145	785	375	145	785	375	145	785	375	145
a)	335.7	335.7	335.6	1.00	0.96	0.95	1.7	1.6	1.6	2.2	2.7	4.0	21.2	37.8	60.4
b)	336.0	336.0	335.9	0.92	0.85	0.83	2.3	1.6	1.5	2.3	1.7	1.6	1.3	5.8	9.0
c)	335.2	335.1	335.1	1.16	1.02	1.02									

In this respect it has to be taken into account, that the quantification using theoretical cross sections is not accurate enough to give a precise absolute ratio of the elements in particular for very low kinetic energies, while relative changes in element ratio of the sample with different information depths or due to changes of the conditions in the XPS chamber can be accurately determined.

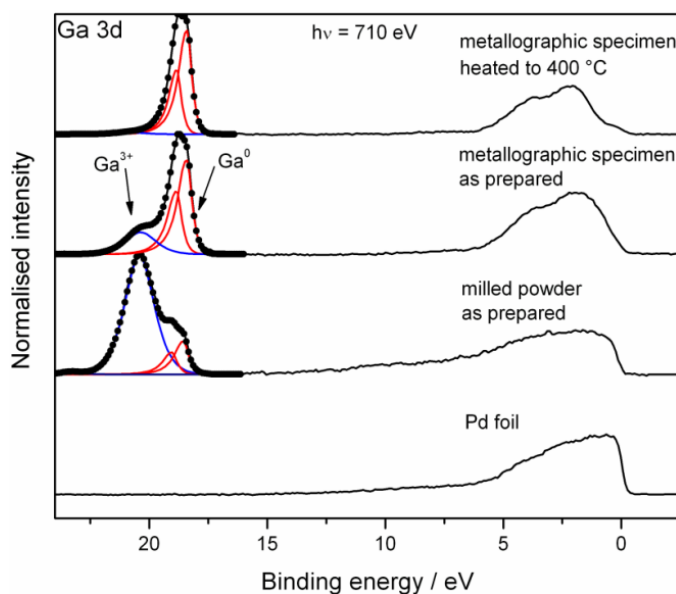


Figure 3-5: Ga 3d and valence spectra of different Pd₂Ga samples. The change of the valence band structure with the amount of oxidized Ga is obvious.

The Pd 3d_{5/2} peak of the as prepared metallographic specimen (before heating) is still almost symmetric, but broader and was observed at a binding energy of 335.6-335.7 eV (see Figure 3-4), as it was reported earlier for unsupported Pd₂Ga^[55]. It is thus located between that,

obtained for elemental Pd and the clean intermetallic surface. This difference is also reflected in the valence band (Figure 3-5) showing an intermediate structure with an increased density of states close to the Fermi edge. The Ga 3d spectra reveal a significant amount of Ga³⁺, increasing from ~21 to 60% with increasing surface sensitivity, (Table 3-2). Lower valent Ga^{δ+} (0 < δ < 3) species were not observed. While the ratio of Pd to the total content of Ga is between 1.7 and 1.6 the ratios of Pd to metallic Ga increases from 2.2 to 4.0 with increasing surface sensitivity. This indicates oxidative decomposition of the IMC resulting in oxidized Ga species and a Pd enriched surface, which must have happened during preparation and/or storing of the sample under Ar atmosphere due to the presence of traces of O₂ and H₂O. The nature of the excess Pd is unclear. In Figure 3-18 we show in detail, that it is not possible to describe the resulting Pd 3d_{5/2} peak by a linear combination of the symmetric peak for clean Pd₂Ga and the strongly asymmetric signal for elemental bulk Pd. Additional fit components are necessary to describe the obtained spectra, whose implementation is subjected to a certain arbitrariness due to the peak overlap of the components and the lack of a suitable reference for the unknown structural nature of the formed Pd species. The peak fitting (Figure 3-18) and the quantification of C 1s (Table 3-5) exclude a Pd-C phase, which would also show a Pd 3d peak between those of Pd₂Ga and elemental Pd. We will see in the following sections that this “intermediate” electronic structure of (not too heavily decomposed) samples is variable and depends on the amount of excess Pd. It is plausible that, deviating from the phase diagram^[77], the (not necessarily equilibrated) near-surface region of Pd₂Ga is able to accommodate much more Pd, leading to smooth transitions in the electronic and structural state between Pd₂Ga and Pd. Furthermore, it is likely that additional intensity in the Pd 3d spectra originates from the presence of small elemental Pd particles or clusters, giving rise to size-related core-level shift with similar extent as with Pd₂Ga^[74]. We will thus restrict the discussion of the Pd 3d spectra in the following on the position and the FWHM of the Pd 3d_{5/2} signal, which as a measure of the degree of surface decomposition into oxidized Ga and Ga-depleted Pd. The observed lines will not be fitted due to the questionable reliability of the derived structural data.

Heating of the specimen to 400 °C in dynamic vacuum is sufficient for a re-forming of an IMC terminated surface. An explanation for the high reducing potential of the dynamic vacuum at higher temperatures can be given by analyzing the C1s spectra (Figure 3-19).

Before heating, a broad peak at around 284.9 eV is observed indicating the presence of hydrocarbons on the surface, which is an unavoidable feature in our *in situ* XPS chamber. After heating of the specimen, the C 1s signal is weaker and asymmetric and its peak shifts significantly to a lower binding energy of about ~284.2 eV, which is a clear evidence for dehydrogenation of hydrocarbons^[78]. Thus, the reduction of the surface Ga oxide in the XPS chamber is likely related to this process.

3. 3. 4 XPS and HR-TEM investigations of milled Pd₂Ga in the as prepared state

The Pd 3d XP spectrum of milled Pd₂Ga is shown in Figure 3-6. A very broad and asymmetric peak indicates a decomposition of the intermetallic compound at the surface to a large extent. The asymmetric peak shape and the shift of the peak position to lower binding energies with increasing surface sensitivity from 335.5 to 335.2 eV indicates that mainly elemental Pd is present at the decomposed surface. In the most surface sensitive Pd 3d spectrum a long tail of the peak to higher binding energies represents undefined species, which are probably due to oxidized Pd species^[79]. It is noted that also intermetallic Pd-Ga compounds with a higher Ga content show peaks at similar positions, but these are unlikely to co-exist with oxidized Ga at the surface. Finally, charging effects might additionally broaden the line shape and residues of intermetallic Pd₂Ga likely also contribute to the spectra as indicated by the small contribution of (inter)-metallic Ga, visible in the Ga 3d spectra in Figure 3-5. The total Pd : Ga ratio shows a vast excess of Ga (Table 3-3), which probably originates from segregation of Ga due to oxidation during the mechanical treatment. However, most of the Ga is oxidized and the ratio between Pd and metallic Ga is by far higher than the nominal composition 2:1 showing that the oxidation of Ga species leaves a Ga-depleted Pd phase at the surface of the Pd₂Ga particles. Accordingly, the valence band (Figure 3-5) of as prepared milled Pd₂Ga clearly resembles that of elemental Pd and not that of clean Pd₂Ga recorded after heating of the metallographic specimen.

In contrast to the metallographic sample, for milled powder the reducing potential in the XPS chamber or the amount of reducing carbonaceous deposits is not sufficient for a complete reduction of the thick surface oxide layer to reform the intermetallic Pd₂Ga. The high temperature treatment at 400 °C in dynamic vacuum leads to a shift of the Pd 3d_{5/2} peak to

335.7 eV, which becomes nearly symmetric but shows still an enhanced broadness. After air exposure for 10 min the sample was measured again. The Ga oxide content increases slightly without observing a shift of the Pd 3d peaks. After storing the sample two months under air no further changes in XP spectra of Ga 3d and Pd 3d could be observed, indicating that the surface readily passivates without further mechanical load and the associated energy input.

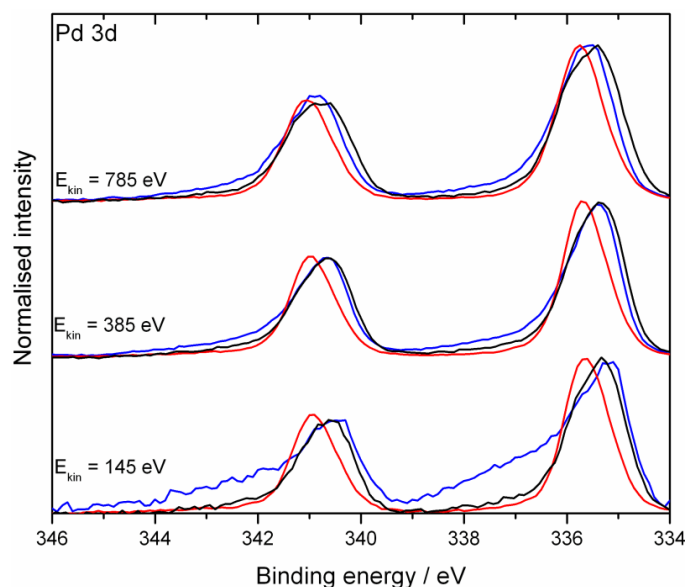


Figure 3-6: Pd 3d depth profiling of milled Pd₂Ga in an as prepared state (blue) and heated to 400 °C (red). The black line represents Pd₂Ga powdered by grinding in air.

HR-TEM images of the Pd₂Ga particles (Figure 3-7) provide a closer look on the local structure and morphology of the surface of the particles. The bulk of the material consists of crystalline Pd₂Ga particles, which is in agreement with the XRD result. The particles are surrounded by a non-uniform amorphous over-layer, which - according to XPS - mainly consists of oxidized Ga species. In this over-layer, crystalline nanoparticles with a diameter of up to 5 nm are embedded and in some case elemental Pd as well as Pd₂Ga could be unambiguously identified. However, Pd and Pd₂Ga cannot be easily distinguished by the diffraction pattern even in atomic resolution TEM because of the close relation of the structures^[58].

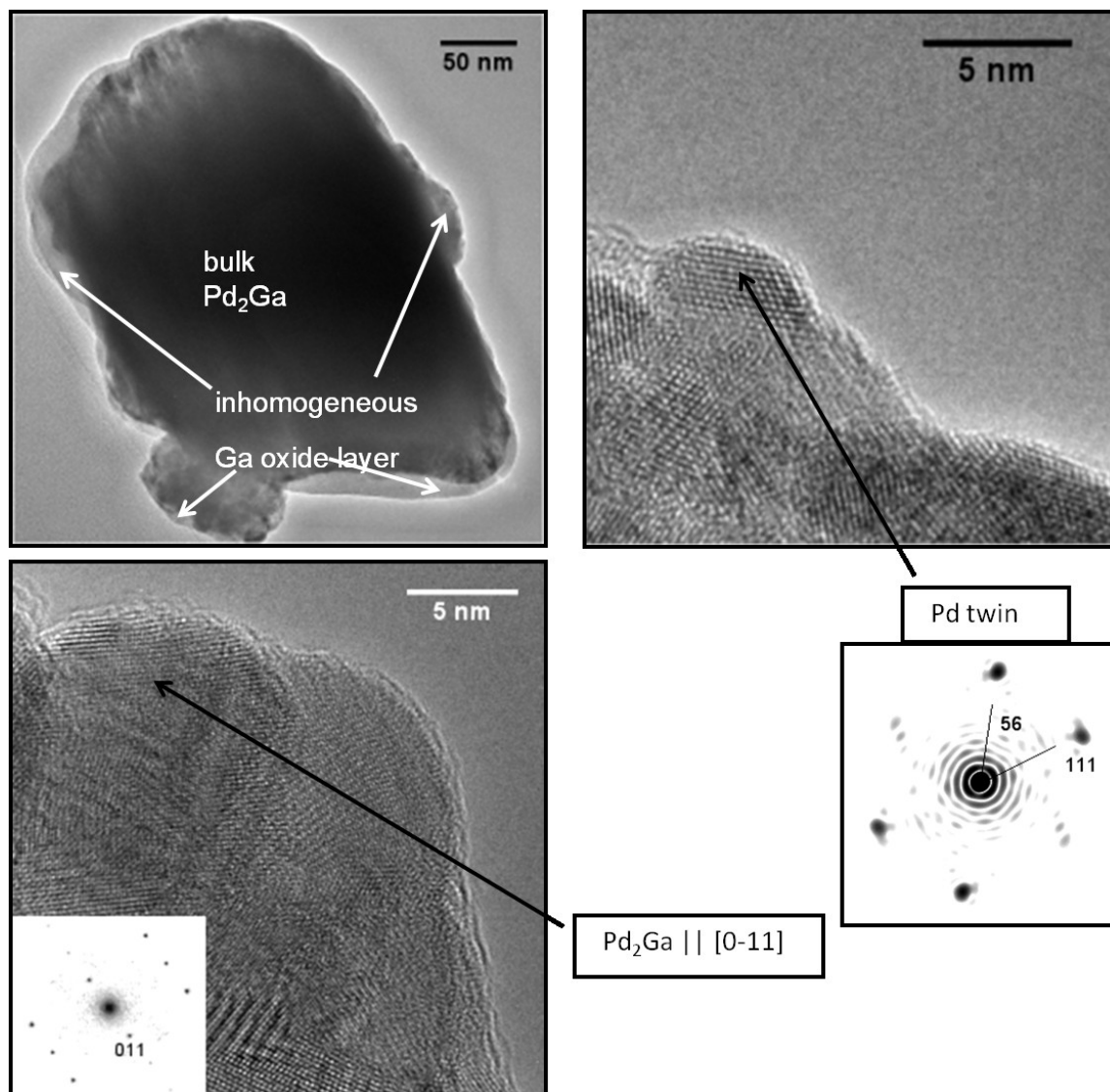


Figure 3-7: HR-TEM of milled Pd_2Ga in an as-prepared state. Large crystalline Pd_2Ga particles are surrounded by an inhomogeneous amorphous Ga oxide layer. At certain parts of the layer nanoparticles are embedded.

3. 3. 5 XPS investigations of ground Pd₂Ga

As shown already in 3. 3. 1 by means of XRD, only grinding instead of milling of Pd₂Ga leads to a lower mechanical load and thus to less stress introduced in the material. However, although the bulk of Pd₂Ga is much less disturbed, the surface of the as prepared ground material is in almost the same manner decomposed as observed for the milled Pd₂Ga. The surface is enriched with Ga which is almost completely oxidized (Table 3-3). Instead of the long tail in the Pd 3d peak only a shoulder is observed (Figure 3-6).

Table 3-3: Comparison of peak maxima and FWHM of Pd 3d_{5/2} at different kinetic energies: milled powder as prepared (a), powder heated to 400 °C in dynamic vacuum (b) and ground powder as prepared (c). The quantification of Pd and Ga always shows a large excess of Ga. Due to the high content of oxidized Ga the surface is enriched on Pd with respect to the present metallic Ga.

E _{kin}	Peak-maximum / eV			Peak-FWHM / eV			Pd ^{total} :Ga ^{total}			Pd ^{total} :Ga ⁰			Ga ³⁺ :(Ga ³⁺ +Ga ⁰)/ %		
	785	375	145	785	375	145	785	375	145	785	375	145	785	375	145
a)	335.5	335.4	335.2	1.32	1.24	n.d.	1.0	0.9	0.6	4.5	7.4	29.8	78.0	88.1	97.9
b)	335.7	335.6	335.6	1.13	1.06	1.05	1.3	1.5	1.4	2.1	2.7	3.0	33.6	46.7	55.6
c)	335.6	335.5	335.4	1.4	1.24	1.17	1.0	0.9	0.6	3.2	5.4	8.9	68.6	83.3	93.4

3. 3. 6 XPS and HR-TEM investigations of *ex situ* pre-reduced milled Pd₂Ga

Because the maximum H₂ pressure in the XPS chamber is limited to ~1 mbar and a full reduction of a thick oxide layer was not possible under these conditions, two *ex situ* pre-reduced samples (5% H₂/Ar, 1 bar total pressure, 4 h, 400 °C) were transferred under Ar into the XPS chamber. The reduction temperature was clearly higher than the reduction peak observed in the DTA/TG/MS measurement (Figure 3-3) with an onset temperature at 180 °C which was assigned to the reduction of the surface oxide layer. The higher temperature allows also a structural healing of the intermetallic surface. One sample was cooled down in Ar after reduction, the other one was cooled down in 5% H₂/Ar. In both cases the surface stoichiometry is close to the nominal composition of 2:1 (Table 3-4), which can be explained by the absence of any mechanical treatment after high-temperature reduction and, as will be shown below, by a mild passivation process. In the latter sample only about 20% Ga are in an oxidized state (on the most surface sensitive XPS measurement, see Figure 3-8 b) and the Pd 3d_{5/2} peak is located at 335.85 eV. Apparently this thin passivation layer is unavoidable if the

environment falls below a certain reduction potential. The reason therefore is likely the uncoordinated sites at the outermost surface with reduced covalent stabilization, which are extremely reactive towards oxygen impurities.

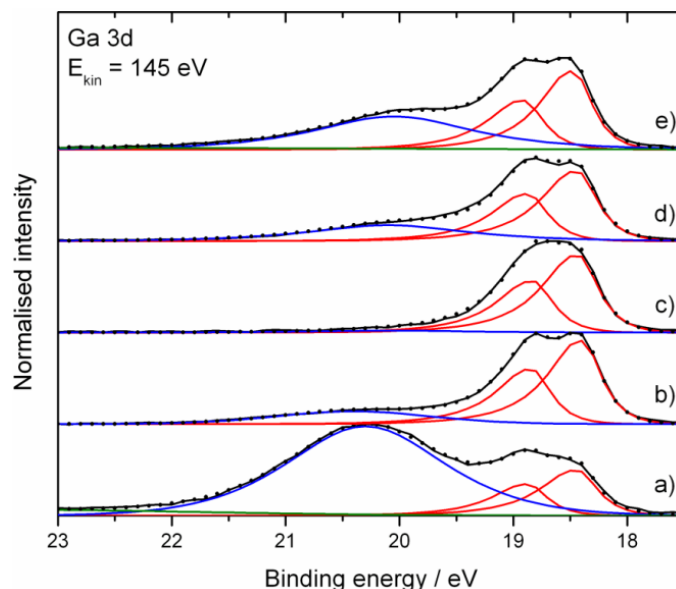


Figure 3-8: Ga 3d spectra of different pre-reduced Pd₂Ga powder samples. a) *ex situ* pre-reduced powder, cooled under Ar b) *ex situ* pre-reduced cooled under H₂ c) *in situ* H₂ treatment after *ex situ* pre-reduction and cooling under Ar d) sample of c) after slow oxidation in the cell and subsequent air exposure e) sample of c) after abrupt exposure to air. Red lines represent fits of the intermetallic Ga 3d doublet while blue lines correspond to oxidized Ga species. In the case of a high oxidation grade also a broad signal of O 2s (green) is observed ~ 23 eV.

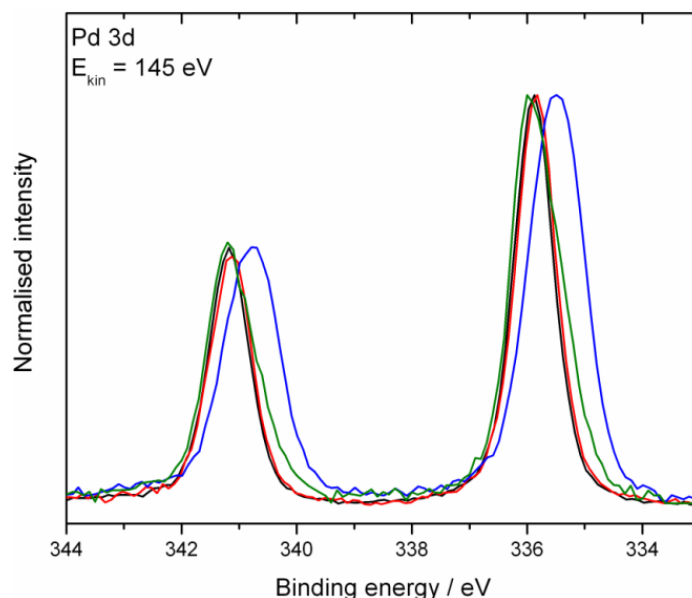


Figure 3-9: Pd 3d spectra of *ex situ* pre-reduced powders at a kinetic energy of 145 eV. The red curve represents the *ex situ* pre-reduced milled powder cooled under 5% H₂/Ar and is almost similar to the metallographic specimen heated to 400 °C (black curve) and the samples treated *in situ* with H₂ at 1 mbar (not shown). *Ex situ* pre-reduction and cooling under 100% Ar leads to significant disruption of the surface (blue curve) as well as the abrupt exposure to air of a freshly reduced sample (green).

In situ H₂ treatment of the sample, leading to the reduction of the surface Ga oxide (see Table 3-4, Figure 3-8), indicate no further shift or change in peak shape and width of the Pd 3d peak and also the valence band structure remain unaltered. This implies that the slightly lower binding energy compared to 336.0 eV in the more bulk sensitive measurements, compare (Table 3-2) originates from a surface core-level shift, rather than the influence of an overlapping Pd component. However, the presence of 20% Ga oxide before *in situ* reduction must involve a Ga-depletion of the remaining Pd near-surface species. On the one hand, Pd₂Ga provides a certain homogeneity range and the formed Ga oxide passivation layer might originate from segregation from the subsurface or the bulk and thus the IMC might balance this loss of metallic Ga. On the other hand, if Ga from the outermost Pd₂Ga layers is oxidized this would leave behind very small Pd accumulations. As already discussed, small Pd clusters might provide a rather similar electronic structure compared to Pd₂Ga^[74]. Furthermore it is clearly visible in Figure 3-18, that also small concentrations of bulk Pd (~1%) are hardly detectable by XPS in our case. Thus, small amounts of elemental Pd are likely to be still present.

The surface is more decomposed, if the sample is cooled in the absence of H₂ under 100% Ar atmosphere (O₂ and H₂O concentration < 100 ppb) after the *ex situ* pre-reduction. It results in a stronger oxidation of about 75% of Ga (Figure 3-8 a) and a slightly asymmetric Pd 3d_{5/2} peak is observed at 335.5 eV (see Figure 3-9). This intermediate core level shift is lower than observed for the as prepared metallographic specimen or the milled sample heated to 400 °C. That lower core level shift is consistent with the larger excess of Pd compared to metallic Ga (7.5:1) but eludes again a reference-based fitting analysis. The difference of the electronic structure is also clearly visible by the different valence band features (see Figure 3-10 b and c). Cooling a pre-reduced sample in Ar, results already in a higher occupation of the d-band close to the Fermi level. These differences strikingly clarify the sensitivity of the intermetallic surface towards oxidative decomposition once the temperature is high and the reducing potential of the environment is not sufficient to outweigh the oxophilicity of the surface Ga species even under condition where gas phase O₂ or H₂O are present only on a minimum impurity level.

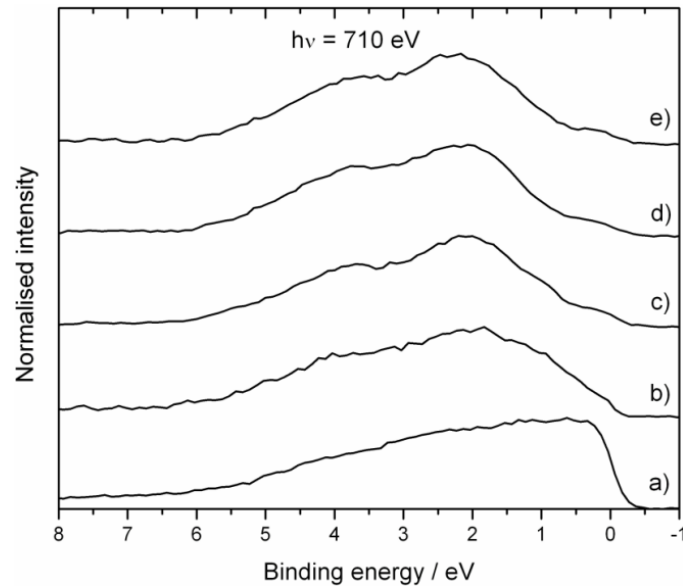


Figure 3-10: XP spectra of the valence band at a photon energy of 710 eV. a) Pd foil b) *ex situ* pre-reduced milled powder and cooled under Ar c) *ex situ* pre-reduced milled powder cooled under H₂ d) metallographic specimen heated to 400 °C and e) sample of b) during treatment in 1 mbar H₂ at 400 °C.

The corresponding HR-TEM images (Figure 3-11) of the pre-reduced particles cooled down in 5% H₂/Ar show again crystalline particles consisting of Pd₂Ga in the bulk which is surrounded by a thinner and more uniform amorphous layer.

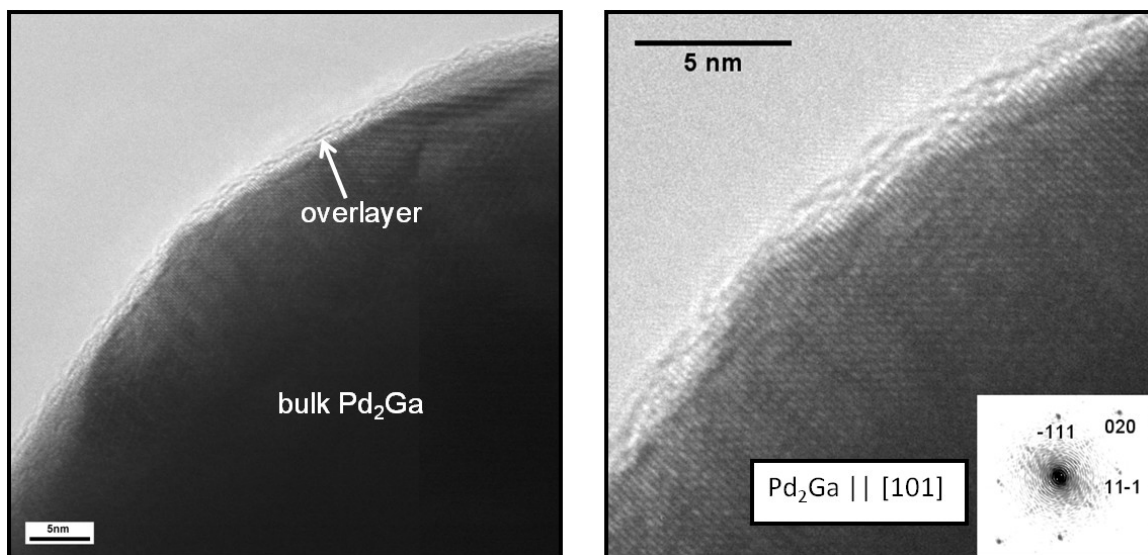


Figure 3-11: HR-TEM of Pd₂Ga powder after pre-reduction at 400 °C. These particles consist of large domains and are surrounded only by a thin amorphous over-layer. According to the XP spectra Ga oxide contribute to the thin over-layer but also contaminations in the microscope likely response therefore.

3.3.7 *In situ* H₂ treatment of pre-reduced milled Pd₂Ga and re-oxidation

Treatment in 1 mbar H₂ at 400 °C in the XPS chamber allows removing the oxide layers almost completely from both (cooled in 5% H₂/Ar and in 100% Ar) *ex situ* pre-reduced samples (Figure 3-8 c). Henceforth also the sample cooled down in 100% Ar provides the electronic structure of Pd 3d core level (Figure 3-9) and valence band (Figure 3-10 e) of pure Pd₂Ga at the surface. However, analyzing the ratio between Pd and Ga both samples are subjected to variations of their surface stoichiometry. The Ar-cooled sample shows an increase of the Pd:Ga ratio to about 2.8 at 400 °C in 1 mbar H₂ and a pronounced decrease to 0.9 when changing to 50 °C in UHV. The H₂-cooled sample also shows a by far too low ratio of about 1.2, in this case even at 400 °C in 1 mbar H₂ atmosphere. These changes are not associated with variations of the Pd 3d peak profile or position, which excludes the formation of more Ga rich or Ga less near-surface alloys. For the latter sample the ratio between Pd and the total content of Ga was much higher at 1.7 when the spectra were recorded at higher kinetic energies of 375 or 785 eV. Because the binding energy of elemental, polycrystalline Ga is very similar to intermetallic Ga^[80] and the resolution of the Ga 3d peaks is not sufficient to distinguish between both, segregation of elemental Ga to the surface is the most likely explanation. However, the ratio stays constant near 1:1 even after abrupt exposure and store of 5 h in air. Since this phenomenon is only observed after reduction in the XPS chamber under reduced pressure and not after *ex situ* pre-reduction, we currently have no explanation for this observation and speculate that this manifestation of dynamic behavior is caused by the special low-pressure conditions in the XPS chamber.

The general sensitivity of the surface redox processes of Pd₂Ga on the exact conditions and the dependence of its reversible character on the sample history is also observed during re-oxidation. If the sample without a protecting oxide-layer is abruptly exposed to air, the amount of oxidized Ga increases to more than 40% and the peak shape of Pd 3d changes and loses its narrow and symmetric profile (Figure 3-9). It is indeed the sole exception, where the observed line profile can approximately be described by a linear combination of 80% Pd₂Ga and 20% bulk Pd (Figure 6 d) evidencing the formation of elemental Pd as it was already assumed by Haghofer et al.^[62]. The situation is different if the sample is carefully oxidized. Slow *in situ* treatment with a step-wise increase of O₂ and H₂O (ratio ~ 1:1) partial pressure

up to 0.6 mbar total pressure at 40 °C within some hours resulted in oxidation of only approximately 25% of Ga at the outermost surface, which is not accompanied with a significant d-band shift or increase in FWHM of the Pd3d peak (Figure 3-9) and a subsequent air-exposure did not lead to further oxidation indicating the formation of a thin passivation layer by very slow oxidation.

Table 3-4: Peak position and FWHM of Pd 3d_{5/2} and elemental quantification of Pd and Ga and Ga oxide content of *ex situ* pre-reduced milled Pd₂Ga recorded at a kinetic energy of 145 eV. a) sample cooled down under 100% Ar, b) *in situ* H₂ treatment (1 mbar) of the sample of a) at 400 °C, c) sample of b) after slow *in situ* oxidation and subsequent exposure to air, d) *ex situ* pre-reduced and cooled down under 5% H₂/Ar, e) *in situ* H₂ treatment (1 mbar) of samples of d) at 400 °C, f) sample of e) after abrupt exposure to air (2 signals).

	Peak-maximum / eV	Peak-FWHM / eV	Pd ^{total} :Ga ^{total}	Pd ^{total} :Ga ⁰	Ga ³⁺ :(Ga ³⁺ +Ga ⁰) / %
a)	335.50	1.07	1.9	7.5	74
b)	335.85	0.85	2.8	2.9	4
c)	335.85	0.79	0.7	0.96	27
d)	335.85	0.82	2.1	2.7	19
e)	335.85	0.85	1.2	1.2	4
f)	335.9 and 335.1	0.85 and 1.0	1.0	1.7	42

3.4 Summary

In this study we investigated the bulk and the surface stability of the intermetallic compound Pd₂Ga. The bulk of Pd₂Ga provides a high chemical stability. Pd₂Ga is inert against hydride formation at low as well as at high temperatures. Oxidative decomposition of the bulk is not observed before ~ 300 °C in 20% O₂/Ar atmosphere. The bulk material is furthermore highly resistant against mechanical load and remains single phase material even after milling. The induced strain effects are easily reversible by a temperature treatment at 400 °C. These observations are in agreement with the results for PdGa and Pd₃Ga₇. However, the high stability of the bulk of Pd₂Ga cannot be transferred to the surface. The dynamics of the surface are complex and depend on the pre-treatment and the actual conditions, which is summarized in Figure 3-12. A metallographic specimen was introduced as reference sample for the XPS studies. The polishing and subsequent storage of this sample under Ar atmosphere at room temperature is already sufficient for partial oxidative decomposition resulting in a Pd enriched metallic state partially covered by Ga oxide (Figure 3-12 A). According to the XPS analysis small Pd accumulations, rather than bulk Pd is present.

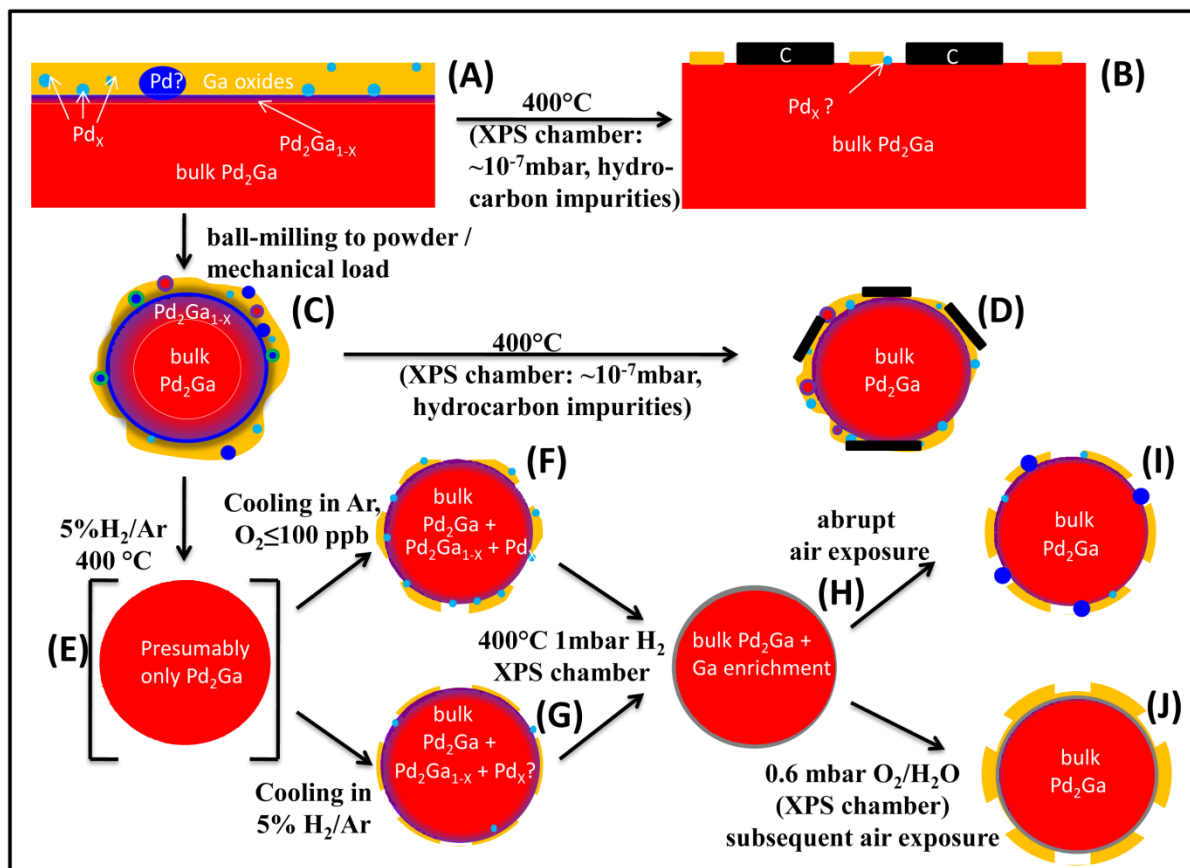


Figure 3-12: Scheme of the observed dynamic changes of Pd_2Ga after different treatments. The rectangle shown in (A) and (B) indicate the metallographic specimen. The spherical sketches (C-J) represent a microcrystalline particle after milling. The non-uniform morphologies and distribution of the nanostructures in particular that of the smaller Pd agglomerates (Pd_x , light blue spheres), larger metallic Pd accumulations (dark blue spheres), Pd oxide (green) and C accumulations (black rectangles) at the surface are simplified. The bulk of Pd_2Ga (red areas) is always stable. Ga oxide is shown in yellow color. A layer of varying thickness at the interface of the bulk and the Ga oxide, shown in purple, marks slightly Pd enriched Pd_2Ga due to Ga surface segregation. The grey cover visible in (H and J) should indicate the irreversible enrichment of metallic Ga on top of the surface during *in situ* H_2 treatment in the XPS chamber.

These Pd particles likely act as nuclei for the re-formation of the IMC at the surface by annealing of the specimen to 400 °C in dynamic vacuum (Figure 3-12 B). The Ga oxide reduction is likely assisted by a Pd induced dehydrogenation of hydrocarbon surface impurities in the XPS chamber resulting in carbonaceous species at the surface. Mechanical load during milling leads to enhanced surface segregation and oxidation of Ga. The surface of an air-milled sample is nanostructured and consists of Pd, Pd oxide and Pd_2Ga nanoparticles embedded in an inhomogeneous Ga oxide layer (Figure 3-12 C). The annealing to 400 °C in dynamic vacuum is not sufficient for a complete re-formation of the IMC at the surface (Figure 3-12 D), whereas under atmospheric pressure the oxide over-layer reduces at ~ 180 °C in 10% H_2/He . The powder was thus (with regard to its application in liquid phase

hydrogenation, see part II^[65]) *ex situ* pre-reduced at 400 °C in 5% H₂/Ar and, presumably, under these conditions the surface is a clean termination of the bulk (Figure 3-12 E). After cooling the sample under this reducing atmosphere and careful handling under Ar we observed the Pd 3d core level as well as the valence band spectra compatible with that of the clean intermetallic surface within the detection limit (Figure 3-12 F). However, a thin passivation layer is unavoidable due to the structural destabilization of Pd₂Ga – likely a consequence of the uncoordinated Ga sites of the termination layer. According to previous literature^[62,63] and our observed activity in hydrogenation, presented in part II of this work^[65], we suggest that the oxide layer is not homogeneous. It is possible that Pd₂Ga tolerates some loss of the metallic Ga, due to its homogeneity range, but traces of elemental Pd could still be present. The situation is much clearer, when the sample is cooled under Ar after reduction (Figure 3-12 G): in absence of H₂ at high temperature smallest traces of O₂ or H₂O are enough for strong decomposition and segregation of the surface even in absence of mechanical load. The *in situ* H₂ treatment *under low pressure conditions* of these samples lead to dynamic enrichment of metallic Ga on top of the surface, apparently without the formation of a more Ga rich IMC, e.g. PdGa (Figure 3-12 H). The mechanism of this process is unclear, but possibly it is an equilibration of the IMC terminated surface. However, despite the Ga enrichment, different surfaces were observed after oxidative treatments (Figure 3-12 I and J): If the material is suddenly exposed to air, this resulted indeed in the partial formation of metallic Pd. In the case of careful, slow oxidization at room temperature under reduced pressure only a thin Ga oxide layer is formed. This passivation layer does not grow after air exposure and, within the detection limit, no further disturbance of the under-lying IMC was observed.

The surface of Pd₂Ga turned out to be highly dynamic. A passivation layer forms rapidly as soon as the environment loses a certain reduction potential. The stability of the passivation layer and the degree of disturbance of the (electronic) structure of the surface strongly depends on the pre-treatment and the environment, i.e. mechanical load, partial pressure of oxidants, total pressure and temperature. Thus the behavior of the intermetallic Ga in Pd₂Ga is comparable to pure elements with high oxophilicity like elemental Ga, Al, Zn or Ti where a passivating layer is rapidly formed without further attack of the bulk. In sharp contrast to the pure elements, the oxidized over-layer of Pd₂Ga can be removed by reduction in hydrogen at relatively low temperatures, which is likely an effect of the presence of finely dispersed

excess Pd, which activates H₂ by dissociative chemisorption. The exact nature of the excess Pd could in most instances not be clarified in this study and is presumably also variable. The presence of Pd enriched phases with intermediate electronic and structural state between Pd and Pd₂Ga could explain the observations. Furthermore, it is likely that small Pd agglomerates with a small size distribution are formed on the surface which are partially embedded in a Ga oxide matrix. Their spectroscopic motifs (core level shift, reduced density of states at the Fermi level) are compatible with the observations and are unfortunately largely indistinguishable from Pd₂Ga itself^[74]. It can be assumed that the catalytic properties of decomposed Pd₂Ga surfaces are dominated by this segregated Pd species rather than by the IMC itself.

3.5 Conclusion

Our study represents a detailed investigation of the surface stability of the Pd₂Ga, which shows high selectivity in the hydrogenation of acetylene in the gas phase as previously reported. Pd and Ga are chemically very different metals and the reaction between both results in the formation of covalent bonds. Contrariwise to alloys, the covalent bonds strongly alter the crystal and the electronic structure. Compared to elemental Pd, the valence band of Pd-Ga intermetallic compounds possesses a structure comparable to a coinage metal with a clear shift of the d-band center away from the Fermi level. These covalent bonds between Pd and Ga, however, are not strong enough to stabilize the material's surface against oxidizing agents and against mechanical load. If the reduction potential falls below a certain value, a passivating over-layer forms and the surface becomes chemically different. The bulk however is protected against further decomposition. The electronic structure of the surface is subjected to a high dynamics with respect to the pre-treatment of the material and the chemical environment. The reason for the reversible character of these disturbances is the formation of metallic Pd accessible to the surface with its ability to activate hydrogen. However, this shows that it is not sufficient to determine the electronic structure and the composition of a freshly prepared intermetallic surface under clean or reducing conditions, since during sample preparation before reaction or under reaction conditions this surface can and will easily change. The termination of the surface may differ substantially from a cut through bulk structure, even if bulk methods still confirm the presence of the intermetallic compound. The

impact of this issue for catalytic reactions will be addressed in part II of this study^[65] by means of the liquid phase hydrogenation of phenylacetylene catalyzed by Pd₂Ga. The discrepancy between surface and bulk with a dynamic behavior that is dependent on the chemical potential of the environment is a manifestation of the well-known materials and pressure gaps that hinder straightforward correlation of structural analysis obtained on model systems with catalytic performance data. It is perspicuous, that these difficulties, demonstrated here by means of Pd₂Ga, must be considered when investigating the bulk and surface structure of other intermetallic compounds containing less noble metals.

3.6 Supporting information

3.6.1 Microscopy

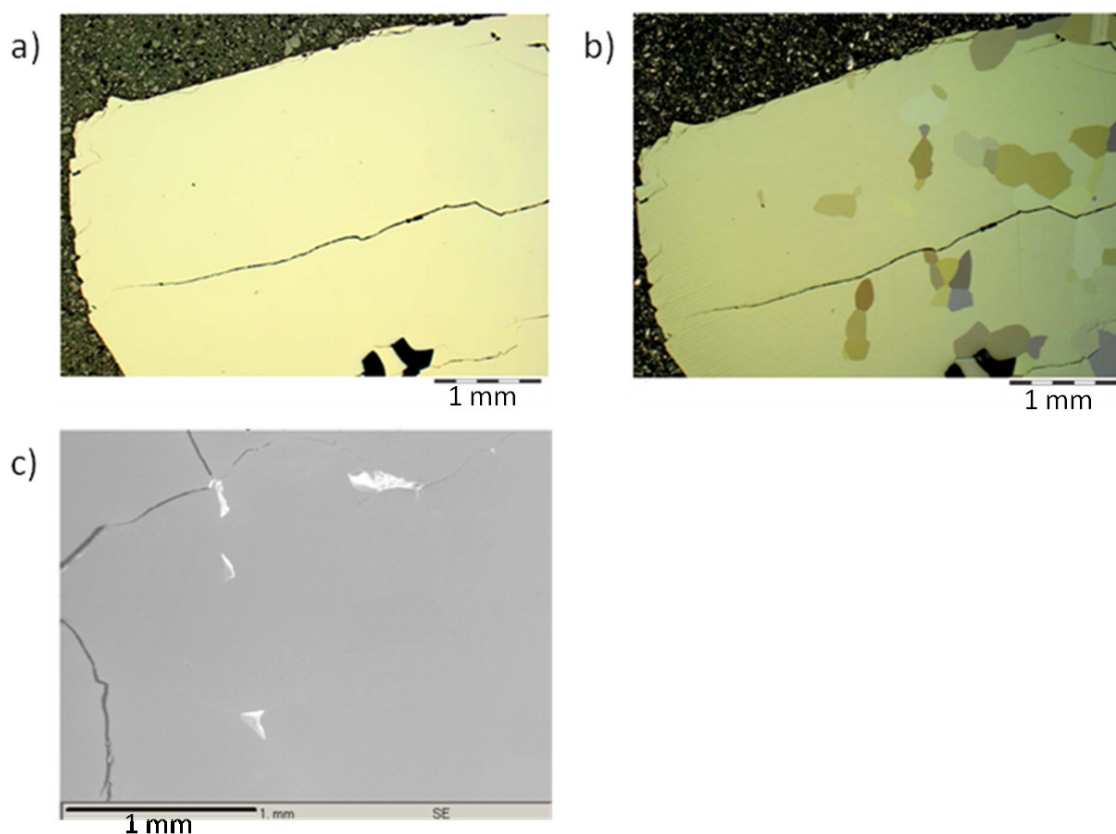


Figure 3-13: Microscopic analysis of an embedded metallographic specimen of Pd₂Ga polished under Ar. The material is homogeneous as visible by optical microscopy (a) and SEM (c). The color shading observed in polarized light (b) indicates the polycrystallinity of the specimen.

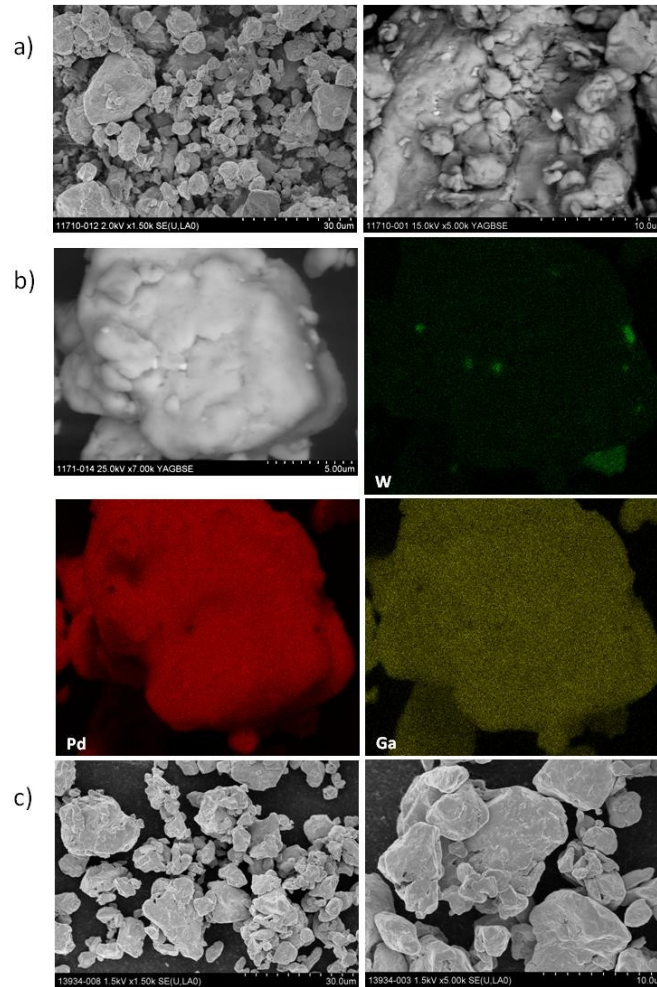


Figure 3-14: SEM images of milled Pd₂Ga. a) overview on the powder in the as prepared state. b) a closer look to a large particle and the elemental mapping of Pd, Ga and W c) overview on the powder after treatment at 400 °C for 4 h in 5% H₂/Ar.

The SEM images reveal a relatively broad particle size distribution between 0.5 – 40 μm of the as prepared (a) as well as the pre-reduced samples (c). Smaller particles cover larger ones. EDX elemental mapping analysis on an agglomerate of the as prepared powder show that Pd and Ga are distributed homogeneously. Impurities of WC are detected, which originates from the WC mill. The amount of WC is below the detection limit of XRD.

3. 6. 2 *In situ* XRD

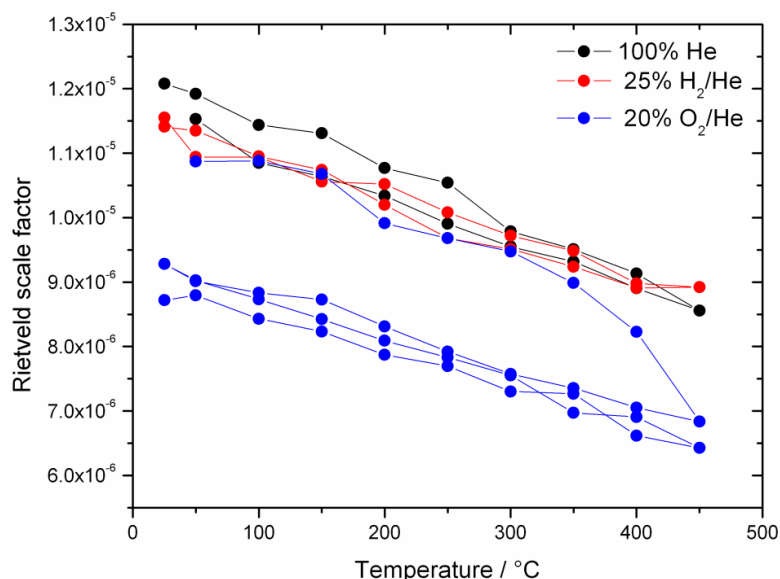


Figure 3-15: Calculated Rietveld scale factor of *in situ* XRD pattern of Pd₂Ga in different atmospheres, representing the overall intensity of the Pd₂Ga reflections. A significant drop starting at about 300 °C in 20% O₂/He indicates starting bulk oxidation.

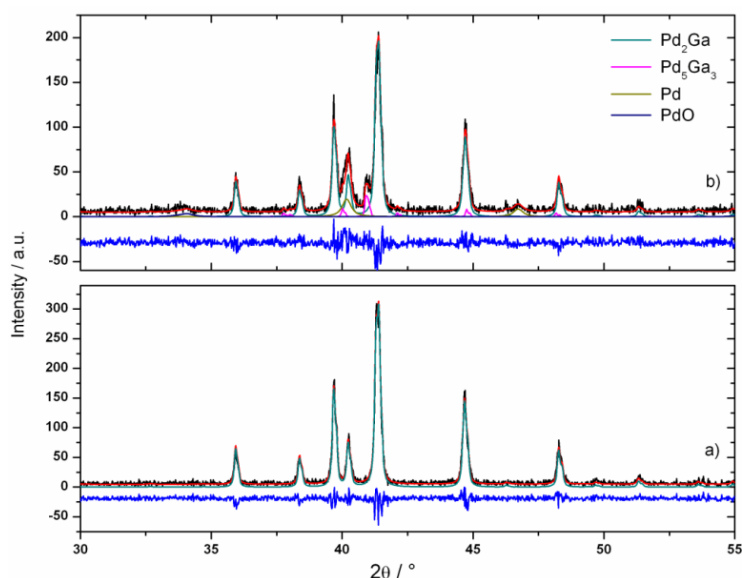


Figure 3-16: Selected *in situ* XRD pattern of Pd₂Ga recorded at 25 °C. a) after stepwise heating and cooling in 100% He and 25% H₂/He respectively. The sample remains single phase b) Decomposition products were detected after high temperature treatment in 20% O₂/He accompanied by a decrease in the overall intensity of the Pd₂Ga diffraction lines. Black lines represent the obtained pattern, red lines correspond to the Rietveld fit and bottom lines reveal the difference between both.

The bulk stability was tested by *in situ* XRD in He, H₂ and O₂ atmosphere. The evolution of the diffraction intensity of Pd₂Ga, which is expressed via the Rietveld scale factor obtained from the fits, is shown in Figure 3-15. Apparently the diffraction intensity is a function of

temperature, as the increased thermal motion of the atoms inside the structure leads to a more diffuse electron density distribution, thus reducing the intensity of Bragg diffraction. Correspondingly, most heating or cooling branches in the plot show an approximately linear, reversible behavior with a common negative slope. However, there are two exceptions from this rule. Firstly, the initial data points for heating in helium deviate slightly from the corresponding cooling branch and the hydrogen cycle. This deviation is likely caused by structural healing of the sample. The diffraction line widths change drastically, which seems to have some impact on the Rietveld scale factor. However no shift of diffraction lines or additional diffraction lines could be observed during temperature treatment in He or H₂ atmosphere (Figure 3-16). Secondly and more significantly, the diffraction intensity decreases at temperatures above 300 °C during the first heating in oxygen. This change is irreversible and does not proceed much further once the maximum temperature has been reached, as demonstrated by the congruence of data points belonging to the corresponding cooling ramp and the second heating-cooling cycle in oxygen. We attribute this intensity decrease to a partial decomposition of Pd₂Ga. Furthermore, diffraction peaks of decomposition products are observed (Figure 3-16 b), though they appear only after some time lag during the cooling branch of the first O₂ cycle, probably as the result of crystallization from an XRD amorphous state triggered by the cooling. The decomposition products are interpreted as a mixture of Pd₅Ga₃, Pd and PdO, although the convoluted nature of the pattern and small contribution of decomposition product peaks make this assignment rather tentative. The simultaneous formation of amorphous Ga oxide is very likely and not detectable by XRD.

3. 6. 3 Further XPS analyses

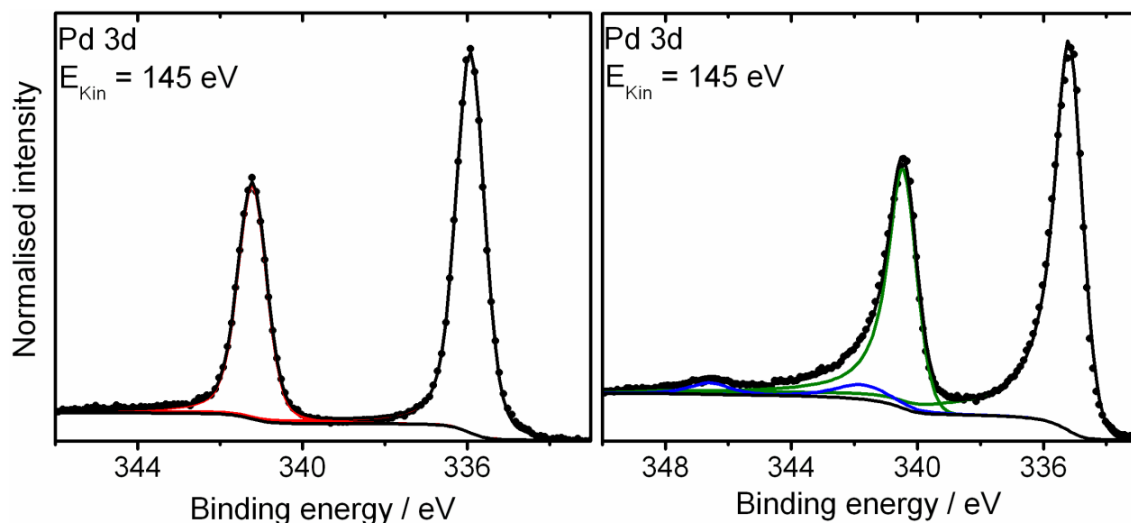


Figure 3-17: Observed Pd 3d reference spectra of the Pd₂Ga metallographic specimen, heated to 400 °C (left) and a Pd foil (right). Both line profiles can be fit with a Donjach-Sunjic function. The asymmetry is very small for the IMC compared to elemental Pd. Blue lines in the Pd spectra represent shake-up satellites due to final state effects.

Figure 3-17 presents the comparison of the Pd 3d spectra of a Pd foil and the Pd₂Ga metallographic specimen heated to 400 °C recorded with electron kinetic energy of ~145 eV ($E_{\text{Exc}} = 485$ eV). Final state effects due to the partial overlap of the d-band with the Fermi edge lead to the peak asymmetry and the observed intensive shake-up satellites in the case of elemental Pd^[75]. The peak maximum is located at 335.1 eV and a Donjach-Sunjic function describes reasonably well the observed peak shapes. In Pd₂Ga the d-band is shifted away from the Fermi edge resulting in an almost symmetric line shape. The formation of the IMC gives rise to a clear shift of the peak maximum to a binding energy of 335.9 eV. At higher excitation energies (higher bulk sensitivity, not shown here) the maximum was observed at 336.0 eV. We attribute the slightly lower binding energy at $E_{\text{Exc}} = 145$ eV to a surface core level shift.

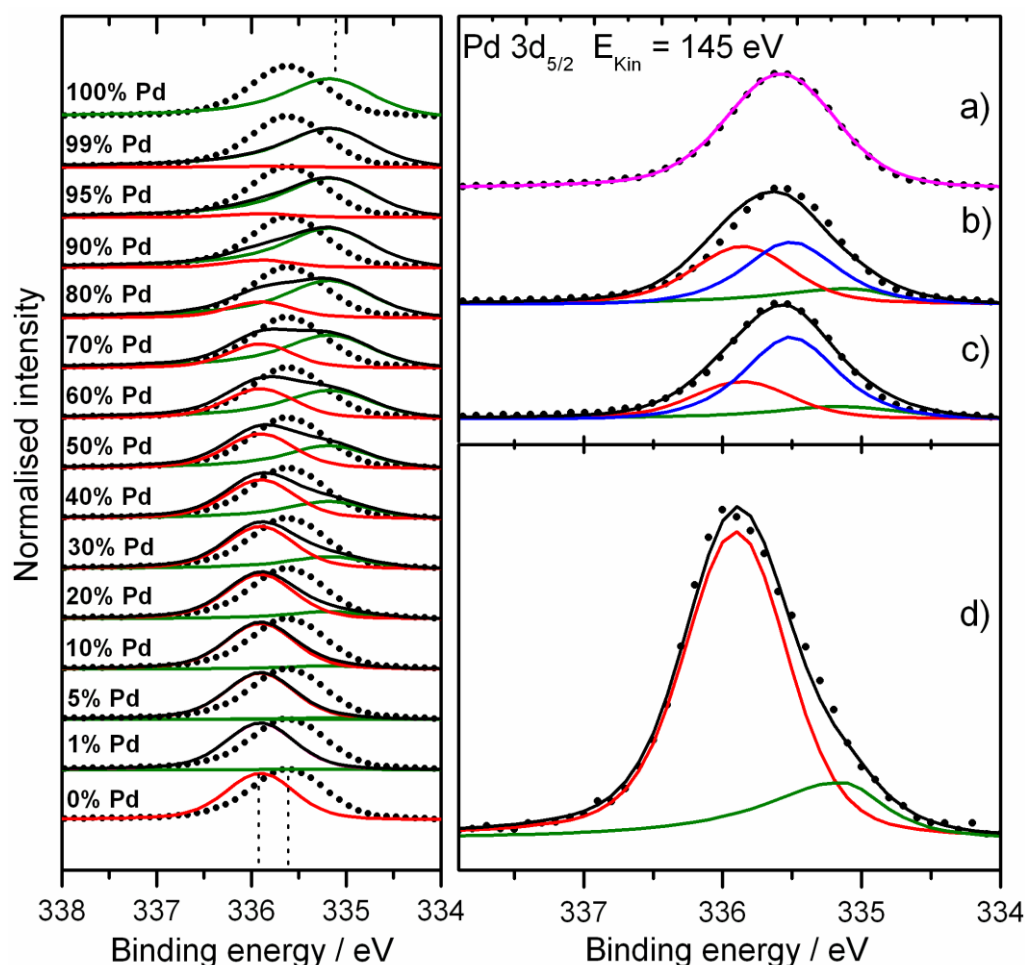


Figure 3-18: Left: The Pd 3d_{5/2} peak of the metallographic specimen in the as prepared state. The almost symmetric but relatively broad peak (black dots) cannot be described with a combination (black lines) of the line shapes of elemental Pd (green) and Pd₂Ga (red). Right: One broad fitting curve perfectly match the obtained line profile (a). The use of three fitting components (b and c), including Pd₂Ga and Pd is somehow arbitrary and do not match a perfect peak fitting. (d) represents a spectra, obtained after *in situ* reduction of milled Pd₂Ga powder, which was abruptly exposed to air and subsequently measured in UHV at room temperature.

Figure 3-18 (left) exemplifies the impossibility to describe a partially decomposed surface of Pd₂Ga by linear combinations of bulk Pd and Pd₂Ga reference line shapes. The Pd 3d XP spectra of an as prepared metallographic specimen recorded at an excitation energy of 485 eV is shown. The observed line shape is almost symmetric and only slightly broadened (compare table 2 in the main part). The quantification of the amount of Pd and metallic Ga revealed a ratio of $\sim 4:1$. Such an excess of bulk Pd would be easily resolvable (Figure 3-18 left). However, it is that very small amounts of elemental Pd would be hardly detectable. Indeed, a resolved shoulder could be only observed when an almost oxide-free sample of Pd₂Ga powder was abruptly exposed to air and subsequently analyzed again in UHV at room temperature (Figure 3-18 d). An approximate, even though not perfect, fit with the two

reference line shapes of the references is possible. In all other cases only the FWHM varies and the peak shift depending on the degree of decomposition. A fit with one peak is able to describe well the observed line profile (Figure 3-18 a) but the resulting FWHM is too high to be attributed to a single compound. Assuming the presence of minimum 40% percentage of Pd₂Ga (roughly corresponding to a ratio of Pd : Ga⁰ of 4:1) and an unknown amount of Pd requires a third compound. Allowing a binding energy of the third component of 335.55 to 335.7 eV and a FWHM between 0.8 and 1.0 eV, which would correspond to a Pd-C phase^[29], the fit clearly fails (Figure 3-18 b). Unconstraining the peak area of Pd₂Ga and the binding energy of the third component yields a better result with finally 30% percentage of Pd₂Ga (Figure 3-18 c). However, even three peaks do not perfectly match the peak profile and it is likely that additional, more or less, arbitrary peaks are necessary.

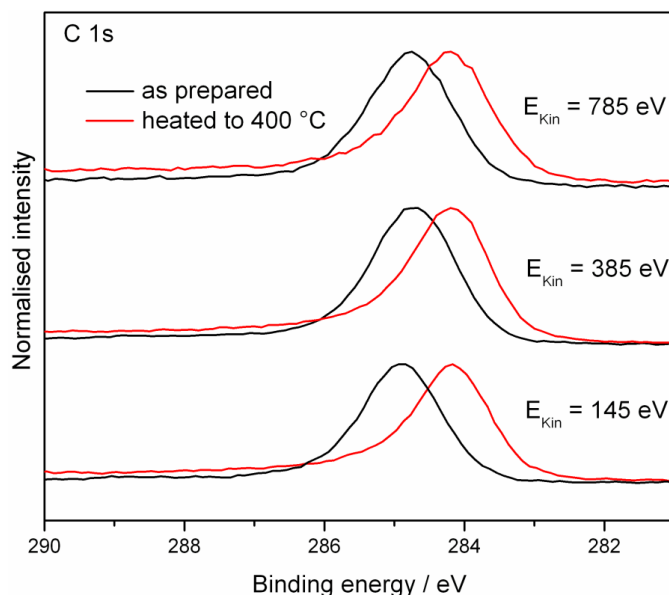


Figure 3-19: C 1s depth profiling of the metallographic specimen in the as prepared state and after heating to 400 °C.

Figure 3-19 shows the C 1s spectra of the metallographic specimen before and after heating to 400 °C. A significant shift of the peak and the arising asymmetry indicate the formation of elemental carbon by dehydrogenation of hydrocarbons. The carbon is present exclusively on the outermost surface as indicated by the analysis of the elemental composition by depth profiling. The carbon originates most likely from hydrocarbon impurities in the XPS cell. The concentration is lowered with increasing information depth, indicating that the carbon is present mainly on the outermost surface. By heating to elevated temperatures a part of the

hydrocarbons can be removed, while another part of the hydrocarbons is converted to elemental carbon.

Table 3-5: Carbon content of different Pd₂Ga samples dependent on the information depth.

$E_{\text{Kin}} / \text{eV}$	$\text{C}/(\text{Pd}+\text{Ga}+\text{C}) / \%$		
	145	385	785
metallographic specimen as prepared	80.2	63.8	49.4
metallographic specimen heated to 400 °C	67.9	56.1	45.1
milled Pd ₂ Ga as prepared	71.2	59.7	50.6
milled Pd ₂ Ga pre-reduced, in situ 400 °C at 1m bar H ₂	64.4	48.4	31.4

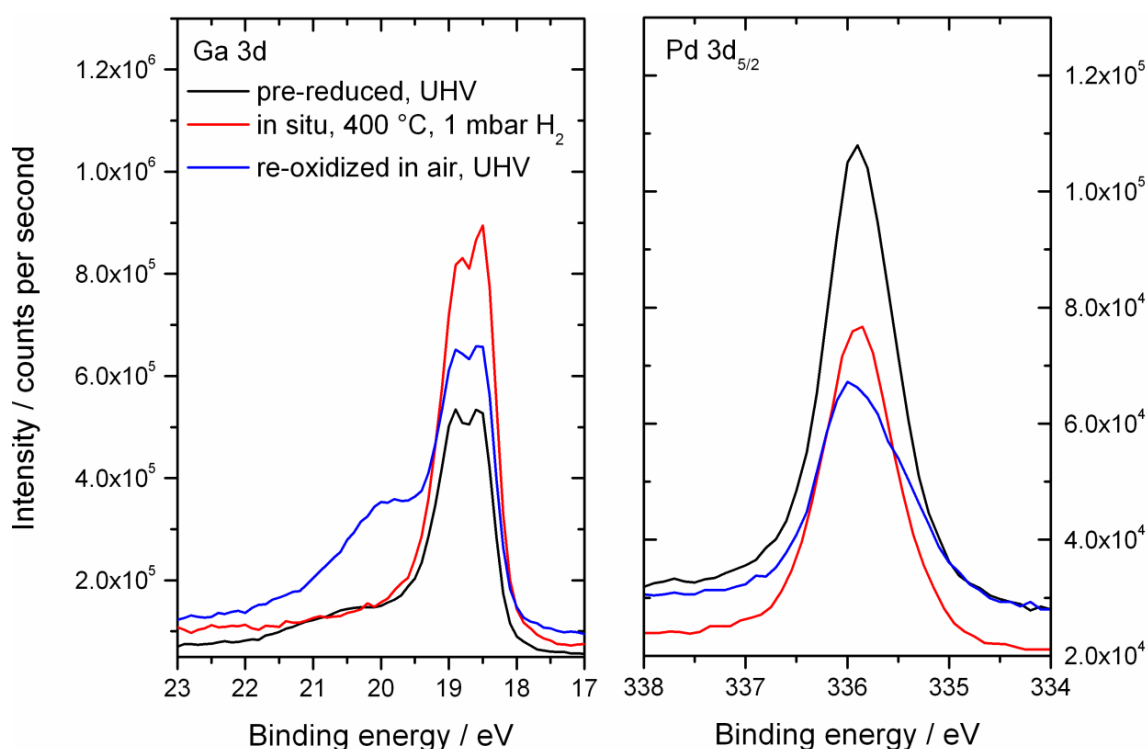


Figure 3-20: Comparison of absolute peak intensities of Ga 3d and Pd 3d recorded at $E_{\text{Kin}} = 145 \text{ eV}$ obtained after *ex situ* pre-reduction and subsequent cooling under H₂ atmosphere.

Figure 3-20 clearly shows the changes in the ratio between Pd and Ga of an *ex situ* pre-reduced sample before and during *in situ* H₂ treatment and after re-oxidation. While the surface stoichiometry of Pd and Ga is ~2:1 under UHV conditions, an enrichment of Ga is observed after removal of the thin oxide during *in situ* H₂ treatment (~0.7:1). The ratio remains too low after abrupt exposure to air and the following measurement under UHV conditions (1:1), which clearly rules out experimental artifacts.

3. 7 References

- [1] H. Arnold, F. Döbert, J. Gaube, in: G. Ertl, H. Knözinger, F. Schüth, J. Weitkamp (Eds.), *Handbook of Heterogeneous Catalysis*, Weinheim, Wiley-VCH, 2008, 3271.
- [2] V. V. Rusak, M. I. Zaretskii, A. S. Mozzhukhin, I. V. Usyshkina, L. A. Pushkina, *Russ. J. Appl. Chem.* 67 (1995) 1066.
- [3] P. Mercier, P. Chabardes, *Pure & Appl. Chem.* 66 (1994) 1509.
- [4] J. Sobczak, T. Bolesławska, M. Pawłowska, W. Palczewska, *Stud. Surf. Sci. Catal.* 41 (1988) 197.
- [5] G. C. Bond, D. A. Dowden, N. Mackenzie, *Trans. Faraday Soc.* 54 (1958) 1537.
- [6] P. B. Wells, *Chem. Ind. (Lond.)* (1964) 1742.
- [7] G. C. Bond, P. B. Wells, *Adv. Catal.* 15 (1964) 205.
- [8] S. Nishimura, *Handbook of Heterogeneous Catalytic Hydrogenation for Organic Synthesis* Wiley-Interscience, New York, 2001, 148.
- [9] J. Horviti, M. Polanyi, *Trans. Faraday Soc.* 30 (1934) 1164.
- [10] P. A. Shet, M. Neurock, C. M. Smith, *J. Phys. Chem. B* 107 (2003) 2009.
- [11] M. Neurock, R. A. van Santen, *J. Phys. Chem. B* 104 (2000) 11127.
- [12] S. Azad, M. Kaltchev, D. Stacciola, G. Wu, W. T. Tysoe, *J. Phys. Chem. B* 104 (2000) 3107.
- [13] G. C. Bond, P. B. Wells, *J. Catal.* 5 (1965) 65.
- [14] A. S. Al-Ammar, G. Webb, *J. Chem. Soc. Faraday Trans. 74* (1978) 195.
- [15] N. Sheppard, C. de la Cruz, *Adv. Catal.* 42 (1998) 181.
- [16] A. N. R. Bos, K. R. Westerterp, *Chem. Eng. Proc.* 32 (1993) 1.
- [17] A. Borodzinski, G. C. Bond, *Catal. Rev.* 48 (2006) 91.
- [18] Á. Molnár, A. Sárkány, M. Varga, *J. Mol. Catal. A* 173 (2001) 185.
- [19] W. M. H. Sachtler, in: G. Ertl, H. Knözinger, F. Schüth, J. Weitkamp (Eds.), *Handbook of Heterogeneous Catalysis*, Weinheim, Wiley-VCH, 2008, 1585.
- [20] V. Ponec, W. M. H. Sachtler in: J. W. Hightower (Ed.), *Proceedings of 5th International Congress on Catalysis*, Amsterdam, 1972, 6541.
- [21] M. García-Mota, B. Bridier, J. Pérez-Ramírez, N. López, *J. Catal.* 273 (2010), 92.
- [22] F. D. Manchester, A. San-Martin, J. M. Pitre, *J. Phase Equilib.* 15 (1994) 62.
- [23] A. M. Doyle, S. K. Shaikhutdinov, H.-J. Freund, *J. Catal.* 223 (2004) 444.

- [24] A. M. Doyle, S. K. Shaikhutdinov, S. D. Jackson, H.-J. Freund, *Angew. Chem. Int. Ed.* 42 (2003) 5240.
- [25] N. A. Khan, S. Shaikhutdinov, H.-J. Freund, *Catal. Lett.* 108 (2006) 159.
- [26] D. Teschner, Z. Révay, J. Borsodi, M. Hävecker, A. Knop-Gericke, R. Schlögl, D. Milroy, S. D. Jackson, D. Torres, P. Sautet, *Angew. Chem. Int. Ed.* 47 (2008) 9274.
- [27] F. Studt, F. Abild-Pedersen, T. Bligaard, R. Z. Sørensen, C. H. Christensen, J. K. Nørskov, *Science* 320 (2008) 1320.
- [28] D. Teschner, E. M. Vass, M. Hävecker, S. Zafeiratos, P. Schnörch, H. Sauer, A. Knop-Gericke, R. Schlögl, M. Chamam, A. Wootsch, A. S. Canning, J. J. Gamman, S. D. Jackson, J. McGregor, L. F. Gladden, *J. Catal.* 242 (2006) 26.
- [29] D. Teschner, J. Borsodi, A. Wootsch, Zs. Révay, M. Hävecker, A. Knop-Gericke, S. D. Jackson, R. Schlögl, *Science* 320 (2008) 86.
- [30] C. N. Thanh, B. Didillon, P. Sarrazin, C. Cameron, US patent 6054409 (2000), to Institut Francais du Petrole
- [31] A. Pachulski, R. Schödel, P. Claus, *Appl. Catal. A: General* 445-446 (2012) 107.
- [32] F. Studt, F. Abild-Pedersen, T. Bligaard, R. Z. Sørensen, C. H. Christensen, J. K. Nørskov, *Science* 320 (2008) 1320.
- [33] P. A. Shet, M. Neurock, C. M. Smith, *J. Phys. Chem. B* 109 (2005) 12449.
- [34] D. C. Huang, K. H. Chang, W. F. Pong, P. K. Tseng, K. J. Hung, W. F. Huang, *Catal. Lett.* 53 (1998) 155.
- [35] S. Zafeiratos, S. Piccinin, D. Teschner, *Catal. Sci. Technol.* 2 (2012) 1787.
- [36] Y. Jin, A. K. Datye, E. Rightor, R. Gulotty, W. Waterman, M. Smith, M. Holbrook, J. Maj, J. Blackson, *J. Catal.* 203 (2001) 292.
- [37] S. González, K. M. Neyman, S. Shaikhutdinov, H.-J. Freund, F. Illas, *J. Phys. Chem. C* 111 (2007) 6852.
- [38] B. Bridier, N. López, J. Pérez-Ramírez, *Dalton Trans.* 39 (2010) 8412.
- [39] M. García-Mota, B. Bridier, J. Pérez-Ramírez, N. López, *J. Catal.* 273 (2010) 92.
- [40] H. Lindlar, *Helv. Chim. Acta* 35 (1952) 446.
- [41] N. Semagina, M. Grasemann, N. Xanthopoulos, A. Renken, L. Kiwi-Minsker, *J. Catal.* 251 (2007) 213.
- [42] S. Nishimura, *Handbook of Heterogeneous Catalytic Hydrogenation for Organic Synthesis* Wiley-Interscience, New York, 2001, 601.

- [43] T. Mallat, A. Baiker, *Appl. Catal. A* 200 (2000) 3.
- [44] N. López, C. Vargas-Fuentes, *Chem. Commun.* 48 (2012) 1379.
- [45] J. Sobczak, W. Palczewska, T. Boleslawska, M. Pawlowska, *Stud. Surf. Sci. Catal.* 41 (1988) 197.
- [46] H. C. de Jongste, V. Poncet, *Bull. Soc. Chim. Belg.* 88 (1979) 453.
- [47] J. C. Fuggle, F. U. Hillebrecht, R. Zeller, Z. Zołnierek, P. A. Bennett, *Phys. Rev. B* 27 (1983) 2145.
- [48] F. U. Hillebrecht, J. C. Fuggle, P. A. Bennett, Z. Zołnierek, *Phys. Rev. B* 27 (1983) 2179.
- [49] K. Kovnir, M. Armbrüster, D. Teschner, T. V. Venkov, F. C. Jentoft, A. Knop-Gericke, Yu. Grin, R. Schlögl, *Sci. Technol. Adv. Mater.* 8 (2007) 420.
- [50] J. Osswald, R. Giedigkeit, R. E. Jentoft, M. Armbrüster, F. Girgsdies, K. Kovnir, T. Ressler, Yu. Grin, R. Schlögl, *J. Catal.* 258 (2008) 210.
- [51] J. Osswald, R. Giedigkeit, R. E. Jentoft, M. Armbrüster, F. Girgsdies, K. Kovnir, T. Ressler, Yu. Grin, R. Schlögl, *J. Catal.* 258 (2008) 219.
- [52] B. H. Verbeek, P. K. Larsen, W. M. Gerits, *Vacuum* 33 (1983) 813.
- [53] M. Klanjšek, A. Gradišek, A. Kocjan, M. Bobnar, P. Jeglič, M. Wencka, Z. Jagličić, P. Popčević, J. Ivkov, A. Smontara, P. Gille, M. Armbrüster, Yu. Grin, J. Dolinšek, *J. Phys.-Condens. Mat.* 24 (2012) 085703.
- [54] M. Armbrüster, H. Borrmann, M. Wedel, Yu. Prots, R. Giedigkeit, P. Gille, Z. Kristallogr. New Cryst. Struct. 225 (2010) 617.
- [55] K. Kovnir, D. Teschner, M. Armbrüster, P. Schnörrch, M. Hävecker, A. Knop-Gericke, Yu. Grin, R. Schlögl, *Bessy Highlights 2007* (2008) 22.
- [56] K. Kovnir, M. Schmidt, C. Waurisch, M. Armbrüster, Yu. Prots, Yu. Grin, Z. Kristallogr. New Cryst. Struct. 223 (2008) 7.
- [57] H. W. King, F. D. Manchester, *J. Phys. F* 8 (1978) 15.
- [58] C. Wannek, B. Harbrecht, *J. Alloys Comp.* 316 (2001) 99.
- [59] M. Armbrüster, K. Kovnir, M. Behrens, D. Teschner, Yu. Grin, R. Schlögl, *J. Am. Chem. Soc.* 132 (2010) 14745.
- [60] A. Ota, M. Armbrüster, M. Behrens, D. Rosenthal, M. Friedrich, I. Kasatkin, F. Girgsdies, W. Zhang, R. Wagner, R. Schlögl, *J. Phys. Chem. C* 115 (2011) 1368.

- [61] A. Haghofer, K. Föttinger, F. Girgsdies, D. Teschner, A. Knop-Gericke, R. Schlögl, G. Rupprechter, *J. Catal.* 286 (2012) 13.
- [62] A. Haghofer, K. Föttinger, M. Nachtegaalm, M. Armbrüster, G. Rupprechter, *J. Phys. Chem. C* 116 (2012) 21816.
- [63] R. Leary, F. de la Peña, J. S. Barnard, Y. Luo, M. Armbrüster, R. Schlögl, J. M. Thomas, P. A. Midgley, *ChemCatChem*, accepted.
- [64] M. Armbrüster, M. Behrens, F. Cinquini, K. Föttinger, Yu. Grin, A. Haghofer, B. Klötzer, A. Knop-Gericke, H. Lorenz, A. Ota, S. Penner, J. Prinz, C. Rameshan, Z. Révay, D. Rosenthal, G. Rupprechter, P. Sautet, R. Schlögl, L. Shao, L. Szentmiklósi, D. Teschner, D. Torres, R. Wagner, R. Widmer, G. Wowsnick, *ChemCatChem* 4 (2012) 1048.
- [65] G. Wowsnick, D. Teschner, M. Armbrüster, I. Kasatkin, F. Girgsdies, Yu. Grin, R. Schlögl, M. Behrens, *J. Catal.* part II of this work, submitted.
- [66] TOPAS version 4.2, copyright 1999, 2009 Bruker AXS.
- [67] R. A. Young in: R. A. Young (Ed.) *The Rietveld Method*, Oxford, Oxford University Press, 1993, 1
- [68] M. Salmeron, R. Schlögl, *Surf. Sci. Rep.* 63 (2008) 169.
- [69] S. Tanuma, C. J. Powell, D. R. Penn, *Surf. Interface Anal.* 43 (2011) 689.
- [70] Casa XPS Version 2.3.10, 1999.
- [71] J. J. Yeh, I. Lindau, *Atom. Data Nucl. Data* 32 (1985) 1.
- [72] J. A. Moulijn, A. E. van Diepen, F. Kapteijn, *J. Mol. Catal. A* 212 (2001) 3.
- [73] H. Kohlmann, *J. Solid State. Chem.* 183 (2010) 367.
- [74] C. Kuhrt, M. Harsdorff, *Surf. Sci.* 245 (1991) 173.
- [75] S. Doniach, M. Sunjic, *J. Phys. C* 3 (1970) 285.
- [76] R. Carli, C. L. Bianchi, *Appl. Surf. Sci.* 74 (1994) 99.
- [77] H. Okamoto, *J. Phase Equil.* 29 (2008) 466.
- [78] P. M. T. M. van Attekum, G. K. Wertheim, *Phys. Rev. B* 43 (1979) 1896.
- [79] K. S. Kim, A. F. Gossmann, N. Winograd, *Anal. Chem.* 46 (1974) 197.
- [80] K. Jacobi, *Surf. Sci.* 192 (1987) 499.

4 Surface Dynamics of the Intermetallic Catalyst Pd₂Ga, Part II – Reactivity and Stability in Liquid Phase Hydrogenation of Phenylacetylene

Authors: Gregor Wowsnick, Detre Teschner, Marc Armbrüster, Igor Kasatkin, Frank Girgsdies, Yuri Grin, Robert Schlögl, Malte Behrens

Abstract

The catalytic properties of unsupported Pd₂Ga for the liquid phase hydrogenation of phenylacetylene are investigated after different pre-treatments with focus on the stability of the intermetallic compound during reaction. Pd₂Ga is highly sensitive against decomposition at the surface in presence of traces of oxidants. Under the conditions of the liquid phase hydrogenation of phenylacetylene the intermetallic surface cannot be re-formed *in situ*. After a reductive pre-treatment, an almost clean Pd₂Ga surface can be obtained. Its hydrogenation activity is significantly lowered compared to elemental Pd, which is due to the intrinsic adsorption properties of the intermetallic surface. However, residues of H₂O or O₂ lead to oxidation of this surface. By applying very inert conditions this decomposition can be suppressed. In this case, the bulk material of Pd₂Ga gets attacked by phenylacetylene during reaction. The controlled modification of the crystal and the electronic structure of Pd is accompanied with a decreased stability.

4.1 Introduction

Liquid phase hydrogenations of C-C triple bonds is widely used in the industrial synthesis of fine chemicals^[1] and pharmaceuticals for example during the synthesis of Vitamin K or as final step in the Linalool synthesis^[2]. After C-C-coupling by alkynylation of an organohalide or ketone the resulting alkyne is semi-hydrogenated to the corresponding alkene, while the full hydrogenation to the alkane is undesired. Another application is the hydrogenation of phenylacetylene, which must be removed from styrene feeds, for the usage in the production of polystyrene^[3]. Various catalysts e.g. Raney-nickel^[4], so called “amorphous Ni-B alloys”^[5] or Fe based^[6,7] catalysts are reported to show good catalytic properties but generally require harsh conditions, i.e. high temperature and pressure. In particular in fine chemical syntheses mild conditions are desired and thus Pd is usually the metal of choice for this reaction^[8]. Reactions are frequently carried out under batch conditions with temperatures far below 100 °C and H₂ pressures of 1 atm or slightly above usually in presence of a solvent. Solvents can influence the reaction behavior^[9] as they might competitively adsorb on the active sites of the catalyst and they might be subjected to interactions with educts, products or transition states. Finally the solubility of H₂ varies with the solvent^[10]. Depending on the substrate and the applied conditions, beside over-hydrogenation and oligomerization, observed in acetylene hydrogenation^[11], cis-trans isomerization^[12], double bond migration^[13] and reduction of other easily to reduce functional groups are the main side-reactions that are also catalyzed by Pd. In this part, the resulting change of the electronic structure of the surface of an unsupported Pd₂Ga model catalyst after different pre-treatments is correlated with its properties for the hydrogenation of phenylacetylene in the liquid phase. The reaction scheme (Scheme 4-1) is comparably simple as stereo-selectivity does not have to be considered and double bond migration cannot occur. The phenyl ring is difficult to reduce and not hydrogenated under mild conditions, but it stabilizes reactive intermediates, e.g. radicals, which makes phenylacetylene and styrene prone to oligomerization even without initiators or catalysts^[14,15]. The hydrogenation of phenylacetylene was studied in numerous publications. Most kinetic studies reveal a zero order kinetics towards the alkyne and first order towards H₂^[16,17,18] and the apparent activation energies are in the range between 22 and 46 kJ/mol. Efficient modifications of Pd can be obtained by using bimetallic system, e.g. Pd-Mg, Pd-Fe, Pd-Ni^[19], Pd-Zn^[20], Pd-Si^[21], Pd-Cu^[22] and high selectivities between 85 and 95% at full conversions are frequently observed. Addition of organic nitrogen bases, e.g. quinoline, often

further enhances the yield of the desired olefin^[23]. However, Molnar et al.^[24] found a comparably high selectivity of ~94% at 100% phenylacetylene conversion for an unsupported Pd catalyst without any modification. Unfortunately, oligomers are hard to detect directly and their possible formation during reaction is not considered in the studies.

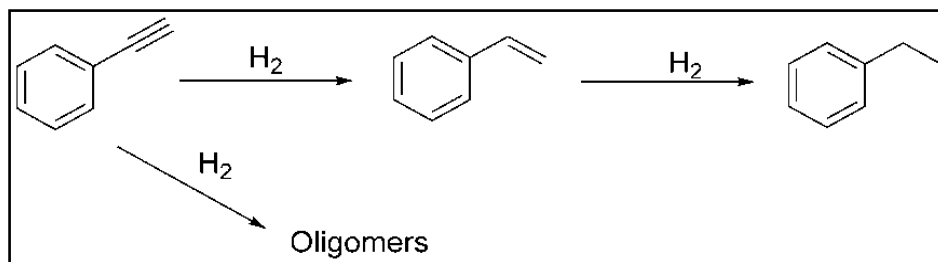
The most prominent catalyst for the selective liquid phase hydrogenation of C-C triple bonds is Lindlar's catalyst^[25] consisting of Pd supported on CaCO₃ and poisoned with Pb(OAc)₂ showing in many cases very high (Z)-alkene yields and low isomerization rates. It is produced by impregnation of Pd(OH)₂ on CaCO₃ followed by reduction in H₂ and subsequent wet-impregnation with Pb(OAc)₂^[25]. The catalyst can be optionally further poisoned by a nitrogen base, e.g. quinoline, before reaction. The H₂ uptake normally significantly decreases or even stops after 1 equivalent H₂ is consumed in the case of internal alkynes^[8]. When phenylacetylene was hydrogenated, Lindlar^[26] and also Sobczak^[27] noticed a considerable further H₂ uptake. However, N-doped polymers as additional modifiers for Lindlar's catalyst gave excellent yields (~98% selectivity at 100% phenylacetylene conversion)^[28]. The role of the support, the Pb additive and the base are still controversially discussed in literature. It was found, that Lindlar's catalyst consists on at least seven different species and the selective sites of Lindlar's catalyst are formed *in situ*^[29]. It is likely that the function of Pb is not an electronic modification of Pd but rather to block sites for alkene adsorption^[29,30]. Palczewska et al.^[31] used H₂ chemisorption and did not obtain evidence for significant diffusion of Pb in the Pd lattice. However they showed that the intermetallic compound Pd₃Pb was even more selective than Lindlar's catalyst for hydrogenation of acetylene, 2-butyne and phenylacetylene to the corresponding alkenes^[27]. The well-ordered structure of the intermetallic compound was claimed to be the reason of enhanced selectivity. García-Mota et al.^[32] used quantum chemical calculations and reached the conclusion that the role of quinoline is to reduce the ensemble size and hence to suppress C-C coupling reactions. The role of Pb was found to reduce the overall amount of H available at the surface and a strong modification in the alkene adsorption strength. In other studies^[33,34] the role of the modifiers of Lindlar's catalyst was attributed to a change in polarization of the Pd-H bond, which leads to different reactivity of H.

Compared to elemental Pd, intermetallic catalysts in the Pd-Ga systems have shown high selectivities and stability in the gas phase hydrogenation of acetylene at high temperatures^[35,36,37,38]. The high stability and selectivity of these catalyst materials was explained by their intrinsically modified crystal and electronic structure, which addresses three critical factors for selectivity: 1) the (partial) isolation of Pd atoms by Ga reduces the ensemble size of Pd 2) the d-band shifts away from the Fermi level, leading to reduced heats of adsorption, in particular favoring alkene desorption 3) the covalent bonds hinder diffusion of C or H in the subsurface and stabilize the intermetallic structure.

Pd₅Ga₂/SiO₂ prepared by impregnation was tested for the liquid phase hydrogenation of toluene by Komatsu et al.^[39]. Its selectivity to stilbene was rather low and falls below 70% at toluene conversions above 90%.

Our first results for the liquid phase hydrogenation of phenylacetylene with unsupported Pd₂Ga and PdGa did not reveal significant differences in the catalytic properties compared to monometallic Pd^[40]. In part I of this work^[41], highly dynamic changes of the surface of Pd₂Ga have been found to contrast the stability of the intermetallic compound in the bulk. Milled Pd₂Ga was single phase according to XRD and no phase transformation, e.g. formation of hydride, was detected during long-time treatment in a 10% H₂/He atmosphere. The bulk remained stable until about 300 °C in O₂ atmosphere. On the other hand the surface of the sample is, according to XP spectra and HR-TEM images, almost completely decomposed: Ga segregation due to mechanical treatment leads to an inhomogeneous overlayer of oxidized Ga species, where nanoparticles of mainly elemental Pd, Pd oxide and presumably undefined Pd species as well as some Pd₂Ga are embedded. A metallographic specimen, polished under Ar, was adopted as reference material for XP spectroscopy, since its comparably marginally disturbed surface could be easily reformed by heating to 400 °C in dynamic vacuum in the *in situ* XPS chamber. This procedure was insufficient for the powdered materials and led only to a partial reversal of the decomposition. An almost clean surface of the powder could be achieved after treatment for 4 h at 400 °C in 5% H₂/Ar and subsequent cooling in this reducing atmosphere. Within the scope of the detection limit of XPS, Pd was solely intermetallic when analyzing the Pd 3d core level spectra. However, the Ga 3d spectra still reveal some oxidized Ga at the outermost surface, which necessarily

involves a Pd enrichment in the near surface. This enrichment might be balanced by the intermetallic compound due to its homogeneity range^[42] but the presence of small amounts of elemental Pd agglomerates could not be excluded. As consequence of the high oxophilicity of Ga on the one hand and the ability of Pd to activate H₂ on the other hand we found a high dynamic of the surface, whose structure strongly depends on the pre-treatment and the actual chemical environment.



Scheme 4-1 Reaction scheme for the hydrogenation of phenylacetylene

Based on the characterization results presented in part I^[41] we address in this part of the work how Pd₂Ga with its strong electronic modification performs under the conditions of a liquid phase hydrogenation.

4. 2 Materials and Methods

4. 2. 1 Synthesis of Pd₂Ga

Pd₂Ga was synthesized as described in part I^[41] by melting stoichiometric amounts of palladium granules (Chempur, 99.95%) and Ga pellets (Chempur, 99.99%) in a glassy carbon crucible in a high frequency induction furnace under Ar atmosphere. The obtained regulus was annealed at 800 °C in an evacuated quartz glass ampoule for three days. To get a fine powder of Pd₂Ga, the material was powdered in a swing mill (Retzsch, MM 200, 4 ml WC pot with two WC balls, 25 Hz) two times for 30 min. The absence of any additional phases was verified by powder X-ray diffraction.

4. 2. 2 X-ray diffraction

For *ex situ* powder X-ray diffraction the sample was placed on a 3 μm Kapton TM foil covered with vaseline. The measurement was performed on an image plate Guinier camera (G670, Huber, Cu K α_1 radiation, $\lambda = 1.54056 \text{ \AA}$, curved Ge monochromator, $3^\circ < 2\Theta < 100^\circ$, CCD detector).

4. 2. 3 X-ray photoelectron spectroscopy

Near ambient pressure X-ray photoelectron spectroscopy^[43] was performed at the ISIS beamline at Bessy II, Helmholtz Zentrum Berlin. Approximately 250 mg of powdered samples were pressed in air to a pill with 8 mm diameter and about 1 mm thickness. For the XPS investigation of a spent sample 300 mg catalyst were used for the hydrogenation procedure described below. After reaction the organic phase was decanted in air and the catalyst was washed three times with n-hexane and dried in vacuum at about 1 mbar. Ga 3d, Pd 3d and C 1s core levels as well as the valence band region were recorded. Spectra were taken with various excitation energies corresponding to kinetic energies of the photoelectrons of 145 eV, 385 eV or 785 eV. Using 3-times the inelastic mean free path given for elemental Pd^[44], these kinetic energies refer to an information depth of 1.3, 2.0 and 3.4 nm as a rough estimation. Analysis of the spectra was performed by the software CASA XPS.

4. 2. 4 HR-TEM

A Philips CM200FEG microscope operated at 200 kV and equipped with a field emission gun, Gatan imaging filter and an energy-dispersive X-ray (EDX) analyzer was used. The coefficient of spherical aberration was $C_s = 1.35 \text{ mm}$ and the information limit was better than 0.18 nm. High-resolution images with a pixel size of 0.016 nm were taken at the magnification of $1.083.000 \times$ with a CCD camera, and selected areas were processed to obtain the power spectra (square of the Fourier transform of the image), which were used for measuring interplanar distances ($\pm 0.5 \%$) and angles ($\pm 0.5 \text{ deg}$) for phase identification.

4. 2. 5 Catalytic hydrogenation

The following reagents were used: n-hexane (Roth > 99%), n-octane (Acros Organics 99%+), n-decane (Acros Organics, 99%+), phenylacetylene (Aldrich, >98%), styrene (Merck, 99%, stabilized), ethylbenzene (Aldrich, anhydrous, 99.8%), Lindlar's catalyst (Aldrich, 5 wt% Pd on CaCO₃, poisoned with Pb), Pd/Al₂O₃ (5 wt% Pd, Aldrich), Pd powder (< 20 µm Aldrich, 99.9%) and H₂ (Westfalengas, 99.999%). Liquids beside n-octane, n-decane and n-hexane were distilled under Ar before use. n-Octane, n-decane and phenylacetylene were optionally stored under Ar adding a 4 Å molecular sieve (Roth).

Most hydrogenation reactions were carried out using a commercial autoclave (Büchi AG, Switzerland, 100 ml glass vessel) equipped with a heating jacket and a hydrogen dosing system. In a typical run the catalyst powder is added to a mixture of 80-100 ml n-octane, 1 ml n-decane as internal standard and ~3 ml (27 mmol) substrate. The mixture is purged with Ar and heated to the reaction temperature, usually 40 °C, under stirring (1250 rpm). The reaction system is flushed with H₂ (total pressure 1-4 bar), which is the starting point of the reaction.

For reactions under very inert conditions a reduction tube can be transferred and connected to a Schlenk line after high temperature reduction of the catalyst. A small part of the catalyst containing tube can be sealed off at $\sim 10^{-5}$ mbar avoiding additional contact with gaseous atmospheres. The ampoule is put in a custom-made glass reactor (~ 200 ml total volume, an image is shown in Figure 4-8). A magnetic stirring bar and three glass-baffles ensure turbulent flow during hydrogenation reaction. H₂-supply, thermocouple and the sample taking system were connected via KF-flanges. The setup allows a bake-out under high vacuum ($\sim 10^{-4}$ mbar). Two spindle valves were attached as inlet for the liquids and for the connection to the Schlenk line, equipped with an oil diffusion pump. The reaction can be started as the stirrer is turned on and the catalyst containing ampoule breaks. Thus the surface of the catalyst contacts immediately the alkyne. For analyses, either an Agilent 7820A GC equipped with a FID detector and a DB-WAX column or an Agilent GC-MS 5975B equipped with a MS and FID detector and a DB-1 column were used. Conversion X_{PA} and selectivity to styrene S_{Sty} for the hydrogenation of phenylacetylene were calculated using the following

formula, where c_{Sty} , c_{EB} and c_{PA} are the concentrations of styrene, ethylbenzene and phenylacetylene and c^0 are the initial concentrations:

$$X_{PA} = \frac{c_{Sty} - c_{Sty}^0 + c_{EB} - c_{EB}^0}{c_{Sty} - c_{Sty}^0 + c_{EB} - c_{EB}^0 + c_{PA}} \quad (1)$$

$$S_{Sty} = \frac{c_{Sty} - c_{Sty}^0}{c_{Sty} - c_{Sty}^0 + c_{EB} - c_{EB}^0} \quad (2)$$

The conversion and the selectivity were reproducible within a scattering of $\pm 0.5\%$. The carbon balance was obtained by:

$$CB = \frac{c_{Sty} + c_{EB} + c_{PA}}{c_{Sty}^0 + c_{EB}^0 + c_{PA}^0} \quad (3)$$

Blindtests of phenylacetylene hydrogenation as well as all hydrogenation reactions using styrene as reactant show a constant carbon balance close to 100% with a scattering of max. $\pm 2\%$. However, a slight decrease of the carbon balance during phenylacetylene hydrogenation was frequently observed. Temporary adsorption^[17], oligomer formation or formation of carbonaceous deposits may account for this behavior. Unfortunately we were not able to quantify oligomers, for which the literature also not provide any description. These effects are not considered in formulas (1) and (2), but they will be discussed separately by means of carbon balances.

The initial activity towards styrene formation A_{Sty} , normalized to the catalyst mass, was calculated by the formula:

$$A_{Sty} = \frac{A_0 \cdot V_{Total}}{m_{Cat}} \quad (4)$$

V_{Total} represents the total volume of the solution during reaction and m_{Cat} is the mass of utilized catalyst for the catalytic run. A_0 is the slope of the plot of styrene concentration

versus time at $t = 0$ and was determined by the derivative of a numerical approximation of the concentration plot by a 4th order polynomial.

Investigations for mass transport influence were performed for hydrogenation of phenylacetylene at 4 bar and 40 °C with milled Pd₂Ga. The initial activity was independent of the stirring rate when using a minimum of 750 rpm. The reaction rate was independent of the catalyst mass, slightly increasing for low catalyst masses, but within the range of systematic error. The corresponding Arrhenius-plot (Figure 4-7) shows a linear dependency and the calculated apparent activation energy was 35.8 kJ/mol. This value is between those reported for an Pd oxide catalyst (46 kJ/mol)^[45] and for Pd/C (26.2 kJ/mol)^[17] or a polymer bound Pd complex (29 kJ/mol)^[18], evidencing the absence of considerable involvement of film diffusion limitation. The initial activity increases proportional with applied H₂ pressure, whereas the selectivity did not changed significantly. Due to the absence of pores in the unsupported intermetallic catalyst, internal mass transport limitations are not considered. Similar activities were detected for the commercial as well as for the custom-made reactor.

4.3 Results and Discussions

4.3.1 Hydrogenation of phenylacetylene with as prepared milled Pd₂Ga, Pd powder, Pd/Al₂O₃ and Lindlar's catalyst

The catalytic results for hydrogenation of phenylacetylene at 4 bar at 40 °C using the as prepared milled powder of Pd₂Ga were compared with different reference catalysts. The observed concentration profiles using Pd/Al₂O₃, Lindlar's catalyst and unsupported elemental Pd powder are shown in Figure 4-1. The corresponding conversion, selectivity and carbon balance plots are shown in Figure 4-10. n-Octane was chosen as solvent to minimize possible solvent effects on the reaction behavior due to the presence of additional functionalities. Pd/Al₂O₃ is a commercial catalyst which was used in earlier work as reference in the acetylene hydrogenation reaction^[36]. With this catalyst, a relatively high selectivity to the semi-hydrogenated product styrene (96.5%) can only be achieved at low conversions compare also Table 4-1, which is typical for a supported monometallic Pd catalyst in this type

of reaction. At full conversion the selectivity is lowered to 82.5%. In contrast, Lindlar's catalyst with its effective modification of the active Pd species provides the highest selectivity to styrene at low and still 94.5% selectivity at full conversion. The selectivity of Pd₂Ga (88.5%) is intermediate between the commercial catalysts, but very similar to that observed for pure Pd powder (90.5%). Similar observations were obtained in the hydrogenation of 1-hexyne and 2-methyl-3-butyne-2-ol (not further discussed here) indicating that the comparable properties of Pd and Pd₂Ga are not significantly substrate dependent. Apart from the selectivity towards over-hydrogenation to ethylbenzene we observed a spontaneous decrease in the carbon balance as soon as the reaction starts and it continuously decreases slightly in all cases, being most pronounced for the Pd/Al₂O₃ catalyst. Jackson et al.^[17] also observed during their analysis that the carbon balance in the beginning of the reaction rapidly decreases, but increases to a certain value during reaction. Adsorption, oligomer formation or carbonaceous deposits are the most likely reasons for this behavior.

The XP spectra of spent Pd₂Ga (Figure 4-9) reveal only the reduction of Pd oxide, which readily occurs under the hydrogenation conditions, while the amount of oxidized Ga is essentially the same and the majority of the Pd remains in elemental state. This suggests that the intermetallic surface cannot be re-formed *in situ* in liquid phase hydrogenation. This can be understood by taking into consideration that the reduction temperature of the oxidic overlayer is 180 °C in 10% H₂/He as shown in part I^[41], whereas the reaction temperature was only 40 °C.

The activities and selectivities summarized in Table 4-1 illustrate, that a direct comparison of the catalysts is rather difficult. The dispersion of the bulk catalysts is extremely low demanding a high amount of catalyst as clearly visible by means of the specific activities. The low specific surface area makes the application of chemisorption methods difficult which unfortunately impede the determination of the active surface area and thus the determination of a reliable turnover frequency.

Table 4-1: Comparison of initial activity and selectivity towards styrene S_{Sty} at low and full conversion and the carbon balance CB of as prepared, milled Pd₂Ga with Pd, Pd/Al₂O₃ and Lindlar's catalyst in the hydrogenation of phenylacetylene at 4 bar, 40 °C in octane in a commercial autoclave.

Catalyst	A _{Sty} / (mmol/(g _{Cat} *h))	S _{Sty} / % (±0.5%) (X _{PA} ≈ 10%)	S _{Sty} / % (±0.5%) (X _{PA} ≥ 99%)	CB / % (±2%) (X ≥ 99%)
Pd ₂ Ga as prepared	478	95.0	88.5	94.5
Pd powder	417	97.0	90.5	96
Pd/Al ₂ O ₃	9828	96.5	82.5	91
Lindlar's catalyst	4939	98	94.5	96.5

As the specific activity is low, the selectivity towards over-hydrogenation is considerably suppressed even with unmodified Pd powder, which might be related to the unusual dispersion of all of our model catalysts. Additionally, compared to acetylene hydrogenation in earlier studies^[35], conclusions on the selectivity behavior in the liquid phase hydrogenation of phenylacetylene are handicapped by a lack of exact quantification of potentially formed oligomers. Nevertheless, the carbon balance of usually 95% and above suggest, that any oligomers are rather minority products. The big advantage of using bulk model catalysts is, that their characterization with XPS and XRD is straightforward and more reliable compared to supported systems. Simultaneously, the absence of any support or modifier allows studying the intrinsic properties of the materials. It was shown in part I^[41] that the surface and the electronic structure of Pd₂Ga is highly dynamic and strongly depending on the pre-treatment. The main focus of this study lies on the comparison of the catalytic behavior of Pd₂Ga after different pre-treatments and the resulting surface state rather than the direct comparison of a series of catalysts. However, finally comparing the rate of ethylbenzene formation in presence of phenylacetylene and the initial rate of ethylbenzene formation from pure styrene allows revealing qualitative differences in the operation mode of the different catalysts.

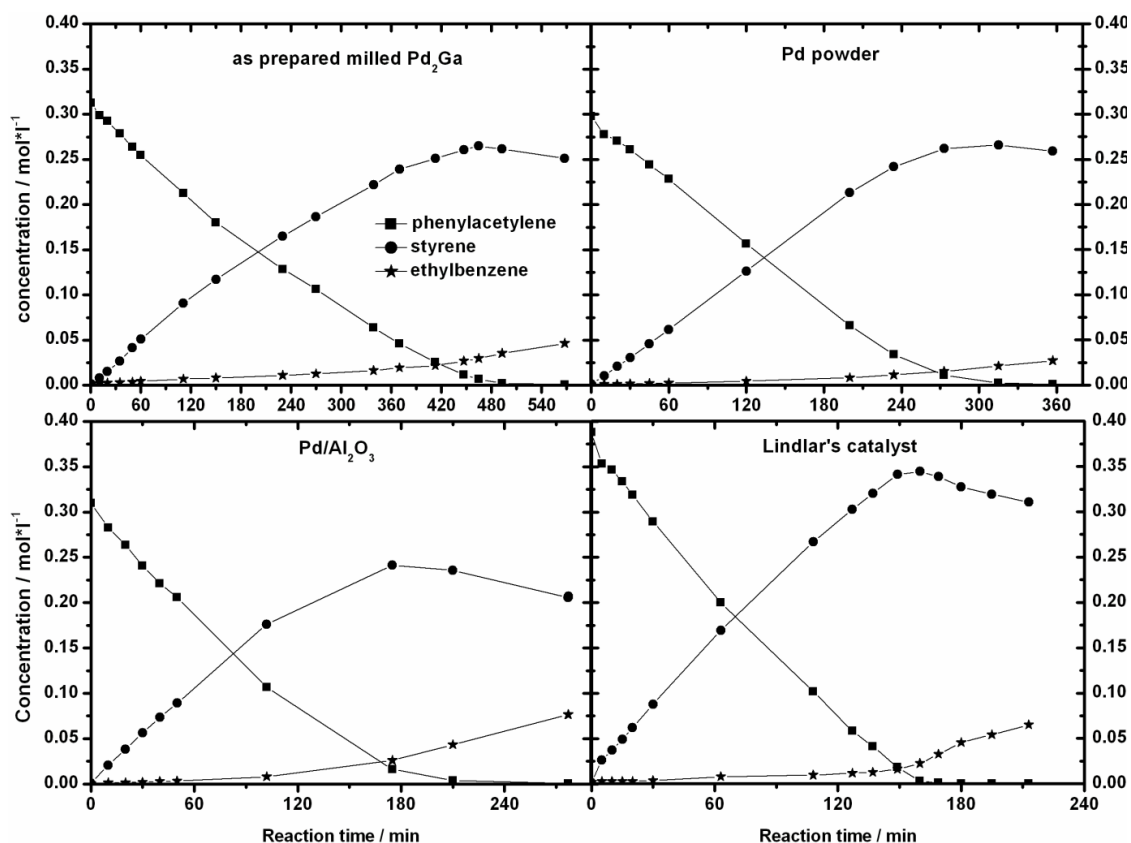


Figure 4-1: Concentration profiles during the hydrogenation of phenylacetylene at 4 bar, 40 °C in octane using Pd₂Ga (10 mg), Pd powder (10 mg), Lindlar's catalyst (3.5 mg, 5 wt-% Pd) and Pd/Al₂O₃ (0.8 mg, 5 wt-% Pd).

4. 3. 2 Hydrogenation of phenylacetylene with Pd₂Ga after different pre-treatments

A reductive pre-treatment at 400 °C is sufficient to heal structural disturbances in the bulk and to regenerate the intermetallic surface to a large extent. Thus, the catalysts were submitted to a corresponding pre-treatment to study the catalytic properties of the intact intermetallic surface. As a first attempt to avoid the re-oxidation of the freshly reduced powder, it was transferred into a glove box without contact to air immediately after reduction and covered with degassed octane, used as solvent in the reaction. The suspension was transferred in a wet state without air-contact into the commercial setup which was baked out at 100 °C and purged with Ar directly before the experiment. This level of effort is appropriate for many air and/or water sensitive reactions. When the reaction is performed after such a pre-treatment, a considerably lower initial reaction rate but a strong increase over time was observed as visible in Figure 4-2 (the corresponding plots for conversion, selectivity and carbon balance are shown in Figure 4-11. This is a clear indication that the surface undergoes modifications during reaction and that the catalyst is not stable. The activating

behavior can be understood considering the significant d-band shift of Pd₂Ga compared to Pd. Due to the significantly lower density of states at the Fermi level one would expect, that the intermetallic compound provides a lower intrinsic activity than Pd. In part I^[41] we have shown that the oxophilicity of intermetallic Ga is still high leading easily to surface oxidation even at very low partial pressures (< 100 ppb) of oxidants similar to elemental Ga. It is likely that the small residues of water or oxygen – hardly avoidable in such a reactor – attack the surface even under these reductive conditions forming a more Pd enriched surface embedded in Ga oxide leading to the increasing activity.

In a further attempt to study the intrinsic catalytic properties of the intermetallic surface and, in turn, to diminish further the influence of residues of water and oxygen, the reaction was performed under even more inert conditions using a tight glass reactor and Schlenk techniques. The freshly pre-reduced catalyst was sealed directly in the glass reduction tube, connected to a Schlenk line. The catalyst-containing ampoule and a magnetic stirring bar were placed in the reactor and subsequently subjected to a thorough bake-out at ~ 100 °C and dynamic vacuum (10^{-4} mbar). The dried liquids were then filled inside the reactor using Schlenk technique. For degassing, the liquids were frozen in liquid nitrogen and degassed under high vacuum at 10^{-4} mbar before defrosting. The sequence was repeated four times. The reaction was started when the atmosphere was changed from Ar to H₂ after the stirrer was turned on and the catalyst-containing ampoule was broken. This procedure provides the advantage that the catalyst does not come into contact with any gaseous atmosphere and is immediately covered by the solved alkyne – the latter binds strongly to the surface of the catalyst and might protect it from oxidation. Under these conditions a more stable initial reaction rate could be achieved (Figure 4-2). Nevertheless, also in this case the reaction rate slowly increased with time indicating instability of the catalyst. The specific activity is significantly lowered by a factor of about 20, compared to the as prepared Pd₂Ga at least at the beginning of the reaction.

The milled Pd₂Ga was also treated in 100% Ar at 400 °C for 4 h but the activity was only slightly lower without an activation period (compare Table 4-3). This indicates that the lower activity of the pre-treated catalyst does hardly originate from changes in surface area during the heat-treatment. The specific surface area was determined before (0.27 ± 0.01 m²/g) and

after pre-reduction at 400 °C ($0.28 \pm 0.01 \text{ m}^2/\text{g}$), revealing no significant change. The increase in reaction rate is furthermore not due to a possible mechanical split of slightly agglomerated particles after high temperature treatment. Such an artifact was excluded by an experiment where an ultra-sonic treatment after breaking the ampoule and before switching to H₂ atmosphere had no influence on the observed activation behavior.

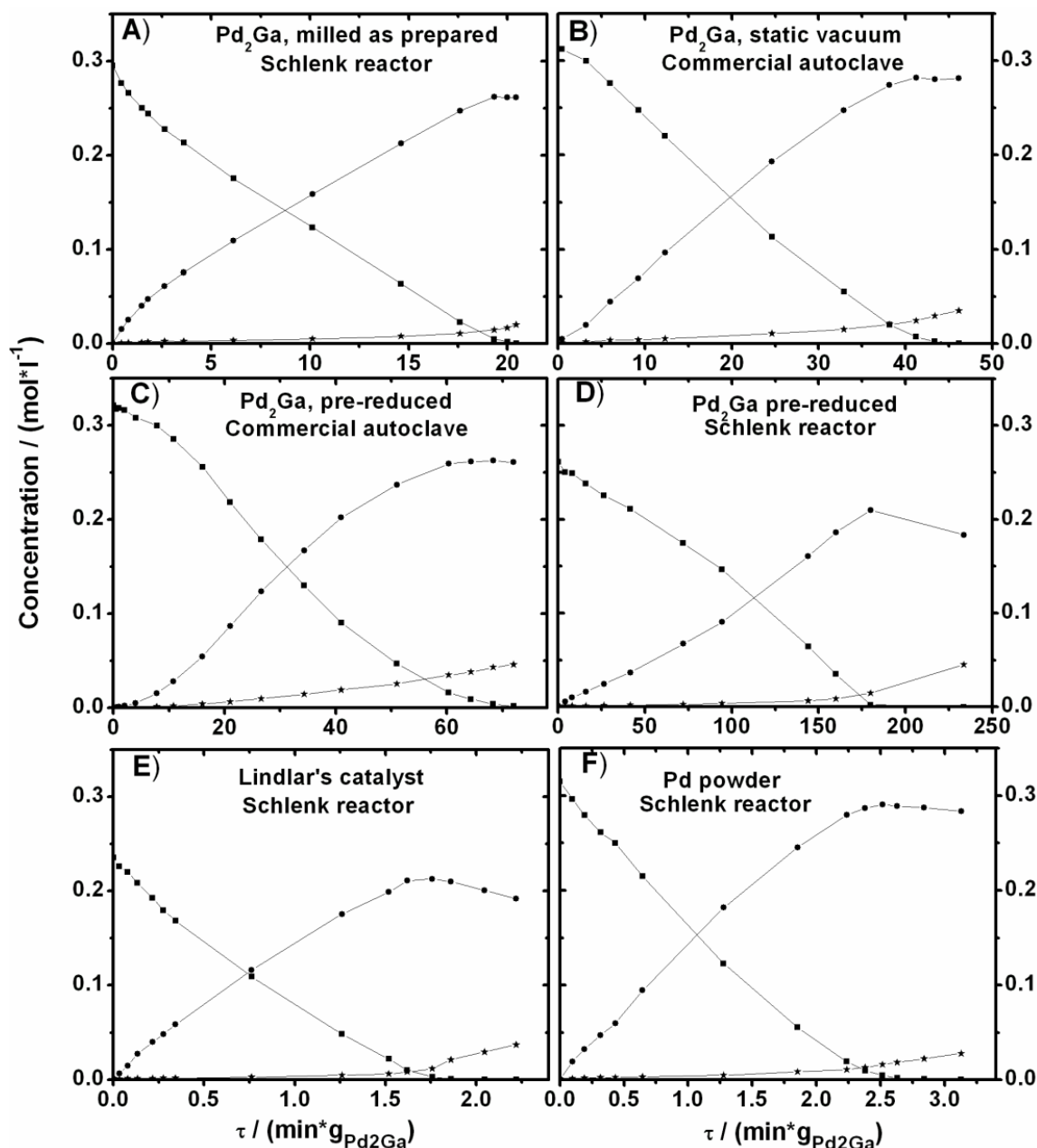


Figure 4-2: Concentration profiles of phenylacetylene hydrogenation for Pd₂Ga after different pre-treatments as well as Pd powder and Lindlar's catalyst as reference catalysts. For better visualization of the strongly different activity of the Pd₂Ga catalyst after the pre-treatments, the reaction time was multiplied by the catalysts mass on the x axis. Note their very different scales. All reactions were carried out at 40 °C in octane at ~ 1 bar, except Pd₂Ga pre-treated in static vacuum (4 bar, compare Table 4-3).

Taking into account that the total concentration of Pd on the outermost surface increases after pre-reduction^[41] we can also exclude that the lower activity originates from a significantly lower Pd surface concentration. In contrast to the pre-treatment at 400 °C in Ar, a pre-treatment at the same temperature in a static vacuum (14 h in static vacuum in a quartz glass ampoule at $p \leq 1 \cdot 10^{-3}$ mbar, then stored in air), showed a very small activation in the beginning of the hydrogenation reaction (Figure 4-2) but yields essentially a stable catalyst afterwards. The reaction rate is ~ 5.7 times lower compared to the sample as prepared or pre-treated in 100% Ar at 400 °C. This result is in agreement with the observation that 400 °C and (dynamic) vacuum is sufficient for a partial reduction of Ga oxide accompanied with an almost symmetric but still relatively broad Pd 3d peak, shifted to 335.6 eV as shown in part I^[41]. After this procedure a passivation layer still exists and the sample is stable even after long time air-contact without mechanical load.

Taking these experiments into account it is most likely that the strongly decreased activity originates from the modified electronic structure of the intermetallic compound, which is expected due to the significantly shifted d-band of Pd₂Ga compared to Pd. However, we are not able to decide unambiguously, whether only Pd₂Ga or very small amounts of probably highly dispersed Pd on top of (inactive) Pd₂Ga catalyzes the reaction. For the still existing increase in reaction rate with reaction time, leaching of Pd and thus contribution of homogeneous catalysis during the reaction might be responsible. To verify the absence of a homogeneous contribution, the catalyst was separated from the solution. After adding fresh phenylacetylene to this solution, no further catalytic activity was observed, which clearly rules out a homogeneous contribution to the catalytic activity. A more likely scenario is that traces of O₂ or H₂O, which cannot be avoided *completely* even with the precautions taken in the Schlenk reactor, lead to advancing decomposition of the surface and surface enrichment of elemental Pd with higher activity. Thus, the intermetallic surface could function like a getter-material for oxygen even in apparently inert atmospheres.

Table 4-2: Lattice parameters and FWHM of the 203 reflection of pre-reduced Pd₂Ga used for hydrogenation of a) phenylacetylene and b) styrene. The values for a fresh sample pre-reduced at 400 °C are given for comparison (c).

Sample preparation	<i>a</i>	<i>b</i>	<i>c</i>	FWHM / °
a)	5.4715(2)	4.0582(1)	7.7849(2)	1.2
b)	5.4799(2)	4.0550(1)	7.7835(3)	0.27
c)	5.4815(1)	4.05556(3)	7.7859(1)	0.23

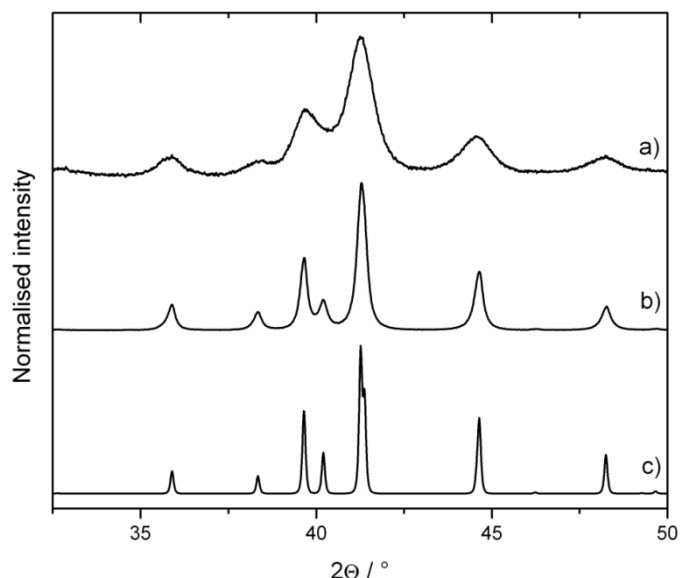


Figure 4-3: X-ray diffraction pattern of pre-reduced Pd₂Ga (a) after liquid phase hydrogenation of phenylacetylene under inert conditions; (b) after styrene hydrogenation. c) represents the calculated pattern according to [46].

XRD analysis of the spent sample (mixed with borosilicate glass, which originates from the broken glass ampoule) revealed a strong broadening of the reflections compared to the freshly reduced Pd₂Ga (Figure 4-3 b). The positions of the reflections do not significantly change and within the detection limit of this method other crystalline phases are absent. The reason for the broadening is visible in TEM images. While the freshly reduced samples show large domains of crystalline Pd₂Ga^[41] with smooth surfaces, the samples after catalysis show ensembles of nanoparticles (Figure 4-4). Also the bulk of the particles exhibits contrast fluctuations indicating that the crystallites have been broken into smaller domains. At the edges of the particles also amorphous material is present between the metallic nanoparticles. The amorphous material is likely related to Ga oxide and also carbon depositions, the latter could partially explain the notably decrease in the carbon balance. However, it is not possible to decide whether Ga oxide is formed already during reaction or by unavoidable contact with air during sample recovery after reaction. Attempts to identify the nature of the metal nanoparticles by HR-TEM did not result in a clear indication for the presence of elemental Pd.

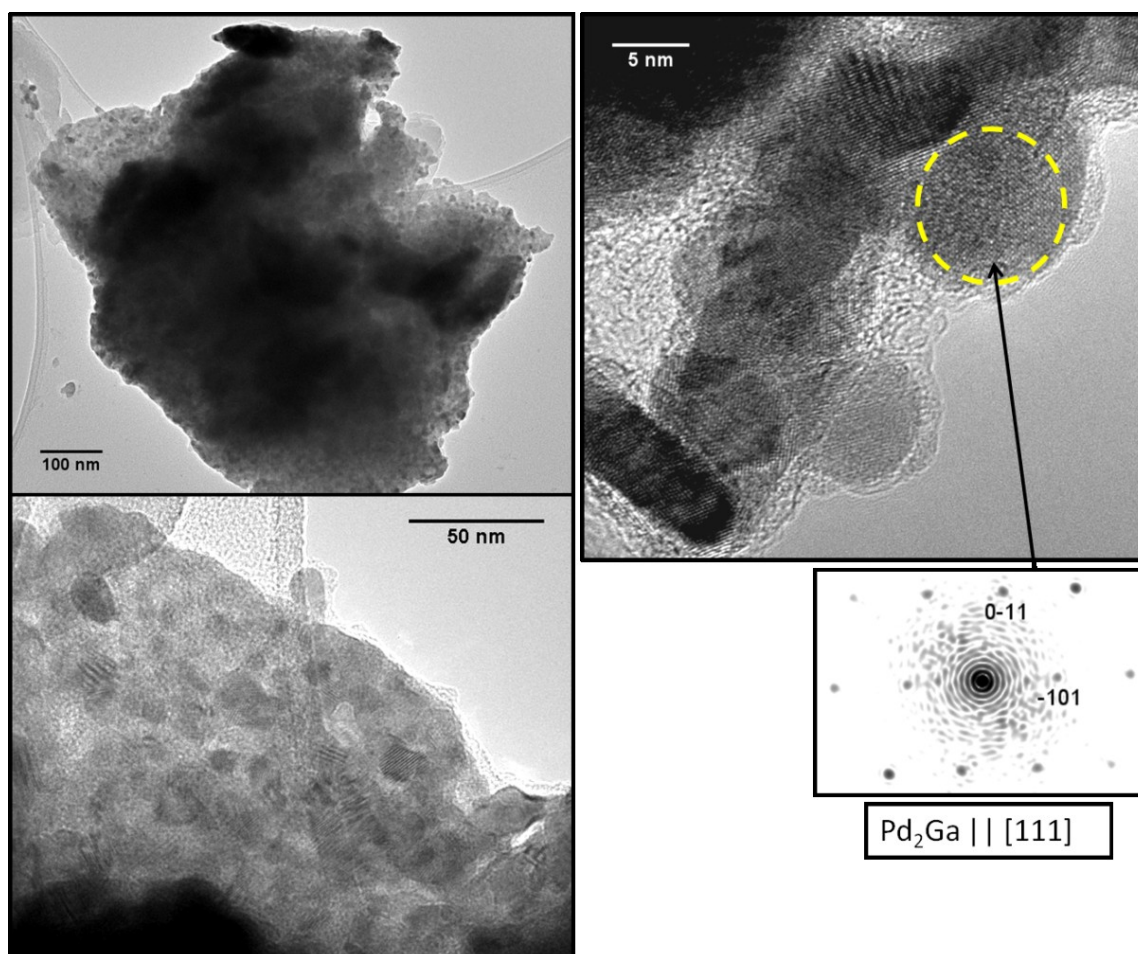


Figure 4-4: HR-TEM of a sample spent for phenylacetylene hydrogenation. In contrast to a pre-reduced fresh sample, the particles are cracked in smaller domains. According to Fourier analysis the surface consists of Pd₂Ga nanoparticles. An amorphous phase is also detected, which can be related either to carbon or Ga oxide. The sample was exposed to air after reaction and before TEM imaging.

Unfortunately, an analysis by XPS was not possible due to strong charging of the glass containing sample. The formation of cracks and small domains might induce the formation of pores, which would certainly enhance the surface area during reaction and thus the reaction rate. This change in the microstructure of the whole catalyst particles and the observed increase in reaction rate can certainly not be explained only by the attack of oxygen or water impurities. Phenylacetylene seems to chemically attack the material.

It is noted that according to the necessary reduction temperature for the oxidized layer of ~180 °C as determined on the unsupported particles, a stable catalytic reaction on the clean intermetallic surface might be possible in gas phase hydrogenation at considerably higher temperatures than usually applied in triple bond hydrogenation reactions as reported earlier. Indeed, at 200 °C and without reductive pre-treatment a clear selectivity difference between

Pd₂Ga and a commercial Pd/Al₂O₃ catalyst was achieved and a stable reaction rate was observed^[35]. However, concerning supported Pd₂Ga nanoparticles a remarkably similar activation behavior during acetylene hydrogenation with time on stream has been observed after pre-reduction at high temperatures^[35]. Alike to the gradual increase in reaction rate in the liquid phase, a long activation period without major changes in the selectivity has been reported. It seems likely that this behavior is also related to a gradual decomposition of the intermetallic surface liberating highly active Pd species from the less active intermetallic compound. Partial surface decomposition of supported Pd₂Ga nanoparticles has also been reported for application in methanol steam reforming, however, under more oxidizing conditions^[47].

Table 4-3: Initial activity towards styrene formation (A_{Sty}) and selectivities to styrene (S_{Sty}) as a function of the pre-treatment and the used reactor for hydrogenation of phenylacetylene. Pre-reduction was 5% H₂/Ar for 4 h at 400 °C. ~ 3 ml phenylacetylene were solved in octane (80-100 ml). The reaction temperature was always 40 °C.

Catalyst	Pre-treatment	Reactor (p / bar)	$A_{Sty} /$ (mmol / (g _{cat} · h))	$S_{Sty} / \% (\pm 0.5\%)$ $X_{PA} \approx 10\%$	$S_{Sty} / \%$ $X_{PA} \geq 99\%$	CB / % $\pm 2\%$
Pd ₂ Ga	none	commercial (1.1)	121	96	88.5	96
Pd ₂ Ga	none	schlenk (1.3)	136	97	93	95
Pd ₂ Ga	400°C ~1·10 ⁻³ mbar	commercial (4)	84	95.5 ($X_{PA} \approx 20\%$)	89	99.5
Pd ₂ Ga	pre-reduced	commercial (1.1)	~5 (rapidly increasing)	(93)	(85)	96
Pd ₂ Ga	pre-reduced	schlenk (1.3)	7.1	97	(94)	86.5
Pd ₂ Ga	400 °C, 100% Ar,	schlenk (1.3)	121	96.5	n.d.	n.d.
Pd powder	none	schlenk (1.3)	641	97.5	93.5	98
Lindlar's catalyst	none	schlenk (1.3)	1154	99	95.5	96

4.3.3 Activity of styrene hydrogenation with pre-reduced Pd₂Ga, Pd powder and Lindlar's catalyst

The loss in the initial activity of pre-reduced Pd₂Ga under inert conditions is not accompanied by an intrinsic gain in selectivity. Compared to reactions carried out in the commercial reactor the selectivity does increase from 88.5% to 93% at full conversion, but such higher selectivity was also obtained with all reference catalysts (Figure 4-2, Table 4-3) in the custom-made reactor and is probably an effect of using distilled and dried phenylacetylene. However, determining the selectivity at 100% conversion for the pre-reduced catalysts is not very meaningful, since the catalyst in this state is already partly decomposed. A clear

difference can be seen in the carbon balance, which decreases to ~86%, which is significantly lower than in the case of all other catalysts and further lowers the overall yield of styrene. We therefore had a closer look on the initial activity in styrene hydrogenation. Using phenylacetylene as educt the initial rate of styrene hydrogenation is very low compared to styrene formation for Pd, Pd₂Ga as well as Lindlar's catalyst.

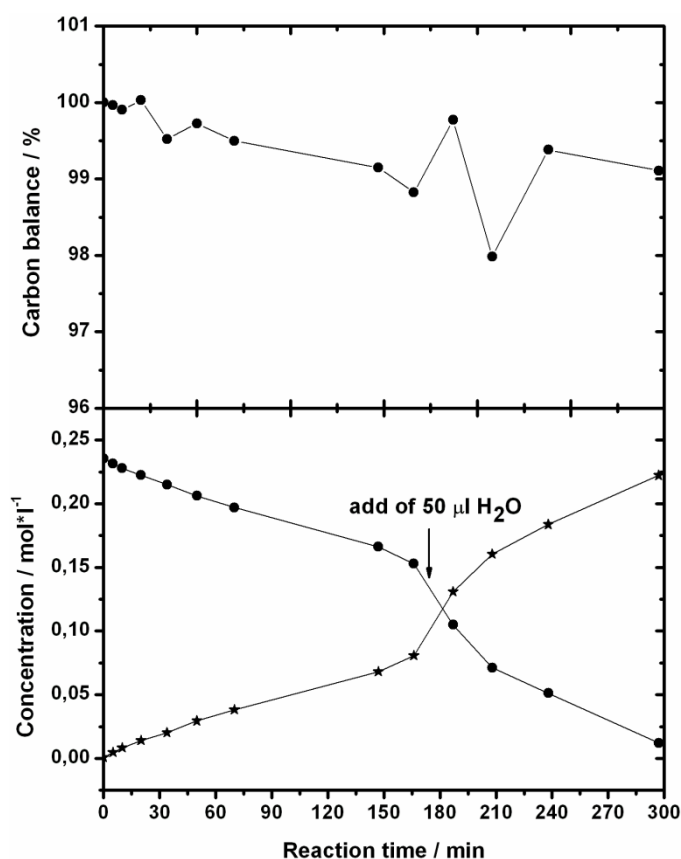


Figure 4-5: Hydrogenation of styrene (circles) with pre-reduced Pd₂Ga to ethylbenzene (stars). Adding small amounts of H₂O under H₂ atmosphere result in spontaneous increase in reaction rate.

Using pure styrene as educt leads in all cases to a significant enhancements of the initial rates of ethylbenzene formation, see Table 4-4. The carbon balance remains constant, close to 100%, indicating that carbonaceous species and oligomers originate from phenylacetylene. Contrariwise to the phenylacetylene hydrogenation, no increase in reaction rate, was observed over time for pre-reduced Pd₂Ga if very inert conditions were applied (Figure 4-5), which suggests that the increase in reaction rate in phenylacetylene hydrogenation is not only caused by O₂ or H₂O impurities, but is a complex convolution of different influences, including the chemical interaction with phenylacetylene, possibly promoted by mechanical load due to stirring. The XRD pattern of such a spent sample revealed only marginal

reflection broadening (Figure 4-3). The crucial role of oxidizing impurities was proven during styrene hydrogenation by adding 50 µl H₂O during the reaction in H₂ atmosphere, which corresponds to a total water concentration of about 500 ppm. We observed a spontaneous sharp increase in reaction rate, indicating oxidative decomposition of the catalyst (Figure 4-5).

Table 4-4: Initial reaction rate of ethylbenzene formation (A_{EB}) for Pd, pre-reduced Pd₂Ga and Lindlar's catalyst. All reactions were carried out in the Schlenk reactor and the reaction conditions for styrene hydrogenation are similar to that described for phenylacetylene hydrogenation. A_{Sty} is given for comparison. The ratio between both activities is calculated for the catalysts.

catalyst	Substrate	$A_{EB} / (\text{mmol}/(\text{g}_{\text{cat}} \cdot \text{h}))$	$A_{Sty} / (\text{mmol}/(\text{g}_{\text{cat}} \cdot \text{h}))$	$A_{Sty} : A_{EB}$
Pd powder	phenylacetylene	16.9	641	37.9
Pd powder	styrene	1096	-	0.58
Pd ₂ Ga pre-reduced	phenylacetylene	0.2	7.1	37.5
Pd ₂ Ga pre-reduced	styrene	7.6	-	0.94
Lindlar's catalyst	phenylacetylene	19.5	1154	59.2
Lindlar's catalyst	styrene	991.2	-	1.16

Comparing the ratio of the initial activities of the phenylacetylene hydrogenation and the hydrogenation of pure styrene, the Pd, pre-reduced Pd₂Ga and Lindlar's catalyst show differences. It is 0.58 for pure Pd powder, meaning that double hydrogenation occurs clearly faster than triple bond hydrogenation. This is typically for Pd catalysts, e.g. in the gas phase hydrogenation of acetylene^[48], and was also reported for the liquid phase hydrogenation of phenylacetylene^[49]. The ability to form hydrides makes Pd highly reactive towards alkene hydrogenation^[50]. The low selectivity towards styrene hydrogenation (see Table 4-4) with pure Pd in phenylacetylene hydrogenation is likely related to the modification of the surface by the alkyne. Irreversible carbon deposits and an *in situ* formed subsurface Pd-C phase^[51,52] reduces the availability of surface hydrogen and suppresses Pd hydride formation. The stability of the Pd-C phase decreases as the chemical potential of the alkyne decreases, which occurs continuously in a batch reaction. Thus at high conversions of phenylacetylene the Pd-C phase vanishes and the reaction becomes unselective. The ratio is 0.94 for pre-reduced Pd₂Ga, thus there is, compared to Pd, a lowered ability for styrene hydrogenation, while no clear difference in ethylbenzene selectivity at low conversions is observed when phenylacetylene is hydrogenated. The explanation is likely the inability of the almost clean intermetallic (sub)-surface to form highly reactive hydrides, which is intrinsic and does not depend on the presence of an alkyne. However, the electronic effect indeed significantly

lowers the activity of Pd₂Ga but does apparently not have a clear influence on the selectivity in phenylacetylene hydrogenation.

In the case of Lindlar's catalyst the initial activity towards styrene formation from phenylacetylene is slightly higher (1.16) than the initial activity towards ethylbenzene formation from pure styrene. In agreement with the literature, there is still a considerably ability for styrene hydrogenation if Lindlar's catalyst^[26,27] is not additionally poisoned with nitrogen bases. However, the rate of ethylbenzene formation from styrene in presence of phenylacetylene is still the lowest compared to the other catalysts. Lindlar's catalyst has a characteristic, which clearly distinguishes it from the other catalysts. There is a short but resolvable increase in rate of ethylbenzene formation when phenylacetylene is completely consumed followed by a sudden decrease at a certain point in time leading finally to a "s"-shape of the ethylbenzene concentration-profile, visible in Figure 4-1 as well as in Figure 4-2 E. A geometric effect of Pb^[29,30] by site-blocking can be considered here. Pb blocks the active sites necessary for alkene hydrogenation but alkynes with their higher heat of adsorption are able to compete for active sites, forcing Pb to restructure. They will be readily hydrogenated over the liberated sites. At the point where the phenylacetylene concentration becomes zero, free active sites are exposed leading to enhanced rates of ethylbenzene formation. Simultaneous restructuring of Pb can occur, which will lead to blockage of these sites diminishing again ethylbenzene formation. The ratio of the velocities of Pb restructuring and ethylbenzene formation determines the degree of over-hydrogenation at 100% conversion using Lindlar's catalyst.

4.4 Summary

The catalytic properties of Pd₂Ga after different pre-treatments for the hydrogenation of phenylacetylene were investigated in the present study. Based on the results of part I^[41] we focused on the stability of this catalyst as function of the pre-treatment with special focus on residual oxidants. The surface of as prepared Pd₂Ga consists mainly of Pd, Pd oxide, Pd₂Ga and Ga oxide (Figure 4-6 a). Despite the reduction of Pd oxide this catalyst is stable under hydrogenation conditions and behaves very similar to the elemental Pd powder used as reference here (Figure 4-6 B). An *in situ* re-formation of a clean intermetallic surface (Figure

4-6 D) does not occur. The powder must be subjected to an *ex situ* pre-reduction in 5% H₂/Ar at 400 °C (Figure 4-6 C). After this treatment the catalyst provides a considerable lower initial activity, which is likely due to the filled valence d-band of Pd₂Ga, shifted away from the Fermi level. However, the contribution of traces of highly dispersed elemental Pd to the activity cannot be excluded (compare also part I of this work [41]). The activity increases quickly over time during reaction and suggests the enrichment of Pd by *in situ* decomposition of the IMC. By applying very inert conditions the increase in activity can be delayed, indicating that the intermetallic surface can be easily oxidized even under reducing conditions in the liquid phase if traces of O₂ or H₂O are present.

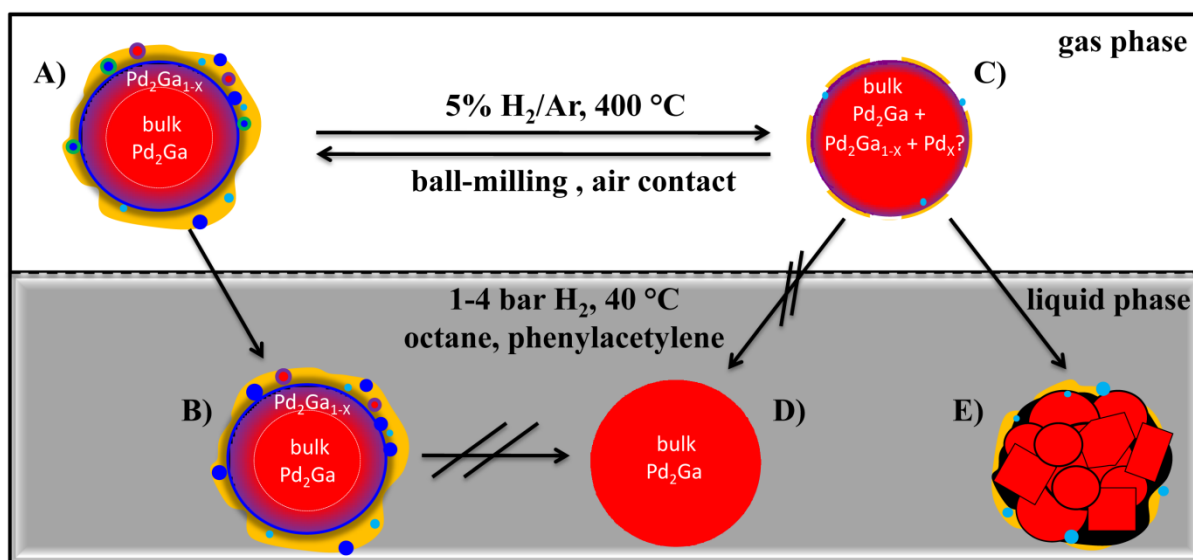


Figure 4-6: Schematic sketch of the structure of a microcrystalline Pd₂Ga particle before and after liquid phase hydrogenation and subsequent air contact. Red: Pd₂Ga, purple: Pd₂Ga_{1-x} (within the homogeneity range), yellow: surface Ga oxide, black: carbon, blue: elemental Pd, green: Pd oxides, light blue particles represent the presence of undefined Pd species. However, the exact nature and morphology of the Pd species is not known.

HR-TEM images as well as XRD of a spent sample show that, independent of the oxidative decomposition of the surface, the bulk gets affected probably by a chemical attack of phenylacetylene (Figure 4-6 E). In no case Pd was leached and thus no homogeneous hydrogenation occurs. The selectivity towards styrene is high even if pure Pd is used and cannot be outperformed by any Pd₂Ga catalyst. This behavior is certainly not comparable to supported systems. Differences in ethylbenzene formation activities are visible when pure styrene is converted to ethylbenzene in terms of a lower initial activity for double bond hydrogenation of Pd₂Ga compared to Pd. That suggests that the resulting surface provides an intrinsically lower ability for double bond hydrogenation, which originates from the

suppressed subsurface chemistry. Lindlar's catalyst still performed slightly better; here the selectivity control is likely a geometric effect due to an *in situ* restructuring of Pb, which competes with alkenes for surface Pd.

4.5 Conclusion

In this study we investigated the reactivity and stability of unsupported Pd₂Ga in the liquid phase hydrogenation of phenylacetylene. We observed a strongly reduced hydrogenation activity for Pd₂Ga when exposing an almost clean intermetallic surface, which originates from the valence d-band of Pd, shifted away from the Fermi level, in agreement with the d-band theory^[53,54]. However, the obtained results during phenylacetylene hydrogenation confirm the high surface dynamics and the tendency for oxidative decomposition of Pd₂Ga at the surface, which was observed in UHV and gaseous atmosphere in part I of this work. Under the mild conditions of the liquid phase hydrogenation this oxidation is not reversible. Besides the surface dynamics, the observed decay of the bulk structure during phenylacetylene hydrogenation is an additional upcoming issue.

The spectroscopic and catalytic results of part I and of this study hold an important aspect for the general concept of modifying catalytic properties by d-band manipulation. In order to take practical advantage of this significant electronic modification by alloying or formation of intermetallic compounds, not only the electronic structure itself, but also its stability needs to be carefully investigated in particular at the surface. The targeted strong electronic modification can be achieved using chemically different metals, e.g. a noble and non-noble component^[55,56]. For instance, compared to Pd the d-band of Pd₂Ga is significantly more shifted than in a Pd-Ag alloy. However, the present results show that for catalytic application one is not completely free in choosing a suitable combination within this concept. The strong modification might be accompanied by an increased instability and propensity towards surface reactions or relaxation that reverses the aimed effect. Covalent interactions between Pd and Ga in Pd₂Ga, lead to a strong electronic modification, but unfortunately not to a sufficient stability. It is the strong oxophilicity of Ga that handicaps practical application in liquid phase hydrogenation catalysis. Intermetallic compounds with their different crystal and electronic structures has been shown to offer interesting potential for various reactions e.g.

methanol steam reforming with Pd₂Ga^[57] or PdZn^[58,59,60] or acetylene hydrogenation with Al₁₃Fe₄^[61] as noble metal free catalyst. However, despite a stable bulk, the IMC surface might rather act as a precursor for the formation of the truly active surface as it is the case for PdZn in methanol steam reforming. The less noble metals like Ti, Zn, Al or In face the same issues like Ga. The surface structure and their electronic structure are dynamic and difficult to control and can get modified by forming a contingent passivation layer with a provisory stability. Thus the catalytic properties will strongly depend on the preparation, pre-treatment and the reaction conditions. For the special case of Pd₂Ga in liquid phase hydrogenation of phenylacetylene we found indications, that the almost clean intermetallic surface without passivation does not protect the surface or the bulk from decomposition. Thus, when making theoretical predictions based on the electronic structure or crystal structure of an intermetallic compound or alloys, chemical dynamics and instabilities need to be considered for application as catalysts. In this case, the price for a concerted d-band manipulation was a practically insufficient stability.

4.6 Supporting information

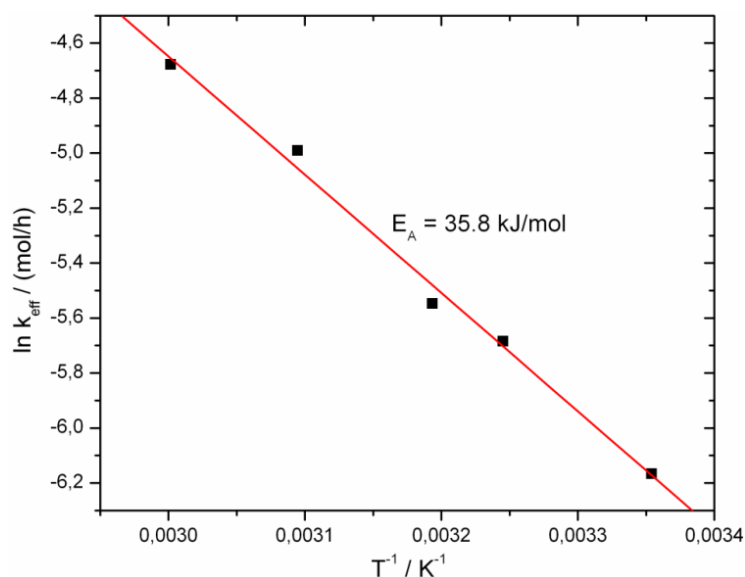


Figure 4-7: Arrhenius-plot for the hydrogenation of phenylacetylene carried out in octane at 4 bar H₂ pressure. The temperature was set to 25 °C, 35 °C, 40 °C, 50 °C and 60 °C.

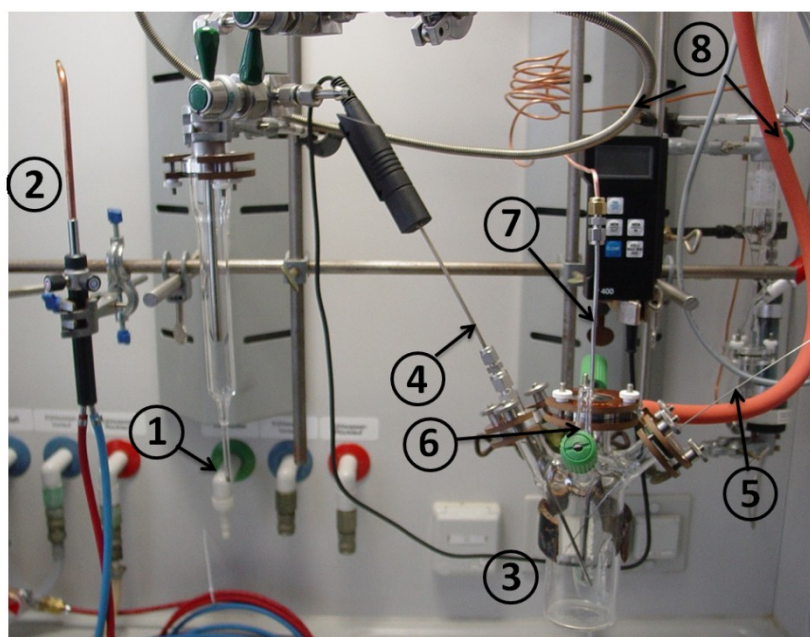


Figure 4-8: Image of a part of the hydrogenation reactor for reactions under very inert conditions: 1 Catalyst containing ampoule, 2 burner, 3 hydrogenation vessel with baffles, 4 thermo-couple, 5 cannula terminated with a 4-way valve (not shown) for sample taking, 6 spindle valve to introduce liquids, 7 H₂ source, 8 connections to the Schlenk line for vacuum and inert gas.

Table 4-5: Comparison of peak maxima and FWHM of Pd 3d_{5/2} at different kinetic energies and quantification of Pd and Ga: a) milled powder as prepared b) spent sample without pre-reduction. The similarity of Ga oxide content and metal ratios is obvious.

E _{Kin} / eV	Peak-maximum / eV			Peak-FWHM / eV			Pd ^{total} :Ga ^{total}			Pd ^{total} :Ga ⁰			Ga ³⁺ :(Ga ³⁺ +Ga ⁰)/%		
	785	375	145	785	375	145	785	375	145	785	375	145	785	375	145
a)	335.5	335.4	335.2	1.3	1.2	n.d.	1.0	0.9	0.6	4.5	7.4	29.8	78.0	88.1	97.9
b)	335.4	335.3	335.4	1.2	1.1	1.2	1.1	0.8	0.6	4.8	6.7	13.4	78.0	88.1	95.3

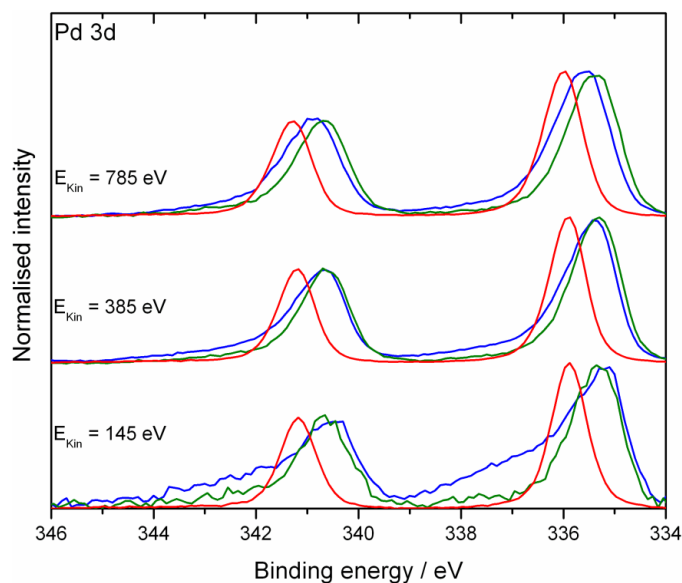


Figure 4-9: XPS depth profiling of the Pd 3d core level for different Pd₂Ga samples. Blue lines represent the as-prepared milled Pd₂Ga consisting mainly of Pd. At the outermost surface oxidized Pd also seems to be present as indicated by the long tail of the peak. Green lines represent a sample used for liquid phase hydrogenation. The Pd oxides vanish during reduction but the surface consists still mainly of elemental Pd, possibly alloyed with some Ga. Red lines represent the metallographic specimen of Pd₂Ga heated to 400 °C and is shown as reference here.

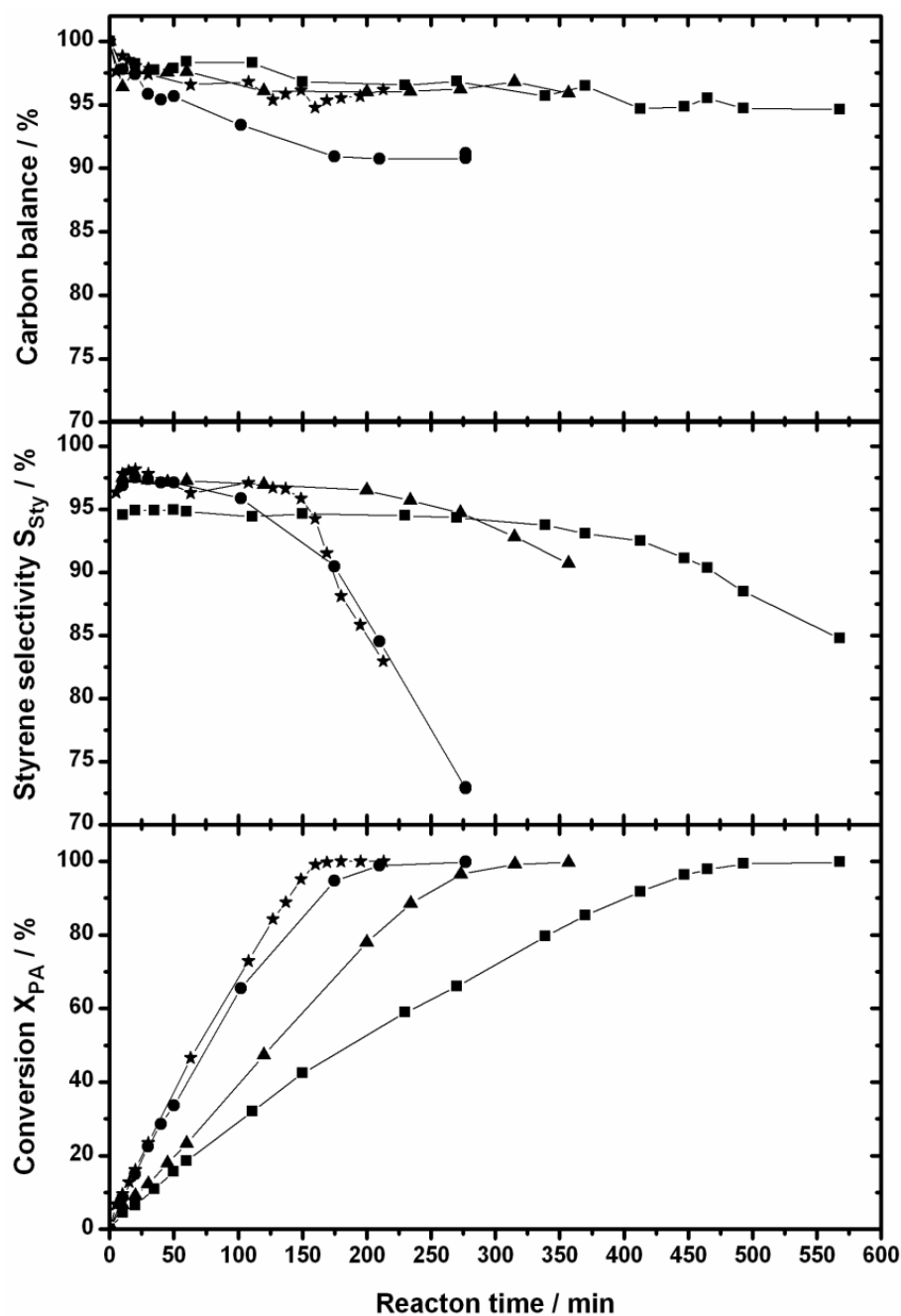


Figure 4-10: Conversion, selectivity and carbon balance vs. time observed for the liquid phase hydrogenation of phenylacetylene at 4 bar, 40 °C with Lindlar's catalyst (stars), Pd/Al₂O₃ (spheres), as prepared milled Pd₂Ga (squares) and Pd powder (triangles)

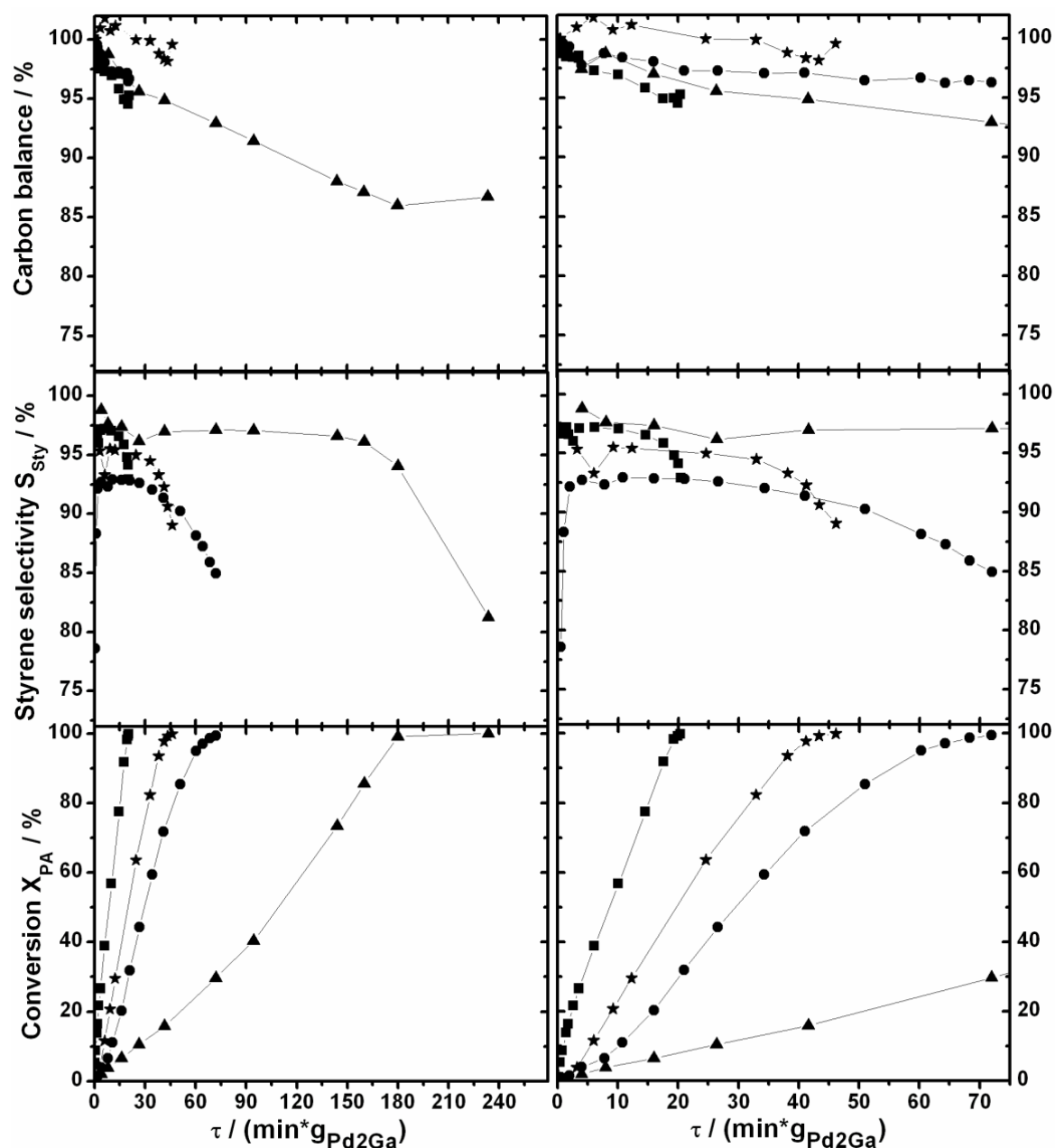


Figure 4-11: Conversion, selectivity and carbon balance versus (time*catalyst mass) for Pd₂Ga after different pre-treatments at ~1.3 bar, 40 °C. On the right site a zoom is shown, to highlight the different initial activities. The highest initial activity is found for as prepared milled Pd₂Ga (squares), followed by milled Pd₂Ga treated at 400 °C in static vacuum (stars, this reaction was performed at 4 bar in the commercial autoclave). A reductive pre-treatment leads to a considerably lower initial activity. It increases rapidly with time, using the commercial autoclave (spheres), but can be stabilized at least in the beginning under very inert conditions (Schlenk reactor). Under these conditions the carbon balance decreases significantly more.

4. 7 References

- [1] H. U. Blaser, A. Schnyder, H. Steiner, F. Rössler, P. Baumeister in: G. Ertl, H. Knözinger, J. Weitkamp (Eds.), *Handbook of Heterogeneous Catalysis*, Weinheim, Wiley-VCH, 2008, 3284.
- [2] N. V. Semagin, A. V. Bykov, E. M. Sulman, V. G. Matveeva, S. N. Sidorov, L. V. Dubrovina, P. M. Valetsky, O. I. Kiselyova, A. R. Khokhlov, B. Stein, L. M. Bronstein, *J. Mol. Catal. A* 208 (2004) 273.
- [3] R. A. Basimova, M. L. Pavlov, S. I. Myachin, A. V. Prokopenko, A. V. Askarova, B. I. Kutepov, S. A. Sychkova, *Petroleum Chemistry* 49 (2009) 360.
- [4] K. N. Campbell, B. K. Campbell, *Chem. Rev.* 31 (1942) 145.
- [5] C. A. Brown, V. K. Ahuja, *J. Org. Chem.* 38 (1973) 2226.
- [6] R. Paul, G. Hilly, *Bull. Soc. Chim. Fr.* 6 (1939) 218.
- [7] W. Reppe, *Justus Liebigs Ann. Chem.* 596 (1955) 38.
- [8] S. Nishimura, *Handbook of Heterogeneous Catalytic Hydrogenation for Organic Synthesis* Wiley-Interscience, New York, 2001, 148.
- [9] V. Vajt, L. Kurc, L. Cervený, *Int. J. Chem. Kinet.* 40 (2008) 240.
- [10] E. Brunner, *J. Chem. Eng. Data* 30 (1985) 269.
- [11] A. Borodzinski, G. C. Bond, *Catal. Rev.* 48 (2006) 91.
- [12] N. A. Dobson, G. Eglinton, M. Krishnamurti, R. A. Raphael, R. G. Willis, *Tetrahedron* 16 (1961) 16.
- [13] S. Nishimura, *Handbook of Heterogeneous Catalytic Hydrogenation for Organic Synthesis*, Wiley-Interscience, New York, 2001, 68.
- [14] F. R. Mayo, *J. Am. Chem. Soc.* 90 (1968) 1289.
- [15] G. N. Bantsyrev, I. M. Scherbakova, M. I. Cherkashin, I. D. Kalikhman, A. N. Chigir, A. A. Berlin, *B. Acad. Sci. USSR Ch.* 19 (1970) 1661.
- [16] E. Shutt, J. M. Winterbottom, *Platinum Metals Rev.* 15 (1971) 94.
- [17] S. D. Jackson, L. A. Shaw, *Appl. Catal. A* 134 (1996) 91.
- [18] M. Terasawa, H. Yamamoto, K. Kaneda, T. Imanaka, S. Teranishi, *J. Catal.* 57 (1979) 315.
- [19] S. Domínguez-Domínguez, Á. Berenguer-Murcia, D. Cazorla-Amorós, Á. Linares-Solano, *J. Catal.* 243 (2006) 74.

- [20] V. Engels, A. E. H. Wheatley, A. Berenguer-Murcia, D. A. Jefferson, B. F. G. Johnson, *Mater. Sci. Forum* 13 (2009) 604.
- [21] R. Tschan, R. Wandeler, M. S. Schneider, M. M. Schubert, A. Baiker, *J. Catal.* 204 (2001) 219.
- [22] A. M. Venezia, L. F. Liotta, G. Deganello, Z. Schay, L. Guzzi, *J. Catal.* 182 (1999) 456.
- [23] T. Mallat, A. Baiker, *Appl. Catal. A* 200 (2000) 3.
- [24] Á. Mólnar, G. V. Smith, M. Bartók, *J. Catal.* 101 (1986) 67.
- [25] H. Lindlar, *Helv. Chim. Acta* 35 (1952) 446.
- [26] H. Lindlar, R. Dubius, *Org. Synth. Coll. Vol.* 5 (1973) 880.
- [27] J. Sobczak, W. Palczewska, T. Boleslawska, M. Pawlowska, *Stud. Surf. Sci. Catal.* 41 (1988) 197.
- [28] D. Dhamodharan, *Chem. Lett.* 235 (1996) 235.
- [29] R. Schlögl, K. Noack, H. Zbinden, *Helv. Chim. Acta* 70 (1987) 627.
- [30] J. Rajaram, A. P. S. Narula, H. P. S. Chawla, S. Dev, *Tetrahedron* 39 (1983) 2315.
- [31] W. Palczewska, A. Jablonski, Kaszukur, *J. Mol. Catal.* 25 (1984) 307.
- [32] M. García-Mota, J. Gómez-Díaz, G. Novell-Leruth, C. Vargas-Fuentes, L. Bellarosa, B. Bridier, J. Pérez-Ramírez, N. López, *Theor. Chem. Acc.* 128 (2011) 663.
- [33] J. Yu, J. B. Spencer, *Chem. Commun* (1998) 1103.
- [34] J. Yu, J. B. Spencer, *J. Org. Chem.* 62 (1997) 8618.
- [35] M. Armbrüster, K. Kovnir, M. Behrens, D. Teschner, Yu. Grin, R. Schlögl, *J. Am. Chem. Soc.* 132 (2010) 14745.
- [36] K. Kovnir, M. Armbrüster, D. Teschner, T. V. Venkov, F. C. Jentoft, A. Knop-Gericke, Yu. Grin, R. Schlögl, *Sci. Technol. Adv. Mater.* 8 (2007) 420.
- [37] J. Osswald, R. Giedigkeit, R. E. Jentoft, M. Armbrüster, F. Girgsdies, K. Kovnir, T. Ressler, Yu. Grin, R. Schlögl, *J. Catal.* 258 (2008) 210.
- [38] J. Osswald, R. Giedigkeit, R. E. Jentoft, M. Armbrüster, F. Girgsdies, K. Kovnir, T. Ressler, Yu. Grin, R. Schlögl, *J. Catal.* 258 (2008) 219.
- [39] T. Komatsu, K. Takagi, K. Ozawa, *Catal Today* 164 (2011) 143.
- [40] M. Armbrüster, M. Behrens, F. Cinquini, K. Föttinger, Yu. Grin, A. Haghofer, B. Klötzer, A. Knop-Gericke, H. Lorenz, A. Ota, S. Penner, J. Prinz, C. Rameshan, Z. Révay, D. Rosenthal, G. Rupprechter, P. Sautet, R. Schlögl, L. Shao, L. Szentmiklósi, D. Teschner, D. Torres, R. Wagner, R. Widmer, G. Wowsnick, *ChemCatChem* 4 (2012) 1048.

- [41] G. Wowsnick, D. Teschner, I. Kasatkin, F. Girgsdies, M. Armbrüster, A. Zhang, Yu. Grin, R. Schlögl, M. Behrens, J. Catal. submitted.
- [42] K. Kovnir, M. Schmidt, C. Waurisch, M. Armbrüster, Y. Prots, Yu. Grin, Z. Kristallogr. New Cryst. Struct. 223 (2008) 7.
- [43] M. Salmeron, R. Schlögl, Surf. Sci. Rep. 63 (2008) 169.
- [44] S. Tanuma, C. J. Powell, D. R. Penn, Surf. Interface Anal. 43 (2011) 689.
- [45] E. Shutt, J. M. Winterbottom, Platinum Metals Rev. 15 (1971) 94.
- [46] K. Kovnir, M. Schmidt, C. Waurisch, M. Armbrüster, Y. Prots, Y. Grin, Z. Kristallogr. New Cryst. Struct. 223 (2008) 7.
- [47] A. Haghofer, K. Föttinger, F. Girgsdies, D. Teschner, A. Knop-Gericke, R. Schlögl, G. Rupprechter, J. Catal. 286 (2012) 13.
- [48] A. S. Al-Ammar, G. Webb, J. Chem. Soc. Faraday Trans. 74 (1978) 195.
- [49] R. V. Chaudhari, R. Jaganathan, D. S. Kolhe, Chem. Eng. Sci. 41 (1986) 3073.
- [50] A. M. Doyle, S. K. Shaikhutdinov, S. D. Jackson, H.-J. Freund, Angew. Chem. Int. Ed. 42 (2003) 5240.
- [51] D. Teschner, J. Borsodi, A. Wootsch, Zs. Révay, M. Hävecker, A. Knop-Gericke, S. D. Jackson, R. Schlögl, Science 320 (2008) 86.
- [52] D. Teschner, E. M. Vass, M. Hävecker, S. Zafeiratos, P. Schnörch, H. Sauer, A. Knop-Gericke, R. Schlögl, M. Chamam, A. Wootsch, A. S. Canning, J. J. Gamman, S. D. Jackson, J. McGregor, L. F. Gladden, J. Catal. 242 (2006) 26.
- [53] B. Hammer, J. K. Nørskov, Surf. Science 343 (1995) 211.
- [54] F. Studt, F. Abild-Pedersen, T. Bligaard, R. Z. Sørensen, C. H. Christensen, J. K. Nørskov, Science 320 (2008) 1320.
- [55] J. C. Fuggle, F. U. Hillebrecht, R. Zeller, Z. Zolnierrek, P. A. Bennett, Phys. Rev. B 27 (1983) 2145.
- [56] F. U. Hillebrecht, J. C. Fuggle, P. A. Bennett, Z. Zolnierrek, Phys. Rev. B 27 (1983) 2179.
- [57] A. Haghofer, D. Ferri, K. Föttinger, G. Rupprechter, ACS Catal. 2 (2012) 2305.
- [58] B. Halevi, E. J. Peterson, A. DeLaRiva, E. Jeroro, V. M. Lebarbier, Y. Wang, J. M. Vohs, B. Kiefer, E. Kunkes, M. Hävecker, M. Behrens, R. Schlögl, A. K. Datye, J. Phys. Chem. C 114 (2010) 17181.
- [59] M. Friedrich, D. Teschner, A. Knop-Gericke, M. Armbrüster, J. Catal. 285 (2012) 41.

- [60] H. Lorenz, M. Friedrich, M. Armbrüster, B. Klötzer, S. Penner, J. Catal. 297 (2013) 151.
- [61] M. Armbrüster, K. Kovnir, M. Friedrich, D. Teschner, G. Wowsnick, M. Hahne, P. Gille, L. Szentmiklósi, M. Feuerbacher, M. Heggen, F. Girgsdies, D. Rosenthal, R. Schlögl, Yu. Grin, Nature Mat. 11 (2012) 690.

5 Summary

In this work the bulk and the surface stability as well as the catalytic properties of the intermetallic compound Pd₂Ga in the liquid phase hydrogenation of phenylacetylene were investigated.

The bulk material is largely stable. In 10% H₂ atmosphere it benefits from a high resistance against hydride formation as detected by *in situ* DTA/TG/MS. *In situ* XRD measurements in 20% O₂/He reveal a high resistance against oxidation below 300 °C. However, compared to elemental Ga, the bonding characteristics do not lead to a sufficiently enhanced thermodynamic or kinetic stabilization against oxidation of intermetallic Ga at the surface. This is a consequence of the reduced coordination of the surface-metal atoms and leads inevitably to a termination which differs from the bulk structure unless very strong reducing conditions are applied. As shown by means of *in situ* XPS and HR-TEM, the degree of surface oxidation and the stability of the resulting passivation layer increases with the temperature, total pressure and partial pressure of potential oxidants. Mechanical load additionally induces Ga segregation and provokes further decomposition. An as prepared milled Pd₂Ga sample consists on Pd and Pd₂Ga nanoparticles embedded in an inhomogeneous Ga oxide over-layer which terminates on the bulk of Pd₂Ga. The ability of the present Pd to activate hydrogen causes an easy reduction of Ga oxide under reducing conditions at high temperatures. In dynamic UHV in the *in situ* XPS chamber a heating to 400 °C induces an at least partial reduction of surface oxide and re-formation of the intermetallic surface. In 10% H₂/He the surface oxide reduction takes place at ~180 °C. The exact nature and morphology of the Pd species formed by partial decomposition cannot be easily determined. The results suggest either the formation of small Pd clusters or the presence of Pd enriched phases with an intermediate electronic and structural state.

The surface cannot be reduced during the liquid phase hydrogenation. After an *ex situ* pre-reduction in 5% H₂/Ar at 400 °C the activity is reduced by a factor of ~20. However, the surface is not stable and can be easily re-oxidized by O₂ and H₂O impurities during phenylacetylene hydrogenation, which is indicated by a strong increase in activity with

reaction time. Minimizing the presence of O₂ or H₂O traces, this decomposition could be impeded but an attack of the bulk of Pd₂Ga by phenylacetylene during reaction was observed.

The overall selectivities towards styrene are varying only in a small range for all catalysts with the low dispersion and are between 88.5 and 94% depending on the conditions. In the case of pre-reduced Pd₂Ga, the carbon balance drops significantly more to 86.5% compared to the other catalysts ($\geq 95\%$), lowering the overall yield of styrene. Thus, clean Pd₂Ga shows inadequate catalytic properties for the liquid phase hydrogenation of phenylacetylene.

The strong dependence of the catalytic properties of Pd₂Ga on the nature of the pre-treatment necessitates a re-investigation with respect to the gas phase hydrogenation of acetylene for the powdered bulk materials of Pd₂Ga and PdGa, which was carried out without a pre-treatment earlier. A re-formation of an as prepared Pd₂Ga sample at 200 °C in feed-gas, containing 5% H₂ might be possible, but other processes e.g. the formation of Pd-C in presence of acetylene, could compete and might also explain the catalytic properties. In the case of Pd₂Ga/MgO/MgGa₂O₄ catalysts a reduction at 500 °C was necessary to form Pd₂Ga nanoparticles from the precursor. After such a pre-treatment the catalyst exhibited a slow pronounced activation from 22% to 94% conversion during 30 h time on stream in acetylene hydrogenation, while the selectivity remains constantly high. One explanation therefore was a slow decomposition of the Pd₂Ga nanoparticles in presence of traces of O₂ and H₂O during hydrogenation, liberating very small Pd accumulations. These were supposed to response for the activity and the high selectivity, rather than Pd₂Ga itself.

The XPS signals presented in previous publications dealing with powdered PdGa samples must be attributed to partially decomposed PdGa, embedded in Ga oxide. The *in situ* formation of PdGa during acetylene hydrogenation is unlikely. The experience reveals that it cannot be obtained in a straightforward manner by H₂ reduction at moderate temperatures (compare also a supporting discussion in appendix). The reason for this difficulty is the primarily formation of Pd₂Ga during reduction. Pd₂Ga might not assist further Ga oxide reduction in presence of H₂.

Independent of the pre-treatment and the thickness of the layer, substitution of Ga by one of its homologues metals will likely result in different stabilities of the passivation layer, with stability increasing in the order $Tl < In < Ga < Al$. The reversibility of the oxidation will be further reduced when substituting Pd with a metal with lower hydrogen activation ability. In general when using less noble metals, a bulk-terminated surface structure might be - if at all - only accessible under strongly reducing conditions and acts rather as a precursor for a less predictable surface especially in presence of oxidants. This fact impedes theoretical predictions based on the electronic structure or crystal structure of an intermetallic compound or alloys for application as catalysts because chemical dynamics and instabilities need to be considered. In the case of Pd_2Ga , the concerted modification of the d-band of Pd leads to a practically insufficient stability.

Appendix

Bulk and surface analyses of PdGa

PdGa was synthesized by melting stoichiometric amounts of Pd granules (Chempur, 99.95%) and Ga pellets (Chempur, 99.99%) in a glassy carbon crucible in a high frequency induction furnace under Ar atmosphere in a glove box ($O_2 < 1$ ppm, $H_2O < 1$ ppm). The obtained regulus was annealed at 800 °C in an evacuated quartz glass ampoule for one week. A metallographic specimen was prepared by cutting 1 mm thick cylinders from the regulus. The slice was polished and stored under Ar. To obtain a fine powder of Pd₂Ga the material was ground in an agate mortar under air. Prior to the XPS measurement the powder was additionally pre-reduced in 5% H₂/Ar at 200 °C for 1 h. 250 mg were pressed to a pill (8 mm diameter), treated again in 5% H₂/Ar at 200 °C, cooled under this atmosphere and subsequently stored under Ar.

The homogeneity of the sample was proven by optical microscopy, elemental mapping and WDX (Figure A1) and XRD (Figure A2 left). An *in situ* TG/MS measurement in 5% H₂/Ar (Figure A2, right) reveals an unexpected carbonate decomposition starting at about 270 °C and a reduction of surface oxide not before 400 °C.

In situ XPS analyses of the metallographic specimen at 1 mbar H₂ at 450 °C reveal only a little amount of oxidized Ga and a narrow Pd 3d_{5/2} signal at 336.3 eV (compare Figure A3 and Figure A4) in agreement with the results of a well-defined PdGa($\bar{1}\bar{1}\bar{1}$) surface after several sputtering/annealing cycles [D. Rosenthal et al., Langmuir 28 (2012) 7848].

The as prepared metallographic specimen is partially decomposed at the surface as indicated by the presence of large amounts of Ga oxide and the binding energies of Pd 3d_{5/2} varying between 335.85 and 336.0 eV. The same is valid for pre-reduced ground PdGa. The pre-reduction leads not to Ga oxide reduction and re-formation of PdGa, as there is no significant change in the binding energy of Pd 3d_{5/2} in comparison to as prepared powdered PdGa [Kovnir et al., Sci. Technol. Adv. Mater. 8 (2007) 420.], which is also in agreement with the

TG/MS data. Complete decomposition in elemental Pd like in the case of Pd₂Ga (compare section 3. 3. 5) is not observed. The reason is likely a considerably stronger and fast Ga segregation from the bulk to the surface and subsequent oxidation due to mechanical load (Table A1), which partially protects remaining intermetallic Ga at the surface. Comparable results were found for air-milled PdGa, pre-reduced at even 400 °C in 200 mbar H₂. The Pd 3d_{5/2} binding energy of this sample was found at 335.7 eV in [J. Osswald et al., J. Catal. 258 (2008) 219.]. It is thus unlikely that PdGa catalyzed the acetylene hydrogenation as reported earlier (T = 200 °C, feed-gas: 0.5% C₂H₂, 5% H₂, 50% C₂H₄ in He, *without* pre-treatment).

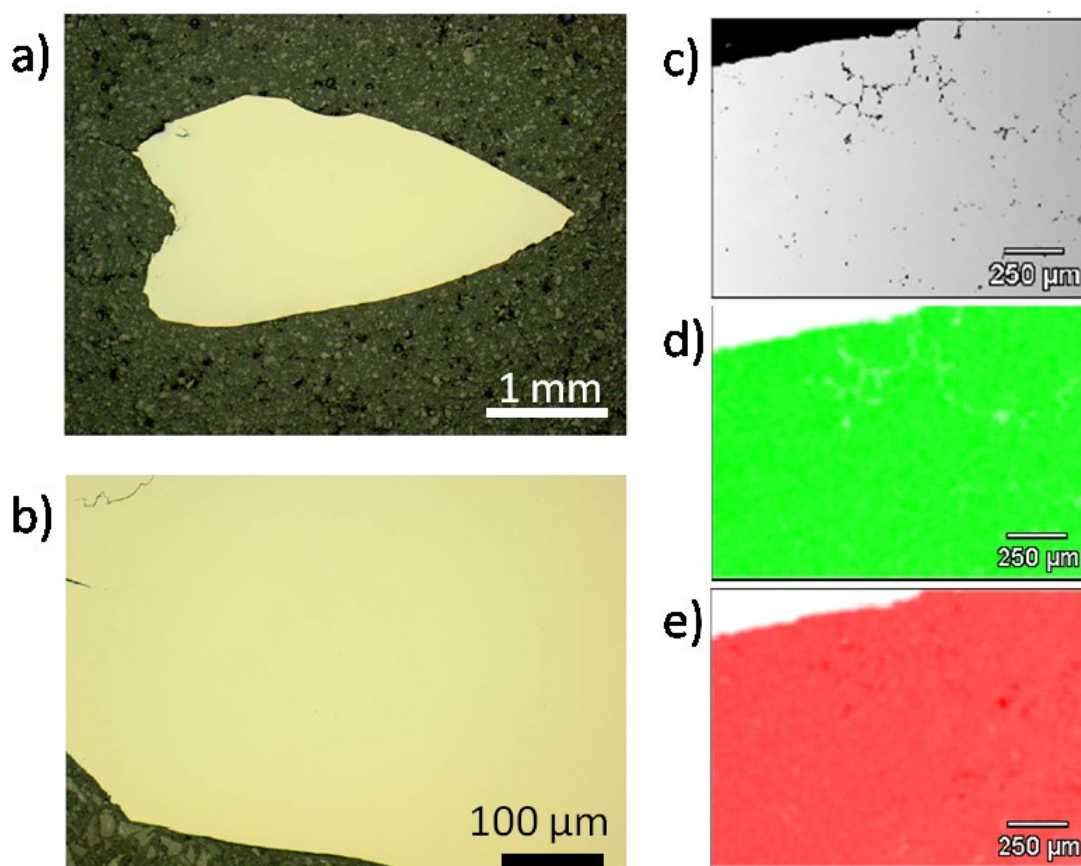


Figure A1: Optical microscopy of an embedded metallographic specimen (a, b) reveals no additional phases. Leaks and rifts, visible in the SEM image (c), are present to a small extent, which certainly originate from sample preparation. The distribution of Pd (d) and Ga (e) is homogeneous with an elemental composition of Pd_{49.8}Ga_{50.2} according to WDX. Small holes, close to the edge are slightly enriched on Ga.

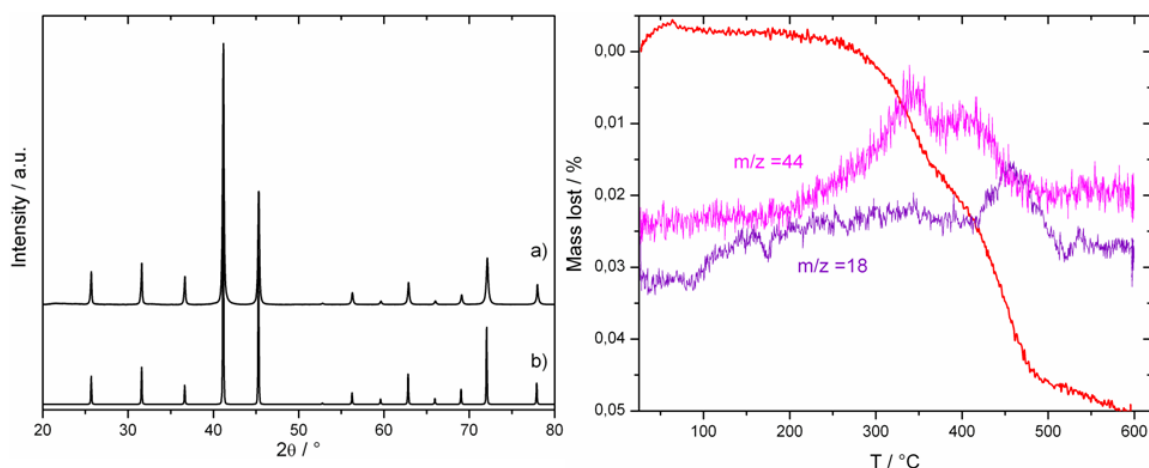


Figure A2 left: X-ray diffraction pattern of ground PdGa (a) and a calculated pattern (b). Right: *In situ* TG/MS of a ground PdGa. The heating rate was 5°C/min in 5% H₂/Ar. The X-ray diffraction pattern of ground PdGa verifies the absence of additional crystalline phases within its detection limit. The *in situ* TG/MS analysis of ground PdGa show a slight mass loss starts at ~270 °C accompanied with the formation of CO₂ which is likely attributed to carbonate decomposition. At 400 °C, a further mass loss accompanied by signals for CO₂ and H₂O is visible, which indicates simultaneous carbonate decomposition and surface oxide reduction.

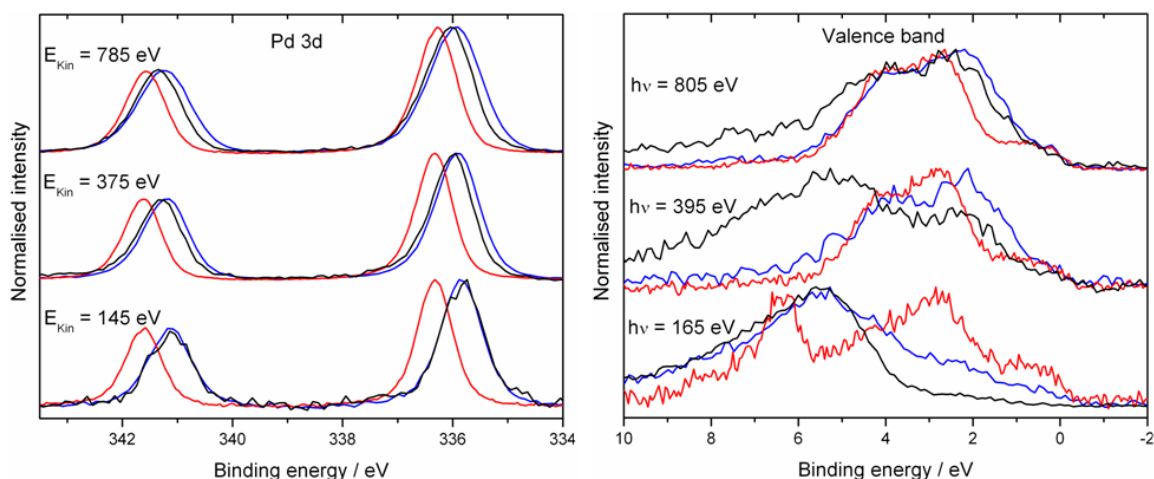


Figure A3 left: XPS depth-profiling of the Pd 3d core-level of the as prepared metallographic specimen of PdGa in UHV at ambient temperature (blue), the metallographic specimen heated *in situ* to 450 °C in 1 mbar H₂ (red) and of ground PdGa, pre-reduced *ex situ* in 5% H₂/Ar at 200 °C for 1 h, recorded under UHV at ambient temperature. A binding energy of 336.3 eV is observed for the *in situ* reduced specimen. This binding energy is similar to that of a PdGa(111) [D. Rosenthal et al., Langmuir 28 (2012) 7848] after several sputtering and annealing cycles. The other signals must be attributed to partially decomposed Pd species. On the right side the corresponding valence bands are shown.

Table A1: Pd 3d_{5/2} peak maxima and FWHM of a) an as prepared metallographic specimen b) metallographic specimen during *in situ* treatment at 450 °C in 1 mbar H₂, c) ground PdGa, pre-reduced *ex situ* in 5% H₂/Ar at 200 °C for 1 h and recorded under UHV at ambient temperature. The calculated surface stoichiometry (ab initio) and the relative content of oxidized Ga are also given. In particular note the massive Ga enrichment for the ground sample c).

E _{kin}	Peak-maximum / eV			FWHM / eV			Pd ^{total} :Ga ^{total}			Pd ^{total} :Ga ⁰			Ga ³⁺ :(Ga ³⁺ +Ga ⁰)/%		
	785	375	145	785	375	145	785	375	145	785	375	145	785	375	145
a)	336.0	335.9	335.9	1.14	0.96	0.92	0.84	0.84	1.17	1.28	1.66	3.62	34.8	49.1	67.8
b)	336.3	336.3	336.3	0.87	0.80	0.77	0.71	0.74	0.75	0.79	0.81	0.78	5.8	8.5	8.8
c)	336.1	336.0	335.9	1.04	0.90	0.95	0.17	0.09	0.05	1.14	1.31	1.31	84.7	92.9	96.3

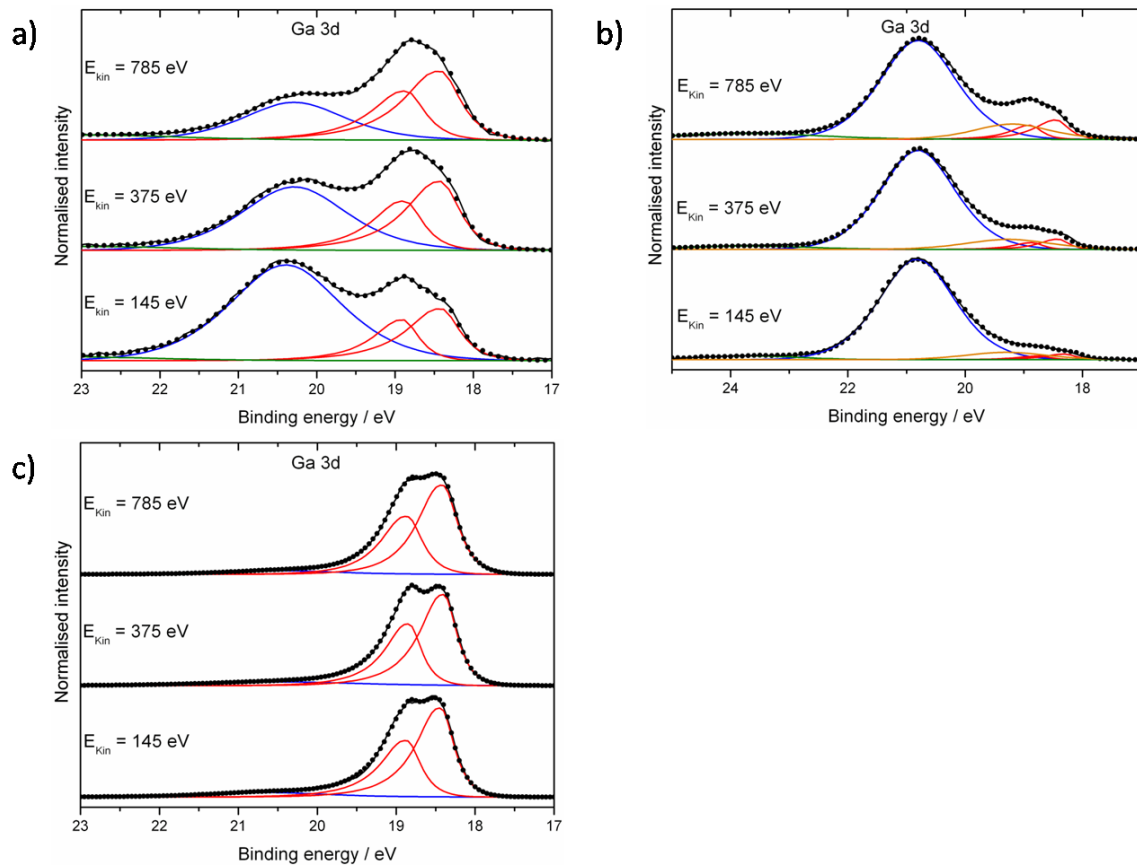


Figure A4: XPS depth-profiling of the Ga 3d core-level. a) an as prepared metallographic specimen of PdGa b) metallographic specimen during *in situ* treatment at 450 °C in 1 mbar H₂, c) ground PdGa, pre-reduced *ex situ* in 5% H₂/Ar at 200 °C for 1 h and recorded under UHV at ambient temperature. In a) and c) large amounts of Ga oxides (blue fitting lines) the relative amount increases with increasing surface sensitivity. The signal at 19.2 eV in c) is attributed to Ga sub-oxides. Only the *in situ* reduced specimen (c) shows Ga almost completely in intermetallic state (red doublet). Green lines correspond to O 2s.

Personal information

Curriculum vitae

Name: Gregor Wowsnick

Date of birth: 12.11.1984

Place of birth: Dresden

Personal status: unwed

Adress: Berliner Straße 123, 10713 Berlin, Germany

Academic education

10/2004-7/2009 Study of chemistry at Technische Universität Dresden qualification:
Diplom-Chemiker

10/2008-7/2009 Diploma thesis; title of thesis: „Nanopartikuläre Darstellung
intermetallischer Pd-Ga-Verbindungen“

since 10/2009 PhD thesis at the Fritz-Haber-Institut der Max-Planck-Gesellschaft in
Berlin; Department of Inorganic Chemistry

Publications

M. Armbrüster, G. Wowsnick, M. Friedrich, M. Heggen, R. Cardoso-Gil: Synthesis and Catalytic Properties of Nanoparticulate Intermetallic Ga-Pd Compounds, *J. Am. Chem. Soc.* 133 (2011) 9112.

R. Leary, Z. Saghi, M. Armbrüster, G. Wowsnick, R. Schlögl, J. M. Thomas, P. A. Midgley: Quantitative High-Angle Annular Dark-Field Scanning Transmission Electron Microscope (HAADF-STEM) Tomography and High-Resolution Electron Microscopy of Unsupported Intermetallic GaPd₂ Catalysts, *J. Phys. Chem. C* 116 (2012) 13343.

M. Armbrüster, M. Behrens, F. Cinquini, K. Föttinger, Yu. Grin, A. Haghofer, B. Klötzer, A. Knop-Gericke, H. Lorenz, A. Ota, S. Penner, J. Prinz, C. Rameshan, Z. Révay, D. Rosenthal, G. Rupprechter, P. Sautet, R. Schlögl, L. Szentmiklósi, D. Teschner, D. Torres, R. Wagner, R. Widmer, G. Wowsnick: How to Control the Selectivity of Palladium-based Catalysts in Hydrogenation Reactions: The Role of Subsurface Chemistry, *ChemCatChem* 4 (2012) 1048.

M. Armbrüster, K. Kovnir, M. Friedrich, D. Teschner, G. Wowsnick, M. Hahne, P. Gille, L. Szentmiklósi, M. Feuerbacher, M. Heggen, F. Girgsdies, D. Rosenthal, R. Schlögl, Yu. Grin, Al₁₃Fe₄ as a Low-cost Alternative for Palladium in Heterogeneous Hydrogenation, *Nature Mat.* 11 (2012) 690.

T. Kandemir, F. Girgsdies, T. C. Hansen, K.-D. Liss, I. Kasatkin, E. L. Kunkes, G. Wowsnick, N. Jacobsen, R. Schlögl, M. Behrens, In Situ Study of Catalytic Processes: Neutron Diffraction of a Methanol Synthesis Catalyst at Industrially Relevant Pressure, *Angew. Chem. Int. Ed.* 52 (2013) 5166.

G. Wowsnick, D. Teschner, I. Kasatkin, F. Girgsdies, M. Armbrüster, A. Zhang, Yu. Grin, R. Schlögl, M. Behrens, Surface Dynamics of the Intermetallic Catalyst Pd₂Ga, Part I – Structural Stability in UHV and Different Gas Atmospheres, submitted to *J. Catal.*

G. Wowsnick, D. Teschner, M. Armbrüster, I. Kasatkin, F. Girgsdies, Yu. Grin, R. Schlögl, M. Behrens, Surface Dynamics of the Intermetallic Catalyst Pd₂Ga, Part II – Reactivity and Stability in Liquid Phase Hydrogenation of Phenylacetylene, submitted to J. Catal.

Oral presentations

G. Wowsnick, D. Teschner, I. Kasatkin, F. Girgsdies, R. Schlögl, M. Armbrüster, M. Behrens Surface Dynamics of the intermetallic compound Pd₂Ga and its catalytic properties in liquid phase alkyne hydrogenation, Third Russian-German seminar on catalysis, 24. - 28. 6. 2013, Burduguz village (Oblast Irkutsk), Russia

Poster presentations

G. Wowsnick, M. Armbrüster, M. Friedrich, Yu. Grin, R. Schlögl: Synthesis and Catalytic Performance of Nanostructured Intermetallic Pd-Ga Compounds, 43. Jahrestreffen deutscher Katalytiker, 10. - 12. 3. 2010. Weimar, Germany

G. Wowsnick, M. Behrens, R. Schlögl, M. Armbrüster: Pd₂Ga as Selective Catalyst for the Semi-Hydrogenation of Phenylacetylene, 44. Jahrestreffen deutscher Katalytiker, 16. - 18. 3. 2011, Weimar, Germany

G. Wowsnick, M. Behrens, R. Schlögl, M. Armbrüster: Stability of Pd₂Ga in Different Atmospheres, EuropaCat X, 28. 8. - 2. 9. 2011, Glasgow, United Kingdom

G. Wowsnick, M. Armbrüster, M. Behrens, I. Kasatkin, A. Zhang, R. Schlögl: Stability of Pd-Ga Intermetallic Compounds under Different Atmospheres and Application in Liquid Phase Hydrogenation, 45. Jahrestreffen deutscher Katalytiker, 14. - 16. 3. 2012, Weimar, Germany.

G. Wowsnick, A.Ota, L. Li, M. Armbrüster, I.Kasatkin, D. Rosenthal, J. Kröhnert, A. Zhang, R. Schlögl, M. Behrens: Pd₂Ga for selective hydrogenation of the C-C-triple bond - syntheses and catalytic properties of model and high performance catalysts, 15th ICC, 1. 7. - 6. 7. 2012, München, Germany